UNIVERSIDAD DE CHILE
FACULTAD DE CIENCIAS FÍSICAS Y MATEMÁTICAS
DEPARTAMENTO DE FÍSICA

TRANSITION TO SPATIOTEMPORAL INTERMITTENCY AND DEFECT TURBULENCE IN SYSTEMS UNDER TRANSLATIONAL COUPLING

TESIS PARA OPTAR AL GRADO DE
MAGÍSTER EN CIENCIAS, MENCIÓN FÍSICA

FABIÁN ADOLFO ÁLVAREZ GARRIDO

PROFESOR GUÍA:
MARCEL CLERC GAVILÁN

MIEMBROS DE LA COMISIÓN:
SALIYA COULIBALY
STEFANIA RESIDORI
ALEJANDRO VALDIVIA HEPP

Este trabajo ha sido parcialmente financiado por proyecto FONDECYT 1180903, el Instituto Milenio de Investigación en Óptica y el Programa de Estadías Cortas de Investigación del Departamento de Postgrado y Postítulo de la Vicerrectoría de Asuntos Académicos de la Universidad de Chile.

SANTIAGO DE CHILE
2020

RESUMEN DE LA MEMORIA PARA OPTAR
AL TÍTULO DE MAGÍSTER EN CIENCIAS, MENCIÓN FÍSICA
POR: FABIÁN ADOLFO ÁLVAREZ GARRIDO
FECHA: 2020
PROF. GUÍA: MARCEL CLERC GAVILÁN

TRANSITION TO SPATIOTEMPORAL INTERMITTENCY AND DEFECT TURBULENCE IN SYSTEMS UNDER TRANSLATIONAL COUPLING

Una dificultad frecuente que se enfrenta al realizar experimentos con retroinyección óptica es el correcto alineamiento de sus componentes. Un desalineamiento puede resultar en un acoplamiento traslacional en la dinámica de las variables físicas estudiadas. Un sistema posee un acoplamiento traslacional cuando la evolución de sus variables físicas en cada punto depende de sus valores locales y de sus valores a una distancia fija. Observaciones experimentales realizadas sobre una válvula de cristal líquido con acoplamiento traslacional en el textit Laboratorio de fenómenos robustos en óptica muestran una transición de patrones de rayas estacionarios hacia ondas viajeras, intermitencia espaciotemporal y turbulencia de defectos. Esta tesis tiene como objetivo caracterizar esta transición en un modelo prototipo de formación de patrones con acoplamiento traslacional.

En el Capítulo 1, explicamos algunos conceptos preliminares de la física no lineal relacionados con la teoría de bifurcaciones y dinámica caótica. Estos conceptos son útiles para comprender los resultados de esta tesis.

El capítulo 2 está dedicado a hacer una breve reseña sobre sistemas con formación de patrones. Explicamos en detalle un mecanismo particular de formación de patrones conocido como las inestabilidades de Turing. También hacemos un resumen sobre el modelo de Swift-Hoheneberg, considerado como la ecuación más simple que tiene una inestabilidad de Turing. Exploramos su fenomenología y derivamos ecuaciones de amplitud que describen sus comportamientos.

En el Capítulo 3, hacemos una reseña sobre la ecuación compleja de Ginzburg-Landau unidimensional. Exploramos su relevancia en diferentes contextos de la física, discutimos sus soluciones conocidas, mostramos su diagrama de bifurcación y explicamos el mecanismo que da lugar a sus regímenes complejos en el sentido espaciotemporal.

En el Capítulo 4, explicamos cómo funciona el experimento de la válvula de cristal líquido con retroinyección, mostramos la fenomenología observada que es de interés para esta tesis y derivamos un modelo teórico que describe parcialmente esta fenomenología. Presentamos una posible explicación al origen de los regímenes complejos en el sentido espaciotemporal que observamos en este experimento.

En el Capítulo 5, presentamos un modelo prototipo de formación de patrones con acoplamiento traslacional: La ecuación de Swift-Hoheneberg con acoplamiento traslacional. Exploramos su fenomenología, la cual exhibe transiciones entre patrones estacionarias, intermitencia espaciotemporal, y turbulencia de defectos. Caracterizamos estas transiciones derivando una ecuación de amplitud: La ecuación compleja de Ginzburg-Landau. Este modelo nos permite revelar el diagrama de bifurcación del modelo prototipo y comprender el mecanismo que

da origen a sus comportamientos complejos. Exploramos brevemente la dinámica bidimensional del modelo prototipo y proponemos generalizaciones utilizando núcleos de interacción. Realizamos comparaciones entre simulaciones numéricas del modelo y observaciones experimentales hechas sobre válvula de cristal líquido desalineada de forma intencional. Finalmente, proponemos una modificación del experimento para explorar los efectos de otras interacciones de largo alcance en sistemas de formación de patrones.

RESUMEN DE LA MEMORIA PARA OPTAR
AL TÍTULO DE MAGÍSTER EN CIENCIAS, MENCIÓN FÍSICA
POR: FABIÁN ADOLFO ÁLVAREZ GARRIDO
FECHA: 2020
PROF. GUÍA: MARCEL CLERC GAVILÁN

TRANSITION TO SPATIOTEMPORAL INTERMITTENCY AND DEFECT TURBULENCE IN SYSTEMS UNDER TRANSLATIONAL COUPLING

A common difficulty faced when performing experiments with optical feedback is the proper alignment of its components. Misalignment may result in a translational coupling in the dynamics of physical quantities under study. A system is said to have a translatioanl coupling when the evolution of its physical variables depends on their values at their local position and their values at some fixed distance from this position. Experimental observations conducted in a liquid crystal light valve with translational coupling in the *Laboratorio de fenómenos robustos en óptica* show a transition from stationary striped patterns to propagation, spatiotemporal intermittency, and defect turbulence of stripped waves. This dissertation aims to characterize this transition in a general pattern forming system with translational coupling.

In Chapter 1, we explain some preliminary concepts of nonlinear physics related to bifurcation theory and chaotic dynamics, which are useful to understand the results of this thesis.

Chapter 2 is dedicated to doing a brief review of pattern formation. We explain in detail a particular pattern-forming mechanism known as Turing instabilities. We also review the Swift-Hoheneberg model, regarded as the simplest equation having a Turing instability. We explore its phenomenology and derive amplitude equations that describe its behaviors.

In Chapter 3, we review the dynamics of the one-dimensional cubic complex Ginzburg-Landau equation. We explore its relevance in different contexts in physics. We discuss its known solutions, show its bifurcation diagram, and explain the mechanism that gives rise to its complex spatiotemporal regimes.

In Chapter 4, we explain how the liquid crystal light valve experiment works, we show the observed phenomenology, which is of interest for this dissertation, and derive a theoretical model that partially describes this phenomenology. We present a possible explanation of the complex dynamics this experiment exhibits.

In Chapter 5, we introduce a prototype pattern forming system with translational coupling, namely the Swift-Hoheneberg equation with translational coupling. We explore its phenomenology, which exhibits transitions to spatiotemporal intermittency and defects turbulence from stationary striped patterns. We characterize these transitions deriving an amplitude equation, namely, the cubic complex Ginzburg-Landau equation. This model allows us to reveal the bifurcation diagram of the prototype model and understand the mechanism that gives rise to the complexity. We briefly explore the two-dimensional dynamics of our prototype model and propose generalizations using interaction kernels. We compare numerical simulations with experimental observations in the liquid crystal light valve. Finally, we propose a modification to the experiment that explores the effects of other long-ranged interactions in pattern-forming systems.

In Chapter 6, we explore and briefly characterize the phenomenology of a different pattern-forming model with an asymmetrical and non-local coupling far from its convective instability, the longitudinal Lugiato-Lefever equation with Raman interaction.

Agradecimientos

El año 2020 es probablemente uno de los años más irregular y caótico de muchos quienes están leyendo esta parte de mi tesis. Ahora bien, tanto la cuarentena y la incertidumbre que se vive han sido una fracción de las dificultades que me ha tocado enfrentar en todo el camino que he recorrido para ir convirtiéndome en un científico. He tenido la fortuna de siempre haber estado acompañado y haberme sentido querido en cada una de estas dificultades, es por esto que me gustaría expresar unas palabras a quienes estuvieron presente en este recorrido:

A mis los miembros de mi familia: Mis padres Gladys y Adolfo, mis hermanos Nicolás., Camilo, Gabriel y Adrián, y mis tíos Marianela y Polo. Quienes han estado conmigo de forma incondicional a lo largo de toda mi vida.

Al profesor Marcel Clerc, por haber sido un excelente guía y un verdadero maestro. Muchas gracias por su constante preocupación y por haberme ayudado a desarrollar una buena disciplina de trabajo. Asimismo, quiero agradecer a Saliya Coulibaly por haberme recibido en Lille y por su constante preocupación durante mi estadía allá. Muchas gracias por tu paciencia a la hora ayudarme con los cálculos más difíciles de esta tesis.

A mis amigos y compañeros del LAFER: Cami, Vale, Gregorio, Gladys, Seba, David, Karin, Michel, Ale, Robert, Martín y Pedro. Muchas gracias a todos por las discusiones científicas, las sobremesas extendidas y todas las buenas experiencias en nuestro subterráneo.

A mis amigos del plan común (también denominados la geobancada unión el Mati) Lore, Kim, Alonso, Mati y Ale. Muchas gracias por todo el apañe, anécdotas, conos robados, por ponerme en diagonal y todos los buenos momentos que hemos vivido los últimos 7 años.

A mis amigos y futuros colegas de la Salita: Archi, Miguel, Cris, Coté, Sca, Tere, Magda, Gerd, Almendra, Chesta, Eli, Rojo, Erick y Aaron. Desde los Carcas, las sobremesas en las banquitas, y las conversaciones profundas (tanto las científicas y las que no, y tanto aquellas que se justificaban y las que no iban a ninguna parte).

A Josefina, por tu amor, compañía y apoyo con el que he contado este último año, me siento muy afortunado de haberte conocido.

A Ignacio Vergara, por todos los encuentros y desencuentros que tuvimos en los años que vivimos y compartimos juntos.

À Marie et Olivier pour avoir fait de le confinement en Willems une belle expérience.

Contents

List of Figures

Introduction

Macroscopic systems under constant injection and dissipation of energy may lead to the formation of dissipative structures [60]. Examples of these structures are fronts, solitons, and patterns [63]. This dissertation is concerned about patterns, which consist of spatially periodic behaviors. They can be found in different contexts in nature, such as the formation of sand ripples, chemical reactions, vegetation self-organization; the emergence of convection rolls in Rayleigh-Benard cells; and development of hexagon and stripes in nematic liquid crystal cells [63, 60, 26, 28, 67, 7, 56, 72], to mention a few. The emergence of these behaviors can be mathematically described in an universal manner by amplitude equations that do not depend on the internal physics of each one of these systems [42, 32]. This feature reflects the universality and robustness of pattern formation.

A nematic liquid crystal cell with optical feedback can be used to study pattern-formation[72]. An external electric field is used to align the liquid crystal molecules in a particular direction. On the other hand, the molecules have a property called birefringence [13], which means they have two different refraction indexes. A polarized light beam traversing a section of the liquid crystal cell will become circularly polarized depending on the local orientation of the molecules. Optical feedback is used to spatially modulate the external electric field according to the local orientation of the molecules. This experiment is called the liquid crystal light valve with optical feedback [3], which exhibits a wide variety of robust phenomena, including stripped and hexagonal patterns [72]. A common difficulty faced in experiments with optical feedback is the alignment. The transition between hexagonal and square patterns has been reported as a consequence of imperfect alignment [1, 69]. It has also been shown that it can induce localized structures emitting vortices resembling a von Karman street [30]. Preliminary experimental observations in the liquid crystal light valve experiment located at the Laboratio de fenómenos robustos en óptica show that an intentional misalignment can also trigger a transition from the stationary striped pattern into traveling, spatiotemporal intermittency and defect turbulence of stripped waves. A full theoretical characterization of the emergence of this complexity has not been done.

A misalignment can be modeled by translational coupling [17, 30]. A spatially extended system is said to have a translational coupling when the local evolution of the physical quantities under study depend on their values locally, and at a given distance. A translational coupling is a particular case of long-ranged and asymmetric interaction. These interactions are not modeled merely by differential terms in the equations that govern the evolution, but rather by integrodifferential terms . This kind of modeling can be found naturally in ecological communities, population dynamics, and optical fibers [33, 56, 22]. Understanding

the effects of a translational coupling we will shed light on the consequences of having more complicated asymmetric couplings.

0.1 Objectives

The main objective of this thesis is to characterize the transition from a steady pattern into complex spatiotemporal dynamics in a pattern forming system with translational coupling. The specific objectives of this dissertation are listed below

- Stablish a minimal Swift-Hohenberg type model with translational coupling.
- Conduct numerical simulations to explore and characterize the dynamical states of this model.
- Derive an amplitude equation that accounts for the observed transitions.
- Reveal the bifurcation diagram of the one-dimensional Swift-Hohenebrg equation with translational coupling.
- Relate the phenomenology of the prototype model with the observed phenomena in the liquid crystal light valve.
- Derive a Swift-Hohenberg equation with translational coupling in some limit of the Liquid crystal light valve experiment.
- Explore the effects of other asymmetric non-local couplings in pattern-forming systems.

Chapter 1

Preliminary concepts

1.1 Bifurcations

A bifurcation is a qualitative change of the solutions of a dynamical system when the parameters on which the system depends on are smoothly modified. These changes can either be: the emergence or destruction of fixed points, periodic orbits, or other invariant sets, such as strange attractors [83], in the phase portrait of the dynamical system; or a change in the stability of any of these structures, likewise, a bifurcation corresponds to a qualitative change in the phase portrait [65]. For illustrative purposes, let us consider the following dynamical system.

$$\partial_t x = \mu x - x^3, \tag{1.1}$$

This example is referred as the Pitchfork bifurcation. When $\mu < 0$, the system only has one equilibrium $x = 0$, which is an attractor of the system. However, when $\mu > 0$, the equilibrium $x = 0$ losses stability and two symmetric stable equilibria emerges $x = \pm\sqrt{\mu}$. A way to visualize this is through a **bifurcation diagram**, which is a plot of the equilibria of the system as a function of the parameters, in this case, μ (see figure 1.1).

1.2 Normal forms

A fixed point in a dynamical system is linearly stable if all the eigenvalues of the Jacobian of the system evaluated at the fixed point have a negative real part. If the real part of one or more of these eigenvalues becomes positive while modifying the parameters of the system, the fixed point turns unstable. A critical situation happens when the real part of at least one eigenvalue becomes zeros while remaining negative for the other eigenvalues. The center manifold theorem states the existence of a center manifold close to the fixed point and tangent to the eigenvector associated with the critical eigenvalue [42]. This manifold is invariant, which means that trajectories starting from the manifold remain contained in it. Since all other directions around the fixed point are attractive, the system dynamics eventually converges into the dynamics of the center manifold, thus the center manifold is attractive. It is possible to parametrize a trajectory inside this manifold with a scalar amplitude. The equation that governs the evolution of this amplitude is known as a normal

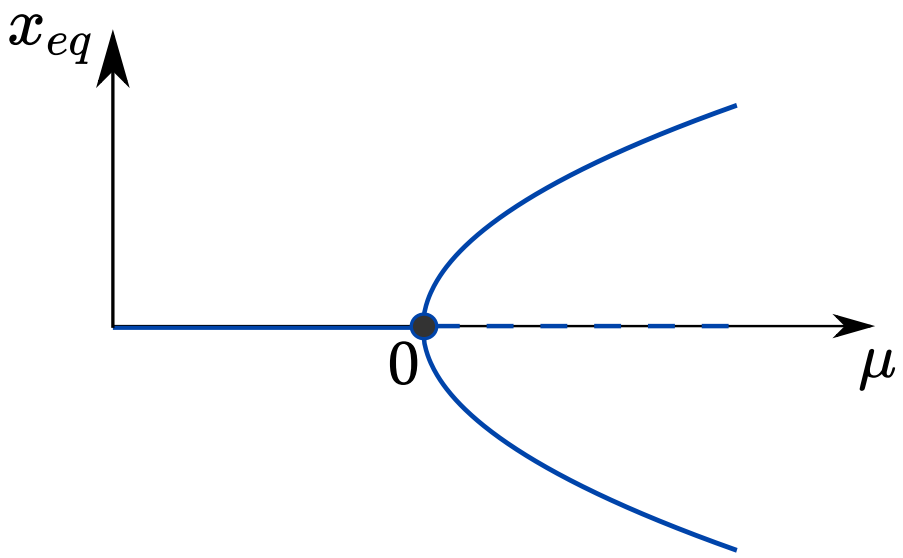

Figure 1.1: Pitchfork bifurcation. Two stable equilibria emegeres at $\mu = 0$ (solid blue line), the solution $x_{eq} = 0$ looses stability at this point (dashed blue line)

form [32]. If there is more than one critical mode, the center manifold has a greater dimension, and then more scalar amplitudes are needed. Having the exact parameters for the system to have a critical mode is not generic; it is only possible to be close to the critical situation in practice. Singular perturbation theory introduces corrections to the normal forms when the parameters are slightly shifted from the critical case [42, 32]. The corrected normal form can always be expanded in powers of the amplitude if one assumes that the dynamics of the system happens close to the fixed point that loses stability. This allows us to capture generic bifurcations, such as equation (1.1), in different physical contexts, since the dynamics are reduced to a scalar amplitude, which is not a physical quantity but is related to real physical quantities by a change of variables. To illustrate how a normal form is obtained, let us consider the following example

$$\partial_t x = \varepsilon x - (x^2 + y^2)x, \tag{1.2a}$$
$$\partial_t y = y - (x^2 + y^2)y. \tag{1.2b}$$

The system has fixed point at $(x, y) = (0, 0)$, the Jacobian $\mathcal{L}$ evaluated at the fixed point reads

$$\mathcal{L} = \begin{pmatrix} \varepsilon & 0 \\ 0 & -1 \end{pmatrix}, \tag{1.3}$$

whose eigenvalues are $\lambda_1 = \varepsilon$ and $\lambda_2 = -1$. When $\varepsilon = 0$, the system is critically unstable, namely, the systems presents an instability. The eigenvector asociated with the critical eigenvalue is

$$\vec{v} = \begin{pmatrix} 1 \\ 0 \end{pmatrix}. \tag{1.4}$$

Assuming $\varepsilon = 0$, we introduce the following Ansatz, which reduces the system to the center manifold (see figure 1.2)

$$\begin{pmatrix} x \\ y \end{pmatrix} = u\vec{v} + \vec{W}(u), \tag{1.5}$$

where $\vec{W}(u)$ is a correction that depends on higher powers of u. We also suppose

$$\partial_t u = a_3 u^3 + a_5 u^5 + ... \tag{1.6}$$

Replacing the Ansatz in the original equation , up to order 3 in powers of u, we get

$$a_3 u^3 \vec{v} = u^3 \vec{v} + \mathcal{L}\vec{W}(u), \tag{1.7}$$

Rearranging terms we get

$$\mathcal{L}\vec{W}(u) = (a_3 + 1)u^3 \vec{v}, \tag{1.8}$$

For the equation (1.8) to have a solution, we must impose the Fredholm alternative [37]. According to this theorem, a linear system of the form

$$\mathcal{L}\vec{X} = \vec{b}, \tag{1.9}$$

has a solution only if $\vec{b} \notin \text{Ker}(\mathcal{L}^\dagger) \iff \vec{b} \cdot \vec{a} = 0 \quad \forall \vec{a} \in \text{Ker}(\mathcal{L}^\dagger)$. It is necesary then to define a proper inner product. For equation (1.8), we choose the euclidean inner product. Since $\mathcal{L} = \mathcal{L}^\dagger$, and $\mathcal{L}\vec{v} = 0$, we must have

$$a_3 = -1, \tag{1.10}$$

from where we conclude

$$\partial_t u^{[3]} = -u^3, \tag{1.11}$$

which implies

$$\vec{W}(u) = 0, \tag{1.12}$$

Now we assume $\varepsilon \ll 1$. Then we have to introduce the following perturbations to our solutions

$$\vec{W}(u) = \varepsilon \vec{W}_\varepsilon(u), \tag{1.13a}$$
$$\partial_t u = -u^3 + \varepsilon f_\varepsilon(u), \tag{1.13b}$$

Replacing the Ansatz in the original system we now obtain

$$\mathcal{L}\vec{W}_\varepsilon(u) = (f_\varepsilon - \varepsilon u)\vec{v}, \tag{1.14}$$

imposing the Fredholm alternative we get

$$f_\varepsilon = \varepsilon u, \tag{1.15}$$

from where we conclude in the normal form

$$\partial_t u = \varepsilon u - u^3. \tag{1.16}$$

To study other examples of normal forms, see textbook [42].

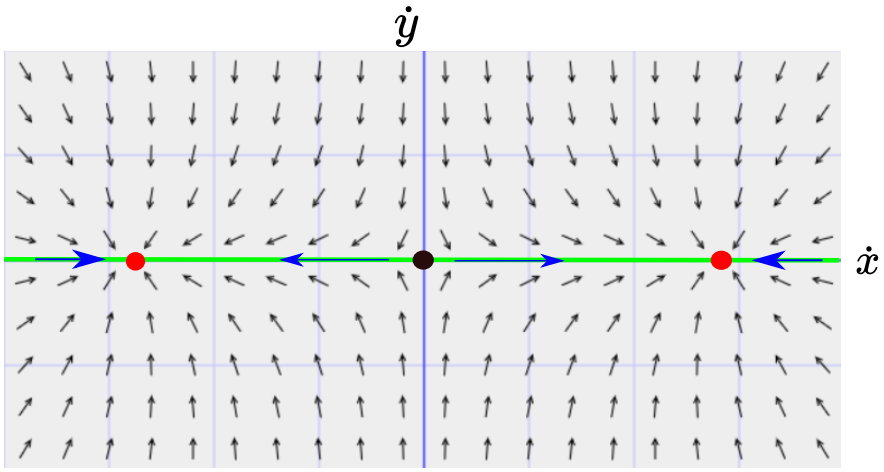

Figure 1.2: Phase portrait of equations (1.2). The red dots correspond to the new equilibria emerging when ε becomes positive. The black dot is the unstable equilibrium. The green solid corresponds to the center manifold of the unperturbed system, in this particular example it coincides with the critical eigenspace.

1.3 Chaos

1.3.1 Lyapunov exponents

A system is said to be chaotic when it exhibits exponential sensibility to initial conditions. This means that when one considers tow arbitrary close initial conditions, the distance between the trajectories evolving from these points diverges exponentially according to a characteristic time scale known as the Lyapunov time [62]. The inverse of this time scale is called the largest Lyapunov exponent [62]. A rigorous definition of this number is the following, let two initial conditions separated by a distance $|\delta\vec{X}_0|$and let $|\delta\vec{X}_0(t)|$ be the evolution of this distance, the largest Lyapunov exponent is given by

$$\lambda = \lim_{t\to\infty} \lim_{\delta\vec{X}_0\to 0} \frac{1}{t} ln \left(\frac{|\delta\vec{X}(t)|}{|\delta\vec{X}_0|} \right), \tag{1.17}$$

these limits do not commute. If the system is not chaotic, then $\lambda \leq 0$. When one introduces a perturbation into a trajectory, the perturbation may expand, contract, or remain unchanged in each direction. If the perturbation is small, its evolution is governed by the equations of the system linearized around the trajectory. Thus, the perturbation evolution is led by an exponential growth characterized by a set of N exponents, where N is the number of degrees of freedom the system has. One can label each one of these exponents by a number i $\in [0, N]$ and order them in a decreasing manner. If this process is repeated many times while averaging every new set of exponents with all the previous ones, the average converges into a set of N numbers. The whole set is referred to as the characteristic Lyapunov exponents [62]. The greatest of this number coincides with the largest Lyapunov exponent defined at (1.17). An algorithm to compute these exponents is presented in the work of Skokos [81]. Any trajectory that does not converge into a single point has at least one exponent equal to 0, associated with perturbations along the trajectory. Consequently, the greatest Lyapunov exponent for stable periodic and quasiperiodic orbits is always 0, which allows us to distinguish between quasiperiodic behaviors that may appear complicated, with generally chaotic dynamics.

Trajectories in a chaotic dissipative system typically converge into an invariant set of points called a strange attractor. These sets are not curves nor surfaces but rather structures of fractal dimension. The Yorke-Kaplan conjecture [46] states that the dimension of a strange attractor is related to the Lyapunov exponents in the following way

$$D_{YK} = j + \frac{\sum_{\mathrm{i}=0}^{j} \lambda_{\mathrm{i}}}{|\lambda_{j+1}|}, \tag{1.18}$$

where j is the maximum integer so that $\sum_{\mathrm{i}=0}^{j} \lambda_{\mathrm{i}} > 0$. Many positive Lyapunov exponents combined with many negative exponents close to 0 result in a greater Yorke-Kaplan dimension; this can be interpreted as many unstable directions with many directions that barely stable. This accounts for a sort of hyperbolic structure. Thus, we can use the Yorke-Kaplan dimension to measure the complexity of the system, and then we can say a system is more complex than others in an objective way.

1.3.2 Spatiotemproal chaos

Spatially extended systems have infinite degrees of freedom, which results in an infinite number of Lyapunov exponent since there is one exponent for each spatial coordinate. There are two possible manifestations of chaos: Low dimensional chaos and spatiotemporal chaos [59]. The difference between these behaviors is how they behave when the size of the system is increased. It is useful to plot the normalized labels $\{\mathrm{i}/N\}$ vs. the set of characteristic Lyapunov exponents $\{\lambda_{\mathrm{i}}\}$, namely, the Lyapunov Spectrum, to distinguish between these two behaviors. If the set of positive Lyapunov exponents always remains discrete, independent of the system's size, we are facing low dimensional chaos; a consequence of this is that in the limit of infinite size, the dynamics converge into a strange attractor of finite dimension. On the other hand, if the set of positive Lyapunov exponents converges into a continuum in the limit when the size of the system approaches into infinity, we are facing spatiotemporal chaos, this means that the dimension of the strange attractor escalates with the size of the system and eventually becomes infinite [74]. In this thesis, we exclusively refer to chaotic spatiotemporal behaviors.

1.4 Turbulence

The turbulence concept was initially introduced in fluid dynamics, where a flow is said to be turbulent when it is highly irregular, chaotic and have and usually large structures, namely vortices, that split into smaller ones (see figure 1.3-a-b). This kind of flow arises as a consequence of high energy injection compared with the fluid's viscosity. Nevertheless, turbulence is not restricted only to flows and should be regarded as sort of spatiotemporal chaos in other contexts in physics. In this thesis, we are concerned with the emergence of turbulent-like behaviors in pattern-forming systems. Due to its chaotic nature, a statistical approach has been mainly used in the characterization of turbulence. Some shared features among in usual turbulent systems are [39, 92, 53]

- The energy is injected into the system in the large scales; this means the energy injected is restricted to the Fourier modes of long-wavelength ($\lambda > l_1$). A pressure difference in a pipe is and the sun irradiating the surface of a planet are examples of this kind of energy injection.

- Dissipation of energy only happens on the short scales of the systems; these means that small wavelength modes are damped ($\lambda < l_2$). Microscopic collisions are an example of this mechanism.
- There is an inertial scale between the injection and dissipation scales ($l_2 < \lambda < l_1$) where energy flows from higher scales into lower scales. For example, in a fluid, big vortices are created in the injection scales; these vortices split into smaller ones, which eventually split into new ones successively upon reaching the dissipation scale. A way of characterizing this energy cascade is trough the power energy distribution $S(k)$; this physical quantity is the square modulus of the Fourier transform of the variable under study; it measures the amount of energy in each mode averaged over time. An energy cascade looks like a power law in the inertial range ($\frac{2\pi}{l_1} < k < \frac{2\pi}{l_2}$) of the power density spectrum (see figure 1.3-c).

The above features describe the well known normal cascade. However, there exist other turbulent behaviors characterized by an inverted cascade, where the injection is in the small scales [39, 57].

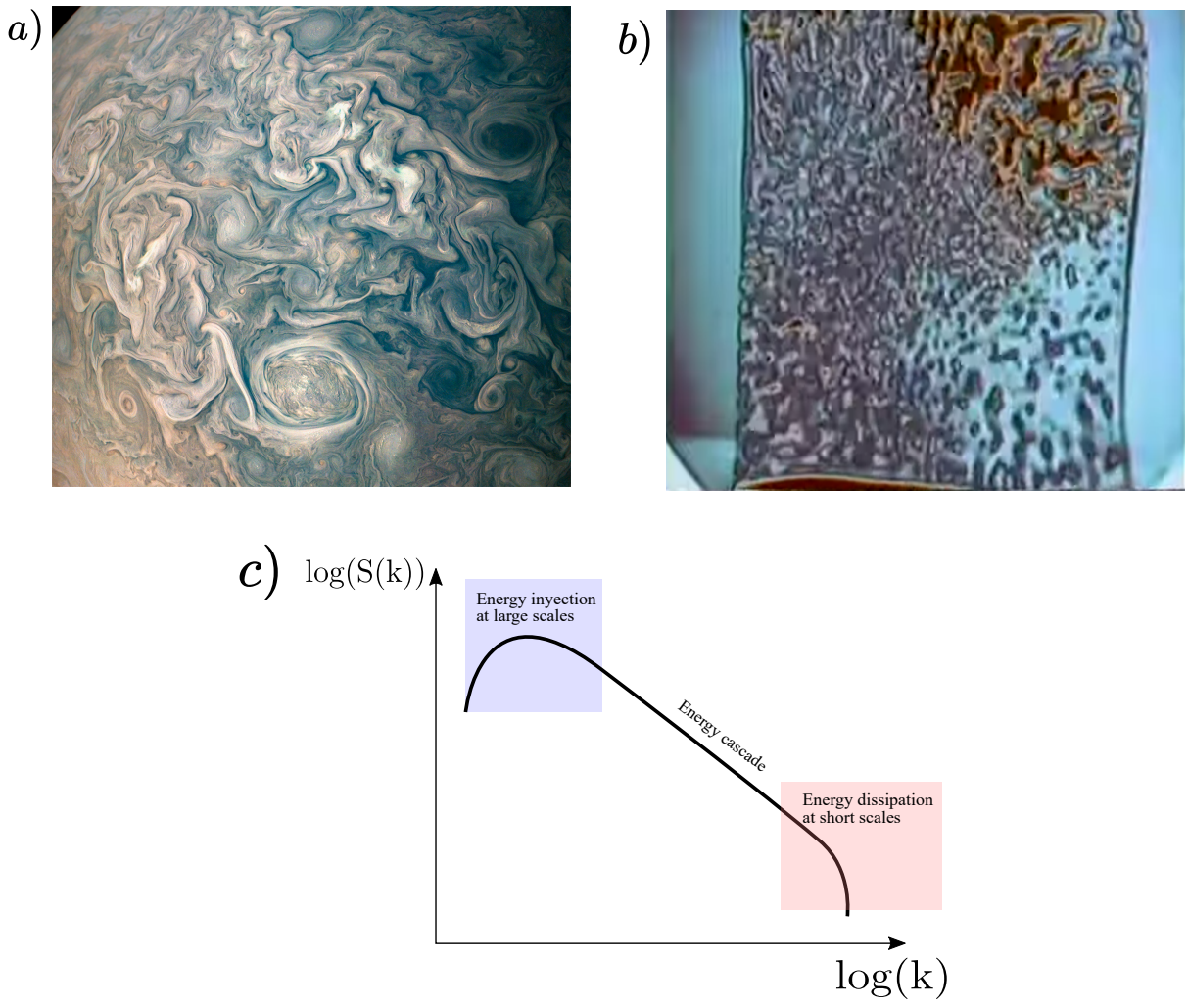

Figure 1.3: Examples of turbulence a) Motions of gas in the surface of Jupiter b) Turbulent dynamics in the a video feedback experiment [29] c) Pictorical image of a energy cascade.

Chapter 2

Pattern formation

Patterns consist of spatially periodic behaviors. They can be found in several contexts in nature, such as Faraday waves, the Taylor-Coutte instability, ripples in the sand, thermal convection rolls, chemical reactions, distribution of biomass in ecological communities, animal fur, and nematic liquid crystal cells, to mention a few [35, 85, 63, 60, 26, 28, 67, 7, 56, 72] (see figure 2.1). A pattern forming mechanism that gives rise to patterns of a specific wavelength was introduced by Alan Turing while shedding light on the origin of morphogenesis [86]. In his article, he proposed that during a chemical reaction, the law of mass action is locally satisfied when the system is divided into cells. The substances involved in the process can flow between adjacent cells. According to Fick's law, this can be modeled as a diffusion when the cells are sufficiently small [25]. A model taking into account the law of mass action and the transport phenomena is known as a reaction-diffusion system, which reads

$$\partial_t \vec{X} = \mathcal{D}\nabla^2 \vec{X} + F(\vec{X}), \tag{2.1}$$

components of $\vec{X}$ are regarded as the local concentrations of the differetn substances involved in a chemical reaction, $\vec{F}(\vec{X})$ is the local production rate of each of these substances, and $\mathcal{D}$ is the diffusivity matrix. Turing showed that under a specific choice of parameters, a fixed point of 2.1 becomes unstable to perturbations of specific wavenumbers. This phenomenon is referred to as a Turing instability. Reaction-diffusion systems have also been proposed in other contexts, such as population dynamics and propagation of genes [36, 47, 44]. Later on, Swift and Honenberg derived a scalar equation exhibiting a Turing instability while studying the appearance of convection rolls in the Rayleigh-Bénard experiment[84, 71, 10]. This equation is known as the Swift-Hohenberg equation, which is the simplest model exhibiting a pattern forming instability. Even more, this equation can be derived as a normal form in some reaction-diffusion systems. The beginning of this chapter is dedicated to discussing the Turing mechanism of pattern formation. In the second part, we talk about the Swift-Hohenberg equation and expose its known behaviors.

2.1 Turing instabilities

Fixed points in dynamical systems can become unstable to spatially modulated perturbations of a specific wavelength when the parameters reach a critical threshold. Let us consider a

Figure 2.1: Patterns in different contexts in nature

dynamical system described by the order parameter $\vec{X}(\vec{r},t)$ having a fixed homogeneous solution $\vec{X}_0$

$$\partial_t \vec{X} = \vec{G}(\vec{X}), \tag{2.2}$$

$$\vec{G}(\vec{X}_0) = 0. \tag{2.3}$$

Let us lineraize 2.2 around $\vec{X}_0$

$$\vec{X} = \vec{X}_0 + \delta\vec{X}, \tag{2.4}$$

$$\partial_t \delta\vec{X} = \mathcal{L}\delta\vec{X}, \tag{2.5}$$

where $\mathcal{L}$ is the Jacobian of the system evaluated at the fixed point. We introduce a representation of the perturbation $\delta\vec{X}$ in a Fourier basis

$$\delta\vec{X} = \sum_{\vec{q}} \vec{X}_{\vec{q}} \mathrm{e}^{\mathrm{i}\vec{q}\cdot\vec{r}+\lambda_{\vec{q}}t}, \tag{2.6}$$

where $\lambda_{\vec{q}}$ is the growth rate of a given Fourier mode. Replacing this representation in equation (2.5) we get an equation for each mode

$$\lambda_{\vec{q}}\vec{X}_{\vec{q}} = \mathcal{L}_{\vec{q}}\vec{X}_{\vec{q}}, \tag{2.7}$$

$$\Rightarrow (\mathcal{L}_{\vec{q}} - \lambda_{\vec{q}}\mathbb{I})\vec{X}_{\vec{q}} = 0, \tag{2.8}$$

with $\mathcal{L}_{\vec{q}}$ being the action of the Jacobian on a Fourier mode. Equation (2.8) is an eigenvalue problem. An expression for $\lambda_{\vec{q}}$ in terms of $\vec{q}$, namely the dispersion relation, can not always be computed analytically but can be determined numerically. The **real** part $\lambda_{\vec{q}}$ is the growth rate of each mode. If $\mathrm{Re}\{\lambda_{\vec{q}}\}$ has a a maximum at $\vec{q}_c \neq 0$ and $\mathrm{Re}\{\lambda_{\vec{q}_c}\} = 0$ (see figure 2.2),

the system is said to have a spatial instability and q_c is referred as a Turing mode, which is determined by solving the following system of equations

$$\mathrm{Re}\{\lambda_{\vec{q}_c}\} = 0, \tag{2.9a}$$
$$\nabla_{\vec{q}}\mathrm{Re}\{\lambda_{\vec{q}_c}\} = 0, \tag{2.9b}$$

When this happens, a pattern of wave number $\vec{q}_c$ emerges. It is important to consider the imaginary part of the dispersion relation at the critical mode

$$\Omega = \mathrm{Im}\{\lambda_{\vec{q}_c}\}. \tag{2.10}$$

When $\Omega = 0$, the pattern is referred as stationary. In the other hand, if $\Omega(q) \neq 0$, the instability gives rise to a traveling wave. If $\Omega(q)$ is even function, the system exhibits an stationary wave, and if it an odd function, the system evolves into a single traveling wave moving in a particular direction, in this case the instability is said to be convective [15]. A

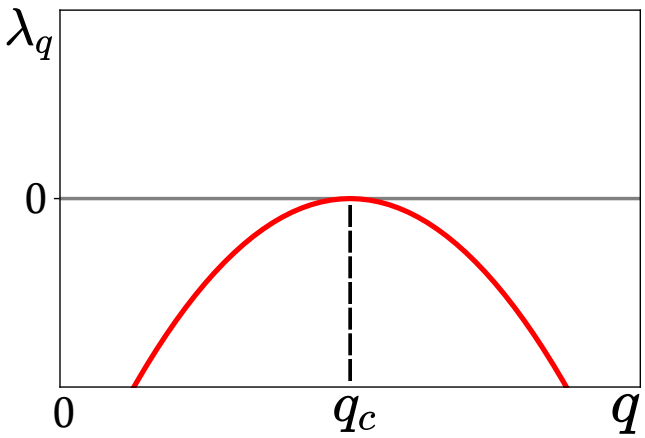

Figure 2.2: Dispersion relation of dynamical system having a Turing mode at $q_c \neq 0$

system may have several Turing modes. The interaction of this modes is what gives origin to more complex structures other than stripes such as hexagons and squares [26]. Normal forms can be used to derive coupled amplitude equations describing the evolution and interaction of these modes [63]. To further illustrate this mechanism, let us consider a reaction-diffusion system having two coupled scalar fields $\vec{X} = (U(\vec{r},t), V(\vec{r},t))$, and let $(U,V) = (0,0)$ be a fixed point of the system

$$\partial_t \begin{pmatrix} U \\ V \end{pmatrix} = \begin{pmatrix} D_1\nabla^2 & 0 \\ 0 & D_1\nabla^2 \end{pmatrix} \begin{pmatrix} U \\ V \end{pmatrix} + \begin{pmatrix} f(U,V) \\ g(U,V) \end{pmatrix}. \tag{2.11}$$

The linearized equation reads

$$\partial_t \begin{pmatrix} U \\ V \end{pmatrix} = \begin{pmatrix} f_U + D_1\nabla^2 & f_V \\ g_U & g_V + D_1\nabla^2 \end{pmatrix} \begin{pmatrix} U \\ V \end{pmatrix}, \tag{2.12}$$

$$\mathcal{L}_{\vec{F}} = \begin{pmatrix} f_U & f_V \\ g_U & g_V \end{pmatrix}. \tag{2.13}$$

Where $\mathcal{L}_{\vec{F}}$ is the Jacobian of the production rate defined in (2.1). If we introduce the Fourier representation of (U, V), the Jacobian of the whole system reads

$$\mathcal{L}_{\vec{q}} = \begin{pmatrix} f_U - D_1 q^2 & f_V \\ g_U & g_V - D_2 q^2 \end{pmatrix}. \tag{2.14}$$

They eigenvalues of this matrix are given by

$$\lambda_{\vec{q}} = \frac{\mathbf{tr}(\mathcal{L}_{\vec{q}}) \pm \sqrt{\mathbf{tr}(\mathcal{L}_{\vec{q}})^2 - 4\mathbf{det}(\mathcal{L}_{\vec{q}})}}{2}, \tag{2.15}$$

having

$$\mathbf{det}(\mathcal{L}_{\vec{q}}) = D_1 D_2 q^4 - (D_1 g_v + D_2 f_u) q^2 + (f_u g_v - f_v g_u), \tag{2.16}$$

$$\mathbf{tr}(\mathcal{L}_{\vec{q}}) = f_u + g_v - (D_1 + D_2) q^2, \tag{2.17}$$

The eigenvalue having the most prominent real part is the one with the + sign. Expanding (2.15) around $q = 0$ one obtains

$$\lambda_{\vec{q}} = C_0 + C_2 q^2 - C_4 q^4 + O(q^6), \tag{2.18}$$

where the coefficients C_0, C_2, C_4 depend on the parameters of the system. For demonstrative purposes, let us assume that all these coefficients are real. A necessary condition for the system to have a Turing instability is that $C_1 > 0$ and $C_2 < 0$. The coefficient C_0 can be adjusted to reach the onset of instability.

2.2 The Swift-Hohenberg model

2.2.1 General remarks

A model having a Turing instability relaying on a single scalar order parameter is the Swift-Hohenberg equation, which reads

$$\partial_t = \varepsilon u - u^3 - \nu \nabla^2 u - \nabla^4 u \tag{2.19}$$

As stated at the beginning of this chapter, this equation was derived close to instability in fluid dynamics while describing the emergence of rolls in the Rayleigh-Benard experiment [84]. In the other hand, if one considers a reaction-diffusion model like the equation (2.11) choosing the parameters so that $C_0 = C_2 = 0$ in equation (2.18), then the system has a critical mode at $q = 0$. When introducing a perturbation into the parameters of the system and applying a normal form analysis to find an equation that describes the evolution of the amplitude of the critical mode, the Swift-Hohenberg equation can be derived (see reference [63] for further details of the derivation). This can be done to any system that haves a dispersion relation like 2.18, which reflects the universality of this model.

An important feature of the Swift-Hohenberg equation is its variational nature, we can define the following free energy

$$\mathcal{F} = \int \left(-\varepsilon \frac{u^2}{2} + u^4 - \nu \frac{(\nabla u)^2}{2} + \frac{(\nabla^2 u)^2}{2} \right) \mathrm{d}V, \tag{2.20}$$

so

$$\partial_t u = -\frac{\delta \mathcal{F}}{\delta u}, \tag{2.21}$$

$$\rightarrow \frac{\mathrm{d}\mathcal{F}}{\mathrm{d}t} = -(\partial_t u)^2. \tag{2.22}$$

This implies that the Swift-Hohenberg equation will evolve until reaching a stationary state. Thus, this equation can not exhibit chaotic spatiotemporal dynamics.

Now we characterize the Turing bifurcation this equation presents. A trivial solution to the Swift-Hohenberg equation is $u(\vec{r}, t) = 0$, we introduce a perturbation δu and express it in the Fourier basis like expression (2.6). The dispersion relation reads

$$\lambda_q = \varepsilon + \nu q^2 - q^4. \tag{2.23}$$

For a fixed ν, the system has a Turing instability at ε_c. The critical mode $\vec{q}_c$ satisfies equations 2.9a, and 2.9b

$$0 = \varepsilon + \nu q_c^2 - q_c^4, \tag{2.24}$$

$$0 = 2\nu q_c - 4q_c^3, \tag{2.25}$$

This allows to solve for ε_c and a expression for q_c^2

$$\varepsilon_c = -\frac{\nu}{4} \tag{2.26}$$

$$q_c^2 = \frac{\nu}{2}. \tag{2.27}$$

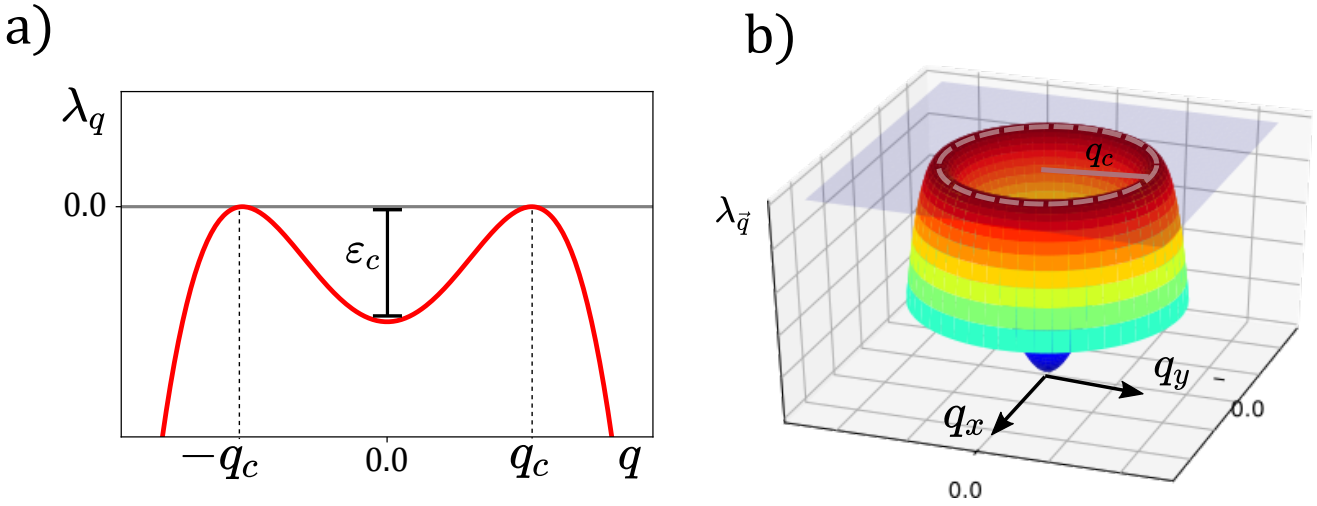

Figure 2.3: **a)** Dispersion relation of the one dimensional Swift-Hohenebrg equation, having only 2 critical modes **b)** Dispersion relation of the two dimensional Swift-Hohenberg equation having a continuum of Turing modes. The light blue plane corresponds $\lambda_{\vec{q}} = 0$. The critical modes correspond to those located at the brown dashed circle

For the one-dimensional Swift-Hohenberg equation, there only exist two critical modes, this is depicted in figure 2.3-a. However, for higher dimensions, there is a continuum of

critical modes which can be seen in figure 2.3-b, which allows the appearance of more complex structures other than stripes.

The Swift-Hohenberg equation describes the emergence of patterns close to the onset of bistability between two symmetric states. In realistic models, this symmetry is usually broken. While deriving the Swift-Hohenberg equation performing a normal form analysis, a term proportional u^2 can appear. Through a change of variables, this is equivalent to add a constant to the Swift-Hohenberg equation

$$\partial_t u = \eta + \varepsilon u - u^3 - \nu\nabla^2 - \nabla^4 u, \tag{2.28}$$

which is known as the generalized Swift-Hohenberg. The homogeneous solution is no longer $u = 0$. However, when deriving the dispersion relation for perturbations to this new solution, its structure looks the same as the case having $\eta = 0$, having 2 Turing modes in one dimension, and a continuum of critically unstable modes for higher dimensions, with the instability happening at another $\varepsilon_c = \varepsilon_c(\eta)$. In one dimension, this additive constant only shifts the point around where the pattern oscillates. Nevertheless, in two dimensions, this constant can account for the emergence of hexagonal patterns.

2.2.2 One dimensional dynamics

The one dimensional Swift-Hohenberg model equation reads

$$\partial_t = \varepsilon u - u^3 - \nu\partial_{yy} u - \partial_{yyyy} u. \tag{2.29}$$

We already know this equation has a Turing instability at $\varepsilon_c = -\frac{\nu}{4}$; beyond this point, striped patterns with wavenumber close to q_c can be found (see figure 2.4) In order to describe the

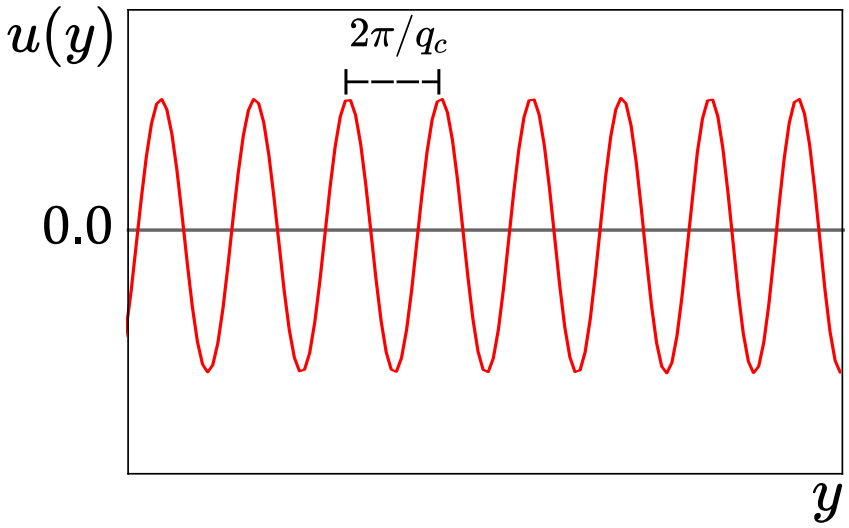

Figure 2.4: Striped pattern observed at $\varepsilon = -0.2, \nu = 1$, with von Neumman boundary conditions.

evolution of the pattern close to bifurcation, we set $\varepsilon = \varepsilon_c + \Delta\varepsilon$, we then propose the following Ansatz

$$u = A(y_1, t)\mathrm{e}^{\mathrm{i}q_c y} + \bar{A}(y_1, t)\mathrm{e}^{-\mathrm{i}q_c y} + W(A, \bar{A}). \tag{2.30}$$

We assume that the amplitude A of the patterns depend on rescalated spatial variable $y_1 = \mu y$, with $\mu \ll 1$ a dummy scaling parameter for the envelope of the pattern. We also need introduce the following inner product between functions

$$f \cdot g = \frac{q_c}{2\pi} \int_{y_0}^{y_0 + \frac{2\pi}{q_c}} \bar{f}(y') g(y') \mathrm{d}y', \tag{2.31}$$

for some arbitrary y_0. In particular we have

$$\mathrm{e}^{\mathrm{i}nq_c y} \cdot \mathrm{e}^{\mathrm{i}mq_c y} = \delta_n^m \quad \text{for} \quad n, m \in \mathbb{Z} \tag{2.32}$$

Introducing the Ansatz into equation (2.29) and keeping up to lowest order in μ we get

$$\begin{aligned} \partial_t A \mathrm{e}^{\mathrm{i}q_c y} + c.c. = \Delta\varepsilon A \mathrm{e}^{\mathrm{i}q_c y_2} + \cancelto{0}{(\varepsilon_c + \nu q_c^2 - q_c^4)} A \mathrm{e}^{\mathrm{i}q_c y} - \mathrm{i}\mu \cancelto{0}{(2\nu q_c - 4q_c^3)} \partial_{y_1} A \mathrm{e}^{\mathrm{i}q_c y} \\ + \mu^2 (6q_c^2 - \nu) \partial_{y_1 y_1} A \mathrm{e}^{\mathrm{i}q_c y} - 3|A|^2 A \mathrm{e}^{\mathrm{i}q_c y} - A^3 \mathrm{e}^{3\mathrm{i}q_c y} + \mathcal{L}W. \end{aligned} \tag{2.33}$$

Where we the linear operator $\mathcal{L}$ is given by

$$\mathcal{L} = \varepsilon - \nu \partial_{yy} - \partial_{yyyy}, \tag{2.34}$$

this linear operator is self-adjoint, so $\mathrm{e}^{\mathrm{i}q_c y_2}$ and $\mathrm{e}^{-\mathrm{i}q_c y_2}$ belong to the Kernel of $\mathcal{L}^\dagger$. Rearranging terms of 2.33 we get

$$\mathcal{L}W(A, \bar{A}) = (-\partial_t A + \Delta\varepsilon A - 3|A|^2 A + 4q_c^2 \partial_{yy} A) \mathrm{e}^{\mathrm{i}q_c y} - A^3 \mathrm{e}^{3\mathrm{i}q_c y} + c.c. \tag{2.35}$$

Applying the solvability condition, we finally get the real Ginzburg-Landau equation [50]

$$\partial_t A = \Delta\varepsilon A - 3|A|^2 A + 4q_c^2 \partial_{yy} A. \tag{2.36}$$

For all these terms to be of the same order, we require that $A \sim \mu \sim (\Delta\varepsilon)^{\frac{1}{2}}$. Thus we expect that beyond ε_c the emergence of patterns supercritically whose amplitude is proportional to $\sqrt{\Delta\varepsilon}$.

2.2.3 Two dimensional dynamics

Since there is a continuum of Turing modes, we expect that the system to have them all interacting. To briefly discuss this, we introduce a new space independent Ansatz to equation 2.19

$$u = \sum_{\vec{q_\mathrm{i}}} A_\mathrm{i}(t) \mathrm{e}^{\mathrm{i}\vec{q_\mathrm{i}} \cdot \vec{r}} + \bar{A}(t) \mathrm{e}^{-\mathrm{i}\vec{q_\mathrm{i}} \cdot \vec{r}} \tag{2.37}$$

where $\vec{q_\mathrm{i}}$ is a different Turing mode. We expect that each amplitude equation looks like

$$\partial_t A_\mathrm{i} = \Delta\varepsilon A_\mathrm{i} - 3A_\mathrm{i}|A_\mathrm{i}|^2 - 6A_\mathrm{i} \sum_j |A_j|^2 \tag{2.38}$$

Solutions to these equations consist in only one dominant mode suppressing all others. We then expect that solutions of the Swift-Hohenberg equation, close to the Turing instability, consist of dominions having patterns of the same wavenumber but different directions, as depicted in figure 2.6. It is possible to derive an amplitude equation to describe the evolution

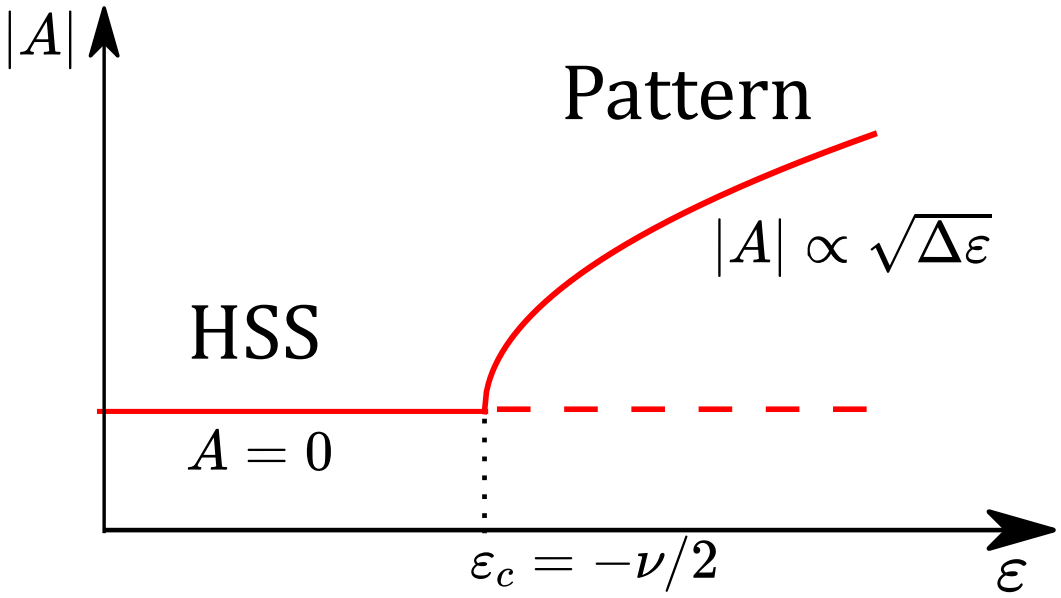

Figure 2.5: Bifrucation diagram of the one dimensional Swift-Hohenberg equation

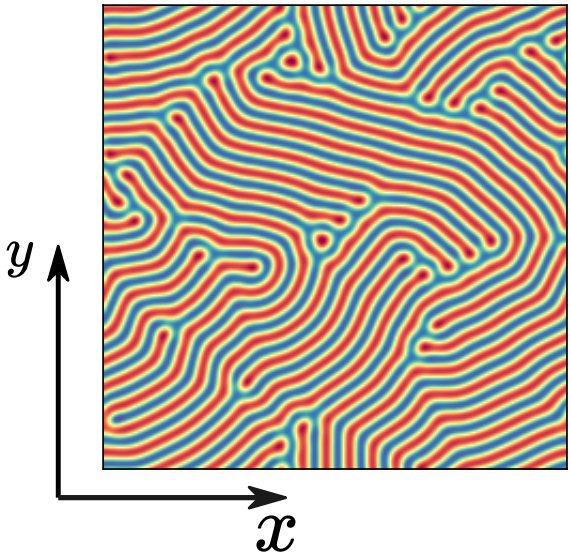

Figure 2.6: Several striped patterns coexisting at $\varepsilon = -.1, \nu = 2$

of each of these domains far from their boundaries. Unlike the one dimensional case, the evolution of the amplitude of a given critical mode is not described by a real Ginzburg-Landau equation but by the Newell-Whitehead-Segel equation [58]. Without loss of generality we choose a critical mode pointing in the y direction, recall that every direction is equivalent and propose the following Ansatz to equation 2.19

$$u = A(x_1, y_1, t)\mathrm{e}^{\mathrm{i}q_c y} + \bar{A}(x_1, y_1, t)\mathrm{e}^{\mathrm{i}q_c y} + W(A, \bar{A}). \tag{2.39}$$

Replacing this Ansatz on equation (2.19)

$$\begin{aligned}\mathcal{L}W(A,\bar{A}) = &\cancelto{0}{(\varepsilon+\nu q_c^2-q_c^4)}Ae^{iq_cy} - i\mu_2\cancelto{0}{(2\nu q_c-4q_c^3)}\partial_{y_1}Ae^{iq_cy} + \cancelto{0}{(2q_c^2-\nu)}(\mu_1^2\partial_{x_1x_1}+\mu_2^2\partial_{y_1y_1})Ae^{iq_cy}\\ &+\Delta\varepsilon Ae^{iqcy} + 4\mu_2^2q_c^2\partial_{y_1y_1}Ae^{iq_cy} - 2i\mu_2q_c\partial_{y_1}(\mu_1^2\partial_{x_1x_1}+\mu_2^2\partial_{y_1y_1})Ae^{iq_cy}\\ &-(\mu_1^4\partial_{x_1x_1x_1x_1}+2\mu_1^2\mu_2^2\partial_{x_1x_1y_1,y_1}+\mu_2^4\partial_{y_1y_1y_1y_1})Ae^{iq_cy} - \partial_tAe^{iq_cy}\\ &-3|A|^2Ae^{iq_cy} - A^3e^{3iq_cy} + c.c. \end{aligned} \tag{2.40}$$

Where we have supposed again that the amplitude A depends on re escalated spatial variables $x_1 = \mu_1 x$ and $y_1 = \mu_2 y$, where the scaling parameters are not necessarily of the same order. Keeping the terms of the lowest order in μ_1 and μ_2

$$\mathcal{L}W(A,\bar{A}) = \Delta\varepsilon A - 3|A|^2A + 4\mu_1^2q_c^2\partial_{y_1y_1}A + 2i\mu_1\mu_2^2q_c\partial_{y_1x_1x_1}A - \mu_2^4\partial_{x_1x_1x_1x_1}A. \tag{2.41}$$

We keep the term proportional to $\mu_1\mu_2^2$ because by demanding that all of the terms in the equation to be of same order we must have $\mu_2 \sim \mu_1^{\frac{1}{2}}$ and then $\mu_1\mu_2^2 \sim \mu_2^4 \sim \mu_1^2$. Applying the solvability condition and returning to the original coordinates we get [58]

$$\partial_tA = \Delta\varepsilon A - 3|A|^2A + 4q_c^2(\partial_{yy}A - i\frac{1}{q_c}\partial_{yxx}A - \frac{1}{4q_c^2}\partial_{xxxx}A). \tag{2.42}$$

comes from the fact that we broke the symmetry by choosing and arbitrary direction on the pattern under study. We showed the scale in the x direction is much shorter than the scale in the y, so stripes are more sensible to bending than to being compressed or extended. This phenomenon is not restricted to the Swift-Hohenberg equation, but general pattern forming systems with rotational symmetry. The effects of breaking this symmetry are discussed in chapter 5.

Let us now consider the generalized Swift-Hohenberg equation. Recall that the additive constant η is equivalent to have a term proportional to u^2 in the original Swift-Hoheneberg equation when applying a change of variables. If we have 3 Turing modes $\vec{q_1}, \vec{q_2}$ and $\vec{q_3}$ satisfying

$$\vec{q_1} + \vec{q_2} + \vec{q_3} = 0, \tag{2.43}$$

known as a resonance conditions, when introducing the Ansatz (2.37) into the Swift-Hohenberg equation with a quadratic term, the condition (2.43) makes it possible to a quadratic term to enter in the amplitude equation of each mode. The equation for A_1 looks like [26]

$$\partial_tA_1 = \Delta\varepsilon A_1 - \alpha\bar{A}_2\bar{A}_3 - A_1\sum_j\beta_j|A_j|^2. \tag{2.44}$$

Equations for A_2, A_3 are of the same form by symetry arguments. System of equations of this form may admit solutions where $|A_1| = |A_2| = |A_1| \neq 0$. Since $q_1 = q_2 = q_3 = q_c$, condition (2.43) is fulfilled by 3 modes forming an angle of $2\pi/3$ between them, this is always possible because there is a continuum of critical modes. This kind of solution accounts for the formation of hexagonal patterns, which may coexist with stripped patterns, as depicted in figure 2.7.

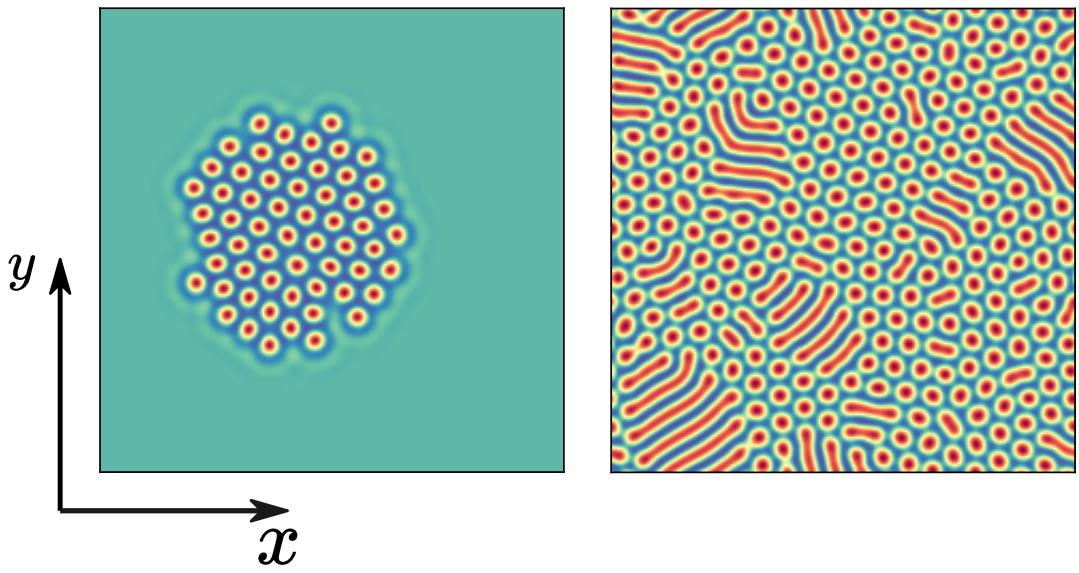

Figure 2.7: Left: Hexagons invading the homogeneus steady state. Right: Hexagons coexisting with stripes.

Chapter 3

The Complex Ginzburg-Landau equation

The dimensionless complex Ginzburg-Landau equation (CGLE) reads

$$\partial_t A = \mu A - (1 + \mathrm{i}\beta)|A|^2 A + (1 + \mathrm{i}\alpha)\nabla^2 A, \tag{3.1}$$

Where μ is the bifurcation parameter, β is the nonlinear frequency response, and α is a dispersion coefficient. As discussed in chapter 1, normal forms describe the dynamics of a system close to instability. A complex order parameter is necessary when describing an oscillatory bifurcation, namely an Andronov-Hopf [5] bifurcation when describing the evolution of a critical mode in a Turing instability or an oscillatory spatial instability. The cubic CGLE describes a slowly varying amplitude rising supercritically from one of these bifurcations when the system is weakly nonlinear, and it has translational and reflection symmetry. This equation was introduced with no time dependency and coupled with a magnetic field by Ginzburg and Landau while developing a theory for superconductivity [50], where the interpretation of the complex order parameter is the generalized wave function. A time-dependent version of this equation was later introduced phonologically by Schmid[76] and formally derived by Gorkov and Eliashberg [40]. The CGLE expressed as (3.1) appeared later in fluid dynamics, where Stuart and Stewartson[82] first derived it while describing an oscillatory spatial instability giving rise to waves in a plane Poiseuille flow. Other physical systems where this equation can be found include the Rayleigh-Benard convection [77], and electroconvection in nematic liquid crystal cells[48] and in laser dynamics [24]. Even though this equation can be derived in various physical systems, there are limitations in its applicability. When describing waves emerging from a convective instability, two coupled amplitude equations are needed to account for waves traveling in opposite directions if the system has reflection symmetry. A second limitation exists for two dimensional systems with spatial instability. If the system is isotropic, when performing a normal form analysis on an unstable mode, an anisotropic differential operator enters in the solvability condition instead of a Laplacian. This phenomenon is briefly discussed in chapter 2 for two-dimensional pattern-forming systems. The amplitude equation derived for this case is known as the Newell-Whitehead-Segel equation [58]. In this chapter, we are mostly concerned about the one-dimensional CGLE.

$$\partial_t A = \mu A - (1 + \mathrm{i}\beta)|A|^2 A + (1 + \mathrm{i}\alpha)\partial_{xx} A. \tag{3.2}$$

We will describe solutions to this equation, explore its dynamical regimes, chaotic on spatiotemporal sense, show its bifurcation diagram, and discuss the origin of complexity. At the

end of this chapter we briefly descibes about the dynamics of the 2 dimensional CGLE.

3.1 Plane wave solutions

The bifurcation parameter μ can always be set equal to 1 by rescaling the time, space and the amplitude. Simple coherent solutions of equation (3.2) are plane waves of the form [6]

$$A_q(x,t) = R_q \mathrm{e}^{\mathrm{i}qx+\omega_q t+\phi}, \tag{3.3}$$

$$R_q = \sqrt{1-q^2}, \tag{3.4}$$

$$\omega_q = \beta(1-q^2)+\alpha q^2. \tag{3.5}$$

Only solutions having $q^2 < 1$ exist. Let us study the linear stability of these solutions by making perturbations on the modulational part of these waves

$$A(x,t) = [R_q + f(t)\mathrm{e}^{\mathrm{i}kx} + g^*(t)\mathrm{e}^{-\mathrm{i}kx}]\mathrm{e}^{\mathrm{i}qx+\omega(q)t+\phi}. \tag{3.6}$$

If we linearize equation (3.2) around the plane wave solution, we get the following linear system for $f(t)$ and $g(t)$

$$\partial_t \begin{pmatrix} f(t) \\ g(t) \end{pmatrix} = \begin{bmatrix} u+z & v \\ v^* & u^*-z^* \end{bmatrix} \begin{pmatrix} f(t) \\ g(t) \end{pmatrix}, \tag{3.7}$$

with

$$\begin{aligned} u &= -(1+\mathrm{i}\beta)R_q^2 - (1+\mathrm{i}\alpha)k^2, \\ v &= -(1+\mathrm{i}\beta)R_q^2, \\ z &= -2qk(1+\mathrm{i}\alpha). \end{aligned} \tag{3.8}$$

Consider solutions of the form $f = f_0\mathrm{e}^{\lambda t}$ and $g = g_0\mathrm{e}^{\lambda t}$. Replacing this Ansatz on equation (3.7), a relation between the complex growing rate of the linear perturbation λ and its wavenumber k can be found [6]

$$\lambda = -\mathrm{i}v_g k - D_2 k^2 + O(k^3), \tag{3.9}$$

having

$$\begin{aligned} v_g &= 2(\alpha-\beta)q^2, \\ D_2 &= \left(1+\alpha\beta+\frac{q^2(1+\beta^2)}{R_q^2}\right). \end{aligned} \tag{3.10}$$

The instability occurs when the real part of the growing rate λ becomes positive. This happens when D_2 becomes negative. This gives a condition for stability of waves which is

$$q^2 < \frac{1+\alpha\beta}{3+\alpha\beta+2\beta^2} = q_E^2. \tag{3.11}$$

This means for fixed parameters α and β only waves having $q^2 < q_E^2$ are stable to linear perturbations. The special case when $q_E = 0$ defines a relation known as the **Benjamin-Feir** relation [11]

$$1+\alpha\beta = 0, \tag{3.12}$$

this relation implies that if $\alpha\beta > -1$, then the homogeneous state $A_0 = \mathrm{e}^{\mathrm{i}\phi}$ is no longer stable

3.2 Localized solutions

Domains of different wave solutions of the CGLE are connected by localized structures. To characterize these solutions the following Ansatz is used

$$A = a(x - vt)\mathrm{e}^{\mathrm{i}\phi(x-vt)+\mathrm{i}\omega}, \tag{3.13}$$

where v, and ω are respectively the characteristic velocity and frequency, which are in principle free parameters. Replacing the Ansatz on equation (3.2) results in a set of 2 differential equations, having defined $\psi = \partial_x\phi$, and $b = \partial_x a$ [88]

$$\partial_x b = a\psi^2 - \frac{1}{1+\alpha^2}[(1+\alpha\omega)a + v(b+\alpha\psi a) - (1+\alpha\beta)a^3], \tag{3.14a}$$

$$\partial_x \psi = 2\frac{b\psi}{a} + \frac{1}{1+\alpha^2}[(\alpha-\omega) + v(\alpha\frac{b}{a} - \psi) - (\alpha-\beta)a^2]. \tag{3.14b}$$

Waves defined by (3.3) correspond to fixed points of this set of equations. Heteroclinic and homoclinic orbits in this phase space describe coherent structures having as their asymptotic state [52]. Characteristic solutions to the CGLE are hole-like solutions, also known as defects [52], they consist of localized dips on the amplitude and localized peaks in the local wavenumber, namely the phase gradient. Holes can emit waves traveling in opposite directions, having different wave numbers, these solutions are known as **Nozakki-Bekki** holes [9] and correspond to heteroclinic orbits of equations (3.14). Holes connecting waves with the same number are known as homoclons as they correspond to homoclinic orbits of equations (3.14); holes connecting the homogeneous state with itself can be found in this category. The dynamics of these defects give origin to the complex spatiotemporal dynamics such as defect turbulence and spatiotemporal intermittency [87]. This will be discussed in the following section. On the other hand, colliding waves form sinks, which look like a bump in the amplitude. Nozakki-Bekki holes and sinks are depicted in figure 3.1.

3.3 Chaotic regimes

The CGLE has complex spatiotemporal regimes, including phase turbulence, defect turbulence, and spatiotemporal intermittency in different parameter space regions. The bifurcation diagram of this equation is shown in figure 3.2[79, 19].

3.3.1 Spatiotemporal intermittency

Below the Benjamin-Feir curve, strange attractors coexist with waves. The dynamics in these attractors consist of patches where the amplitude remains homogeneous, and the wavenumber is close to 0. These patches appear and disappear over temporal evolution. The spatiotemporal evolution looks like a characteristic fractal pattern known as a Sierpinski carpet.[80](see figure 3.3). These almost homogeneous regions patches may coexist with regions where the wavenumber is different from 0 separated by Nozzak-Bekki holes and sinks (see figure 3.3 a)).

Holes connect the homogeneous patches. As the wavenumber, there is approximately 0; holes can be regarded as homoclons. The dynamics of these holes come from the fact that they are unstable [87]. They may evolve in two ways, either they decay, or the peak in its

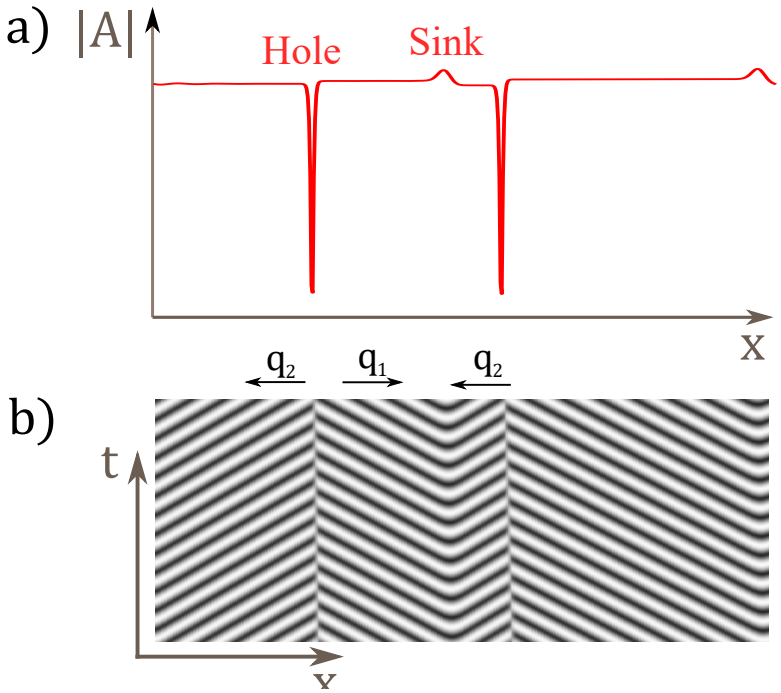

Figure 3.1: **a)** Envelope of $A(x,t)$ the depicting 2 Nozzaki-Bekki holes and a sink **b)** Spatiotemporal diagram showing the evolution of the holes and sink. Waves traveling in opposite directions can be seen.

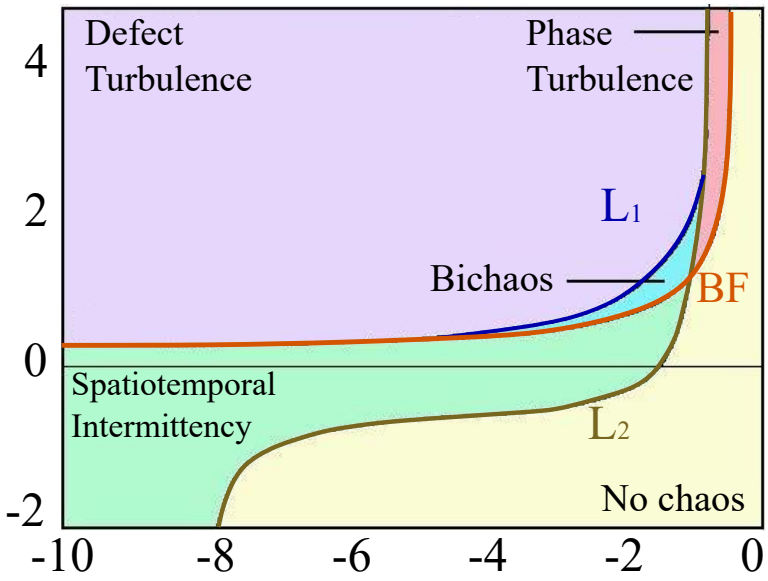

Figure 3.2: Bifurcation diagram of the CGLE in one dimension (Image from: https://codeinthehole.com/tutorial/coherent.html).

phase gradient, namely ψ, starts to grow into a phase slip. A second negative in the phase gradient appears, so the total phase across the hole is conserved. Eventually, a new hole is nucleated, traveling in the opposite direction that later may suffer the same instability. The motions of holes create a characteristic zig-zag motion of holes [87]. The conservation of the phase gradient across the hole can be deduced from integrating equation (3.14b) across the

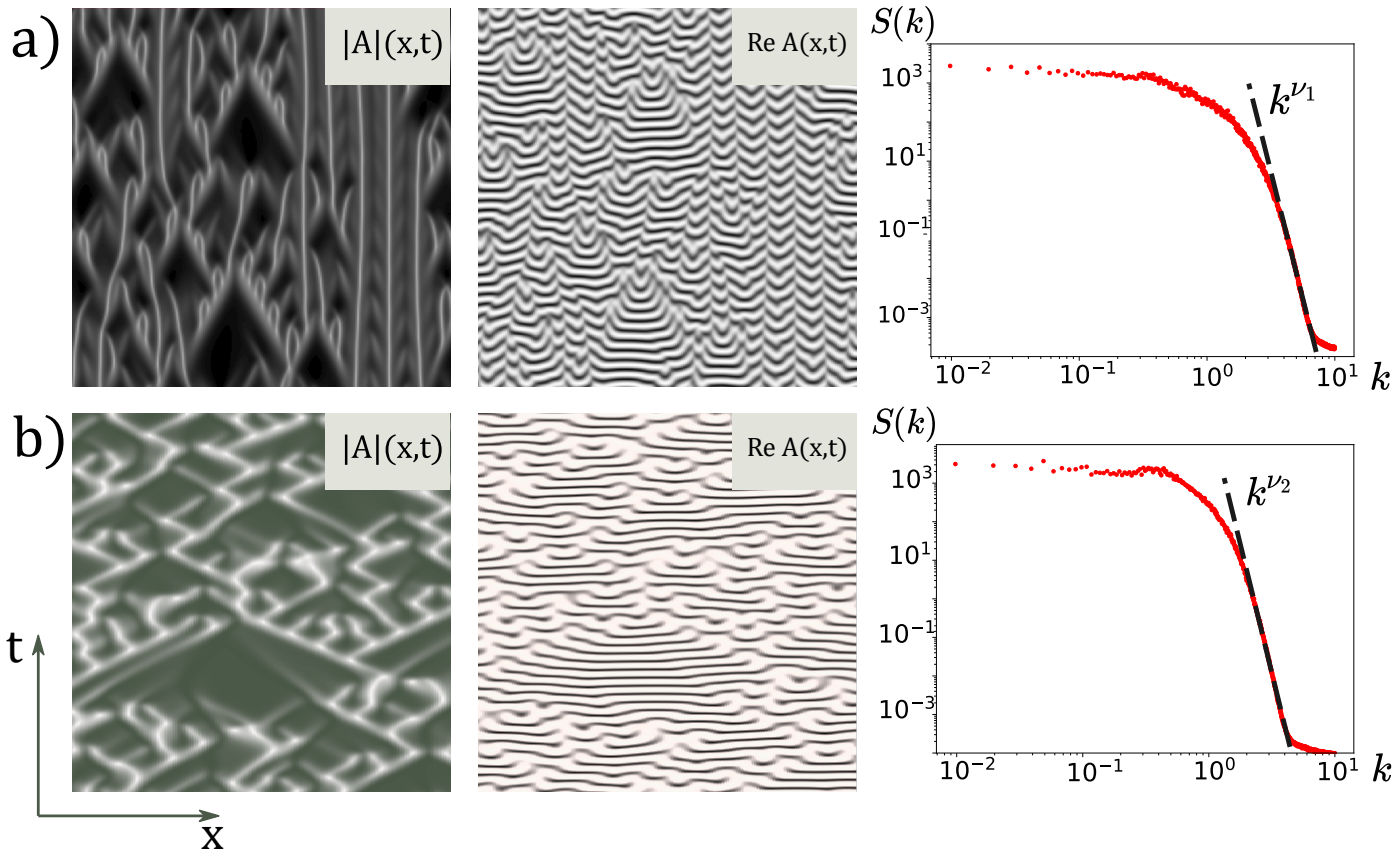

Figure 3.3: Spatiotemporal interrmittency at 2 different points of the parameter space **a)**$\alpha = -0.5$ and $\beta = -4.0$, Sierpinsky carpet is coexisting with traveling waves. **b)** $\alpha = 0.5$ and $\beta = -1.75$.

hole and using that the asymptotic state of the phase gradient is well defined and that the gradient of the amplitude, namely $\partial_x a$, is an odd function. L_2 transition line is determined numerically simulating the equation and slowly tuning the parameters until there are no more collisions of localized structures [19]. We also computed the spectral energy distribution

$$S(k) = \langle |\tilde{A}|^2(k) \rangle_T, \tag{3.15}$$

where the brackets represent an average over time, and the tilde denotes the spatial Fourier transform. In both examples in figure 3.3, we observe a power law in the in the spectrum, which is consistent with the self-similar behavior

3.3.2 Phase turbulence

The homogeneous state is no longer stable above the Benjamin-Feir curve ($\alpha\beta > -1$). However, there is a region in the parameter space where this does not lead to the appearance and disappearance of holes. Rather the amplitude of the field remains close to the homogeneous, and ripples appear over this state, which presents venous structure when recording its spatiotemporal evolution (see figure 3.4). To describe this behavior, we start by taking the Ansatz of the homogeneous state $A_H = e^{i\phi}$ and promoting the ϕ into a slowly varying function of time and space. A gradient expansion is made in order to respect phase invariance, and

the linear coefficients are matched, so the equation has the same linear stability properties as equation (3.7). Non linearities are included by replacing q by $\partial_x\phi$ in the definition of D_2 in equation (3.10)[45]. When doing so, the Kuramoto Sivanchinky equation is derived from [49, 73]

$$\partial_t\phi = D_2\partial_{xx}\phi - D_4\partial_{xxxx}\phi + c_1(\partial_{xx}u)^2. \tag{3.16}$$

This equation is known to exhibit spatiotemporal chaos, which accounts for the dynamics observed in this regime of the CGLE. The spectral energy distribution decays as a power law,

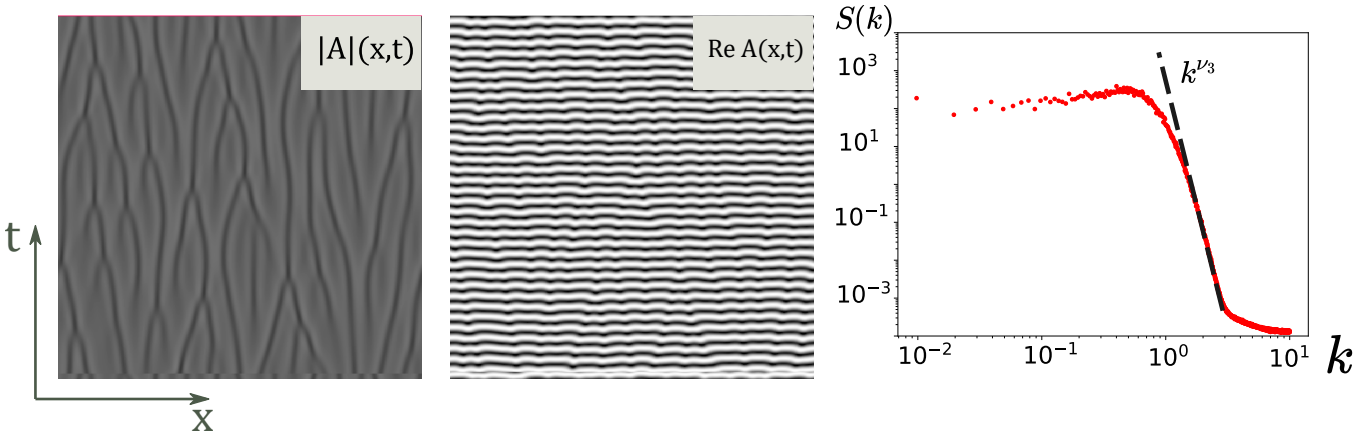

Figure 3.4: Spatiotemporal evolution of phase turbulent regime at $\alpha = 2$ and $\beta = 0.9$. Ripples over the homogeneous state can seen on the evolution of the envelope

that it why this state is referred as turbulence. In the region labeled as bichaos it is possible to find coexistence phase turbulence and spatiotemporal intermittency.

3.3.3 Defect turbulence

Further up the Bejanmin-Feir curve, the homogeneous patches that characterize spatiotemporal intermittency shrink and disappear, leaving a large isotropic region of creation and destruction of defects. The L_1 transition line is determined by measuring extrema in the correlation functions [31], or by measuring where the density of defects vanishes [79]. Its power density distribution also shows a power law, which is the reason why this state is called defect turbulence .

3.4 Two-dimensional dynamics

Waves are also solutions in tow dimensions. They have the described by relation (3.3) promoting q into a vector $\vec{q}$:

$$A_q(x,t) = R_q e^{i\vec{q}\cdot\vec{r}+\omega_q t+\phi}, \tag{3.17}$$

A linear stability analysis yields similar conditions for stability. Using the Ansatz (3.6), but promoting k into a a vector $\vec{k}$, the complex growth rate of each mode is given by

$$\lambda = -i\vec{v}_g'\cdot\vec{k} - D_2'k^2 + O(k^3), \tag{3.18}$$

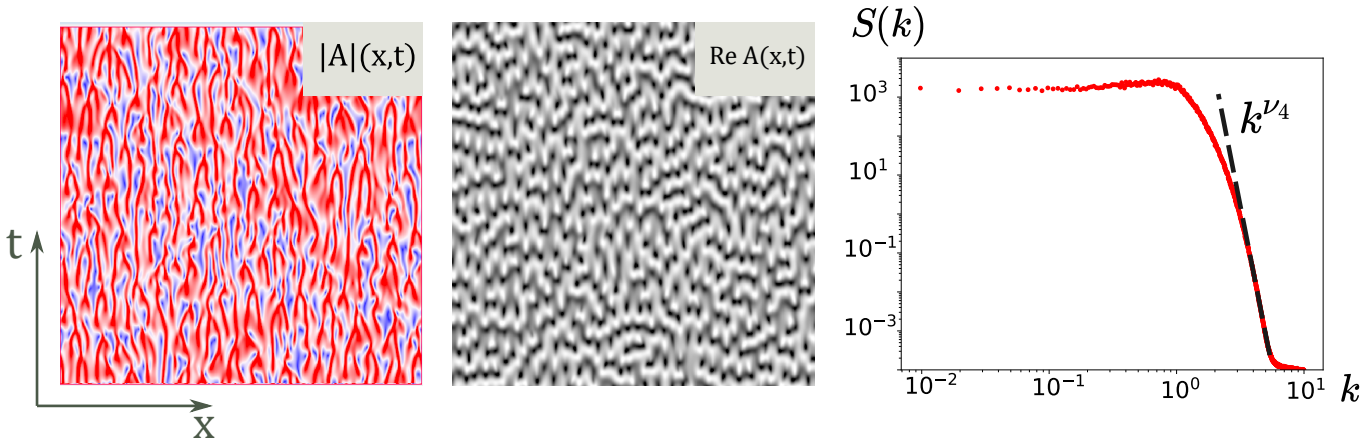

Figure 3.5: Defect turbulence observed at $\alpha = 2$ and $\beta = -1.9$. On the left panel, blue regions correspond to zones where the amplitude is close to 0.

where

$$\begin{aligned} \vec{v}_g' &= 2(\alpha - \beta)\vec{q}, \\ D_2' &= \left(1 + \alpha\beta + \frac{q_k^2(1+\beta^2)}{R_q^2}\right), \\ q_k &= \frac{\vec{k}\cdot\vec{q}}{k}. \end{aligned} \tag{3.19}$$

When perturbations are parallel to $\vec{q}$, the conditions are the same as the one-dimensional case. Thus, the Benjamin-Fair condition for the stability of the homogeneous state can be derived.

A hole like solutions behaves differently. They are located at the intersections of the nullclines of the real and imaginary parts of $A(x, y)$; they correspond to singularities in the field phase, and these solutions are topological. Integrating the local wavenumber $\nabla\phi$ along a path enclosing the hole gives integer multiples of 2π:

$$m = \frac{1}{2\pi}\oint \nabla\phi \cdot \mathrm{d}\vec{r} = \frac{1}{2\pi}\oint \mathrm{d}\phi \quad m \in \mathbb{Z}, \tag{3.20}$$

Quantity m is called the topological charge of the defect. The total topological charge in the CGLE is a conserved quantity [64]; thus, defects can only be created or destroyed in pairs of opposite charge, differently from the one-dimensional case holes can fade out or nucleate new ones. Holes emitting spiral waves exist. Their asymptotic wavenumbers correspond to the ones of the stable waves given by (3.3). Colliding waves emitted by source holes form shocks, similar to sinks in the one-dimensional case. Holes that absorb waves are formed at the corners where shocks intersect. The system can evolve into a glassy state, made of domains having a spiral in its center, and separated by shocks and vortexes at their intersections.

A new mechanism of the emergence of complexity is observed, where creation and annihilation oh defects are always happening or in the form of phase turbulence [55] where no defects are observed. There is no direct analogy to the one-dimensional spatiotemporal intermittency. However, in chapter 5, a modified two-dimensional CGLE is presented where a behavior resembling this chaotic regime is observed.

Chapter 4

The liquid crystal light valve experiment

The liquid crystal light valve (LCLV) is an experiment that takes advantage of the optical properties of nematic liquid crystals to observe diverse phenomena such as localized structures, hexagonal and striped patterns, and spatiotemporal chaos. In this chapter, we explain how the experiment works, show the phenomenology of interest for this thesis, derive a theoretical model describing this phenomenology partially, and offer a possible explanation of the complex dynamics this experiment may exhibit.

4.1 Nematic liquid crystals

Liquid crystal corresponds to an intermediate state of matter between isotropic fluids and crystalline solids; this means it can flow while its molecules preserve a crystal-like orientation. In this thesis, we are interested in a nematic liquid crystal [66]. Its molecules are rod-like shaped tend to preserve **locally** the same orientation, but having no positional order (see figure 4.1). The molecular orientation is characterized by a unitary vector $\vec{n}(\vec{r})$ called the director

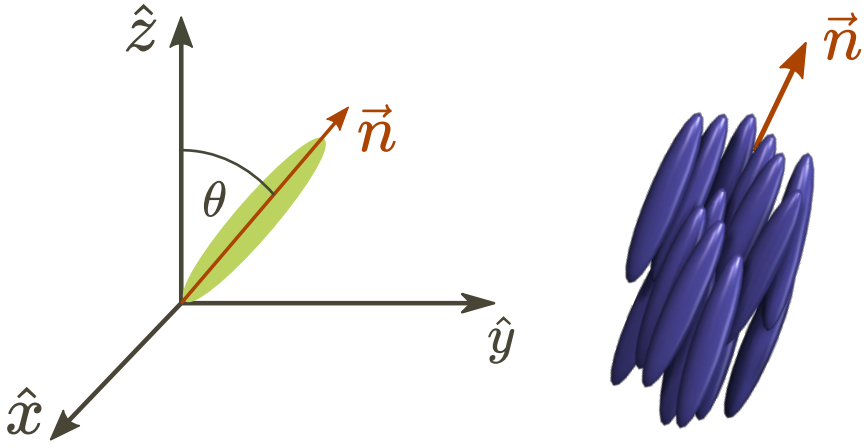

Figure 4.1: Left: Shape of nematic liquid crystal. Right: Representation of the nematic phase.

4.1.1 Electrical properties

The anisotropy of the liquid crystal molecules implies they dielectric permittivity is a tensor ε_{ij} with 2 degrees of freedom rather than a constant. In other words, they have a dielectric permittivity $\varepsilon_{\parallel}$ for the longitudinal axis of the molecules, namely the extraordinary axis, and other dielectric constant $\varepsilon_{\perp}$ for the other two directions, namely the ordinary axes. We define the dielectric anisotropy as the difference between the dielectric permittivities of the ordinary and extraordinary axes: $\Delta\varepsilon = \varepsilon_{\parallel} - \varepsilon_{\perp}$.

The quadrupole moment of the liquid crystal molecules allows them to align themselves parallel or perpendicular to an external electric field depending on the sign of its dielectric anisotropy. Recall the definition of the electric displacement on a linear anisotropic medium and energy density of an electric field [18]

$$D_i = \varepsilon_{ij} E_j = \varepsilon_{\perp} E_i + (\varepsilon_{\parallel} - \varepsilon_{\perp}) E_j n_j n_i = \varepsilon_{\parallel} E_i + \Delta\varepsilon E_j n_j n_i, \tag{4.1}$$

$$u = -\frac{1}{2} E_i D_i = -\frac{1}{2}(\varepsilon_{\parallel} E_i E_i + \Delta\varepsilon (E_i n_i)^2). \tag{4.2}$$

The second term on (4.2) is the square of the projection of the external electric field on the director. When the sign of $\Delta\varepsilon$ is positive (negative), the potential energy is minimized when the molecule is oriented parallel (orthogonal) to the electric field.

We are concerned in a nematic liquid crystal cell, which consists of two parallel glass plates filled with a nematic liquid crystal of positive dielectric anisotropy ($\Delta\varepsilon > 0$). Glass plates are treated so that the molecules located just over their surfaces remain parallel to them, the cell is said to have a planar anchoring. A sinusoidal voltage of amplitude V_0 is set between the plates, taking the precaution that the voltage period is shorter than the characteristic timescale of the molecular reorientation. A photoresistive wall is located at the back of the cell, so the voltage can be modulated using a light beam. As explained before, the molecules would like to orient themselves in the direction of the external electric field; however, its elasticity and the boundary conditions imposed at the glass plates constrain the rotation of the molecules. Experimentally, it has been observed that for voltages below a threshold V_F, the molecules remain parallel to plates. Over this threshold, the inclination angle of the molecules averaged along the thickness of the cell is given by

$$\theta = \frac{\pi}{2}\left(1 - \sqrt{\frac{V_F}{V_0}}\right), \tag{4.3}$$

V_F is known as the Fréedericksz voltage, and this phenomenon is known as the Fréedericksz transition [38].

4.1.2 Optical properties

Having tow different electric permittivities also implies the existence of two refraction indexes. This property is called birefringence and is characterized by the difference $\Delta n = n_{\parallel} - n_{\perp}$. When a linearly polarized wave traverses a liquid crystal cell, it comes out with circular polarization depending on how the polarization is oriented with respect to the mean direction of the director across the cell. If we consider a cell of thickness d when a linearly polarized wave traverses the cell, the two components of its polarization acquire a phase difference

φ because each polarization propagates with a different speed inside the cell. The relation between the envelope of the electric field before and after it passes through the cell, $\vec{E}_{in}$ and $\vec{E}_{out}$ respectively, is given by [13]

$$\vec{E}_{in} = \begin{pmatrix} \cos\psi_1 \\ \sin\psi_1 \end{pmatrix} E_0, \tag{4.4}$$

$$\vec{E}_{out} = \begin{bmatrix} \mathrm{e}^{-\mathrm{i}\varphi} & 0 \\ 0 & 1 \end{bmatrix} \begin{pmatrix} \cos\psi_1 \\ \sin\psi_1 \end{pmatrix} E_0 \tag{4.5}$$

$$\varphi = k\mathrm{d}\Delta n \cos^2\theta(x,y) + O(\Delta n^2), \tag{4.6}$$

Where θ is the local molecular orientation averaged over thickness of the cell, which may not be homogeneous along the cell

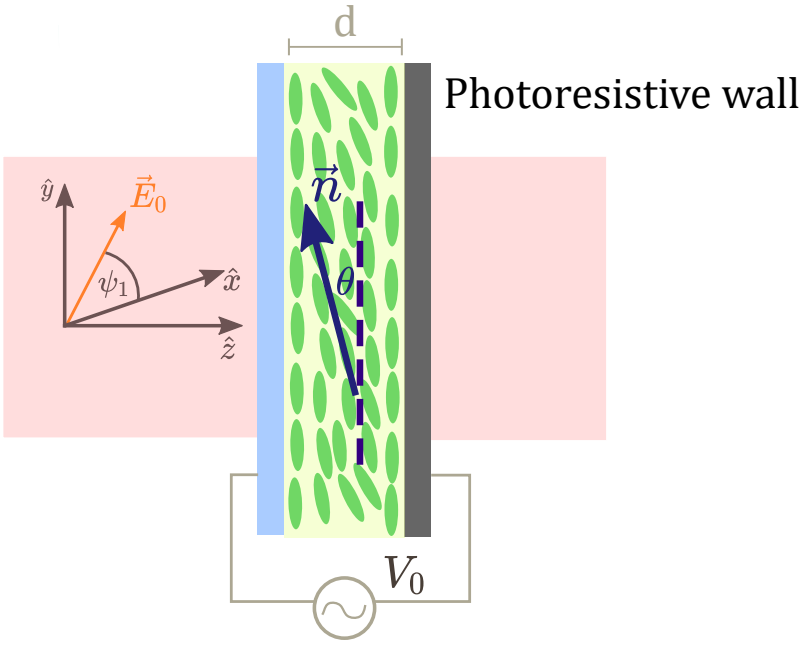

Figure 4.2: Nematic liquid crystal cell with planar anchoring. At the boundaries liquid crystal molecules are oriented parallel to the plates. A photoresistive wall is located at the back of the cell which allows to spatially modulate the voltage at the cell using light.

4.2 Experimental setup

The liquid crystal light valve experiment (see figure 4.3) was originally designed Akhmanov et al. [3]. It consists of a liquid crystal cell whose voltage is spatially modulated according to the averaged orientation of the molecules at each point. This is done through optical feedback and the photoresistive wall. A laser beam with a given polarization is directed into the cell; the beam is reflected by a mirror located at the back of the cell and traverses back the cell. The components of the polarization acquire a phase difference of $\varphi = 2k\mathrm{d}\cos^2\theta(x,y)$.The factor 2 comes from the beam traversing the cell twice. The local phase difference is converted into spatial modulation of the envelope using a polarizer. Through the optical feedback the

modulated wave is directed to the photoresistive wall at the back of the liquid crystal cell. A spatial light modulator (SLM) is used to set the shape of the beam. A quasi-one-dimensional mask or a two-dimensional one can be used.

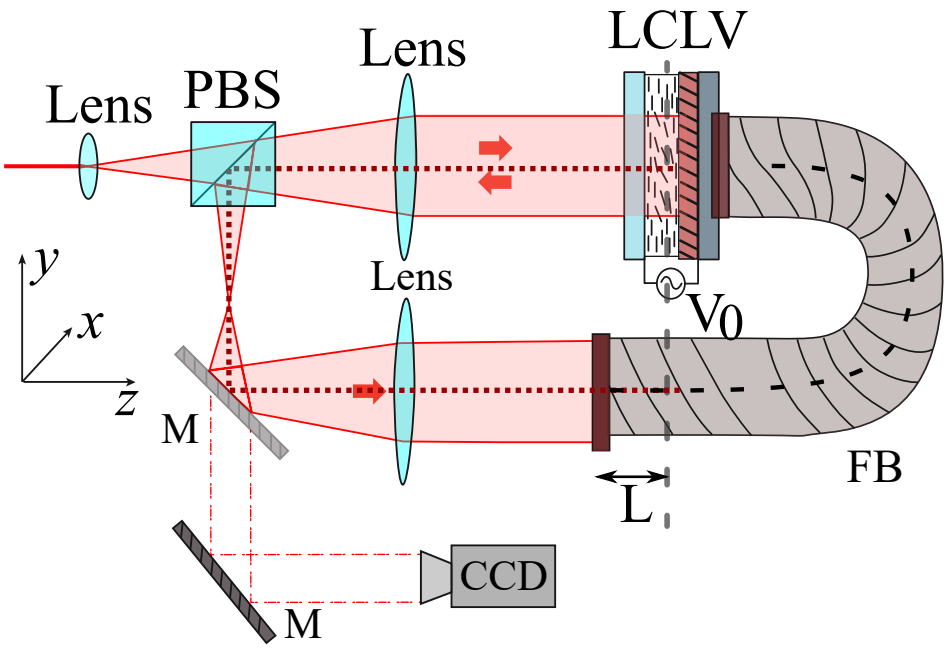

Figure 4.3: Liquid crystal light valve with optical feedback setup. An incident laser beam passes through a polarized beam splitter where it acquires a fixed polarization. The beam then enters into a liquid crystal cell and is reflected by a mirror located at the back of the cell, when coming out of the cell, the beam has a circular polarization. The polarization is converted into amplitude modulation by the polarized beam splitter and an arrange of mirrors and lenses is used to direct the beam into a fiber bundle, where ir later directed into a photoresitive wall at the back of the liquid crystal cell.

4.2.1 Optical components

Polarized beam splitter (PBS)

We use a PBS to set the polarization of the incoming beam and convert the polarization modulation into amplitude modulation of the outcoming wave [75]. A PBS (see figure 4.4) transmits light with a specific polarization, characterized by an angle ψ_1 while it reflects light with the orthogonal direction of polarization. Let us consider a linearly polarized wave of amplitude E_0. When the wave passes the first time on the PBS, the electric field is given by $\vec{E}_{in}$, when it comes out of the liquid crystal cell is given by $\vec{E}_{out}$, and when it passes a second time on the PBS, the value of the electric field is given by $\vec{E}_m$ (see figure 4.4)

$$\vec{E}_{in} = \begin{pmatrix} \cos\psi_1 \\ \sin\psi_1 \end{pmatrix} E_0, \tag{4.7}$$

$$\vec{E}_{out} = \begin{pmatrix} e^{-i\varphi}\cos\psi_1 \\ \sin\psi_1 \end{pmatrix} E_0, \tag{4.8}$$

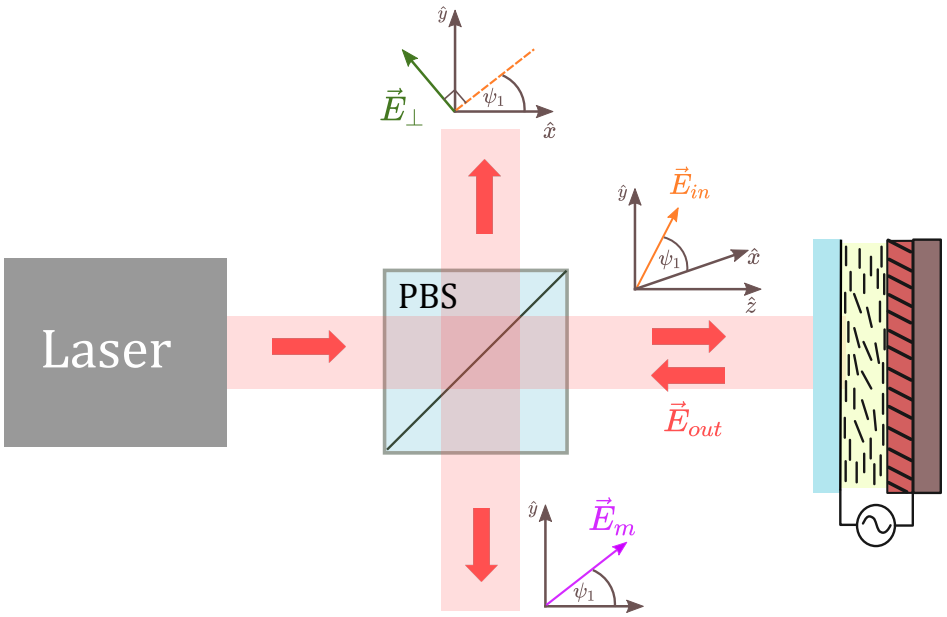

Figure 4.4: Polarized beam splitter

$$\vec{E}_m = (-\mathrm{e}^{-\mathrm{i}\varphi} \sin\psi_1 \cos\psi_1 + \cos\psi_1 \sin\psi_1) \begin{pmatrix} -\sin\psi_1 \\ \cos\psi_1 \end{pmatrix} E_0. \tag{4.9}$$

The 4-f array

We require to reproduce the intensity profile of the modulated beam into the photoresistive cell. A 4-f array allows us to reproduce an image four focal distances further away. This arrangement works with two convergent lenses. When an image is located at the focus of the first convergent lens, its Fourier transform is formed one focal distance from the back of the lens, called the Fourier plane [75]. Another convergent lens is located at a focal distance away from the Fourier plane. This equivalent to taking another Fourier transform. The composition of 2 Fourier transforms forms an inverted version of the original image four focal distances away from it (see figure 4.5). A slot can be located at the Fourier plane to filter out the dynamics of any of the transversal directions.

The fiber bundle (FB)

To transfer the resulting image from the 4-f array, we use the fiber bundle, a collection of optical fibers. The FB is twisted in 180°, so the projected image into the photoresistive wall is oriented in the same way as the original one. The FB can be displaced along the optical axis by a distance L (see FB at figure 4.3). The paraxial equation [?] can describe the evolution of the amplitude of the wave along with the distance

$$\nabla_{\perp}^2 E + 2\mathrm{i}k\partial_z E = 0, \tag{4.10}$$

the resulting amplitude E_w can be computed applying a diffraction operator on E_m

$$E_w = \mathrm{e}^{-\mathrm{i}\frac{L}{2k}\nabla_{\perp}^2} E_m = \mathrm{e}^{\mathrm{i}\frac{L}{2k}\nabla_{\perp}^2} (-\mathrm{e}^{-\mathrm{i}\beta\cos^2\varphi(x,y)} \cos\psi_1 \sin\psi_1 + \cos\psi_1 \sin\psi_1) E_0. \tag{4.11}$$

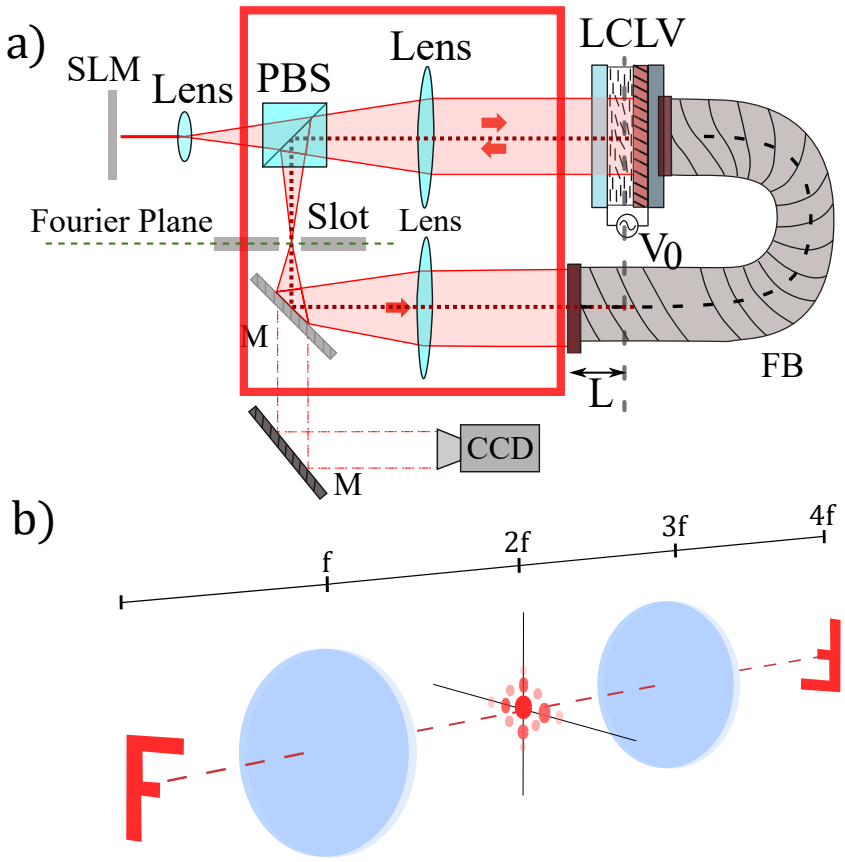

Figure 4.5: a) Physical location of the 4f array in the LCLV. b) A typycal 4-f array

Choosing $\psi_1 = 45°$. Since the intensity of light reaching the photoresisitve wall is porportional to $|E_w|^2$ we have

$$I_w = \frac{I_0}{4}|\mathrm{e}^{-\mathrm{i}\frac{L}{2k}\nabla_\perp^2}(1 - \mathrm{e}^{-\mathrm{i}\beta\cos^2\varphi(x,y)})|^2, \tag{4.12}$$

where I_0 is intensity of initial beam.

4.3 Experimental observations

4.3.1 Pattern formation

The LCLV exhibits a wide variety of dissipative structures such as fronts, solitons, and patterns [72]. For this thesis, we will be interested in the dynamics of the last ones. Typical snapshots of two-dimensional patterns of different kinds are depicted in the upper panels of figure 4.6. The bottom panels are snapshots of the far-field observations of each of the patterns above. Looking at the far-field is equivalent to look at the Fourier plane [13]

4.3.2 Spatiotemporal chaos

Patterns are not necessarily static; it has been shown that if one keeps track of their temporal evolution, they may exhibit complex spatiotemporal dynamics [20]. In figure 4.7 a) there are two snapshots of the experiment, one using a quasi one- dimensional mask and the other

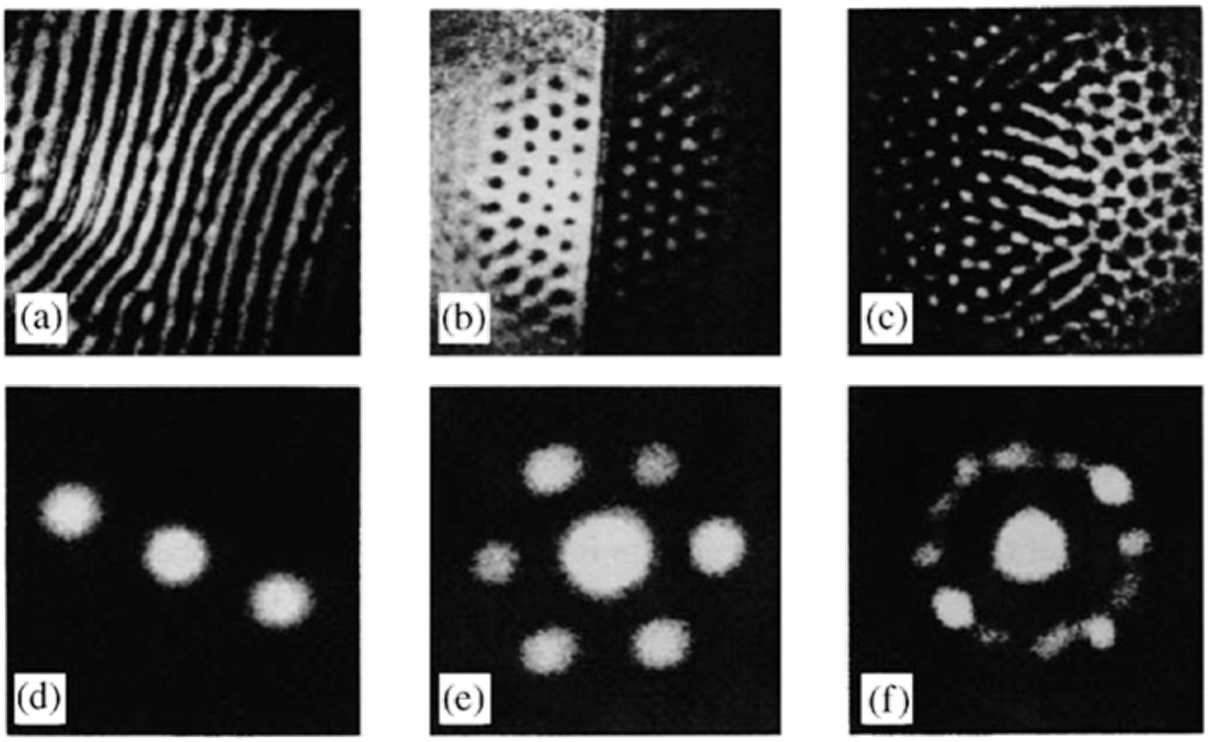

Figure 4.6: **Upper line**: Near field observations of **a)** Stripped pattern **b)**Hexagonal pattern **c)** Coexitence between stripped and hexagonal patterns. **Botom line**: Far field observations of the patterns above. Figure from [72]

using a rectangular one. The dashed red line represents a section of the pattern tracked over time. A slot is used to filter out the dynamics in the x direction, forcing the patterns to be in the y direction. It is possible to distinguish stationary, quasiperiodic, intermittent, and turbulent like dynamics for different values of V_0

Figure 4.8 a) represents the power density spectrum for distinct values of V_0 exhibiting different regimes. The blue corresponds to the stationary case, with only one characteristic frequency, whereas the red represents a quasiperiodic regime, characterized by several incommensurable frequencies. The black curve resembles a power law, which is characteristic for turbulent like dynamics. Figure 4.8 b) represents the largest Lyapunov exponent of the system measured for different values of V_0. Recall that for positive values of this physical quantity, the system is said to be chaotic. This plot shows transitions from stationary and quasiperiodic patterns to complex spatiotemporal dynamics.

4.4 Theoretical description

A simple reaction diffusion equation describing the evolution of $\theta(x, y)$ reads [21].

$$\partial_t \theta = -(\theta - \theta_0(x, y)) + l^2 \nabla^2 \theta, \tag{4.13}$$

$\theta_0(x, y)$ is the angle of equilibrium of the Frederikz transition. Recall (4.3), describing the equilibrium inclination angle in a liquid crystal cell, we replace V_0 with effective voltage at

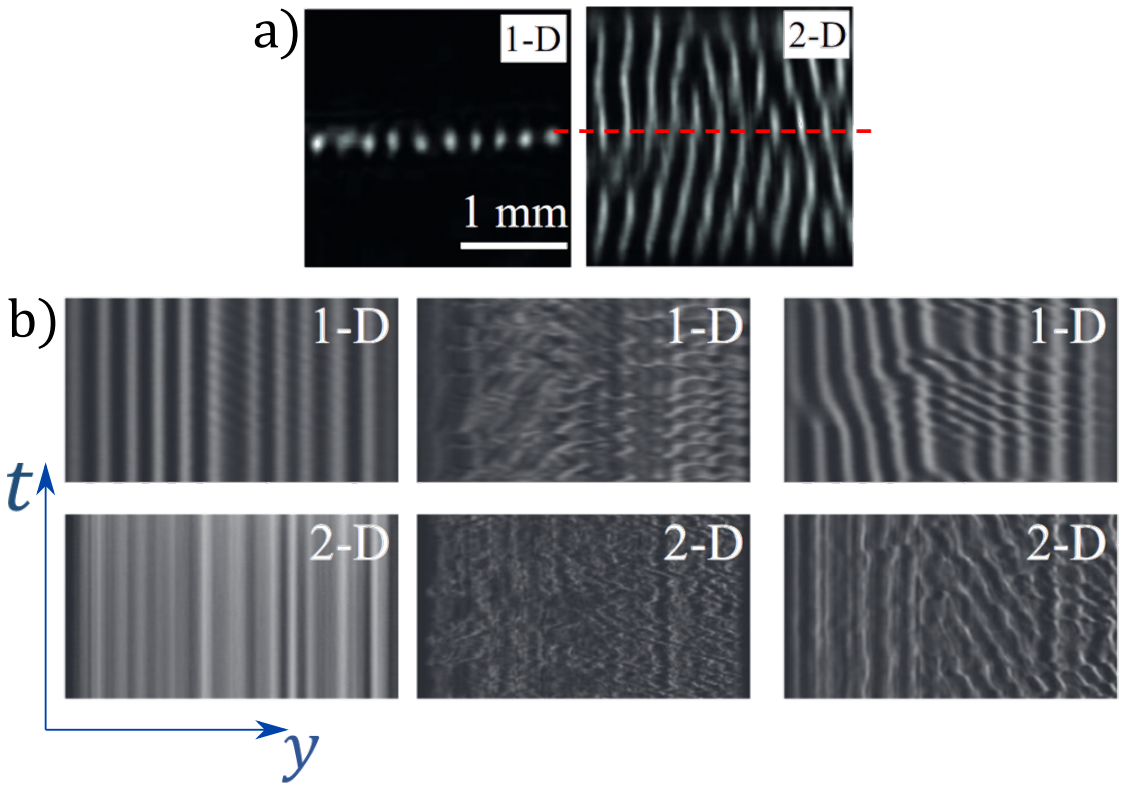

Figure 4.7: **a)** Snapshots of typical patterns observed in the LCLV for a quasi one dimensional and two dimensional masks. **b)** Spatiotemporal diagrams of a one dimensional section of the patterns using both masks depicting different dynamical regimes for the. Figure from [20].

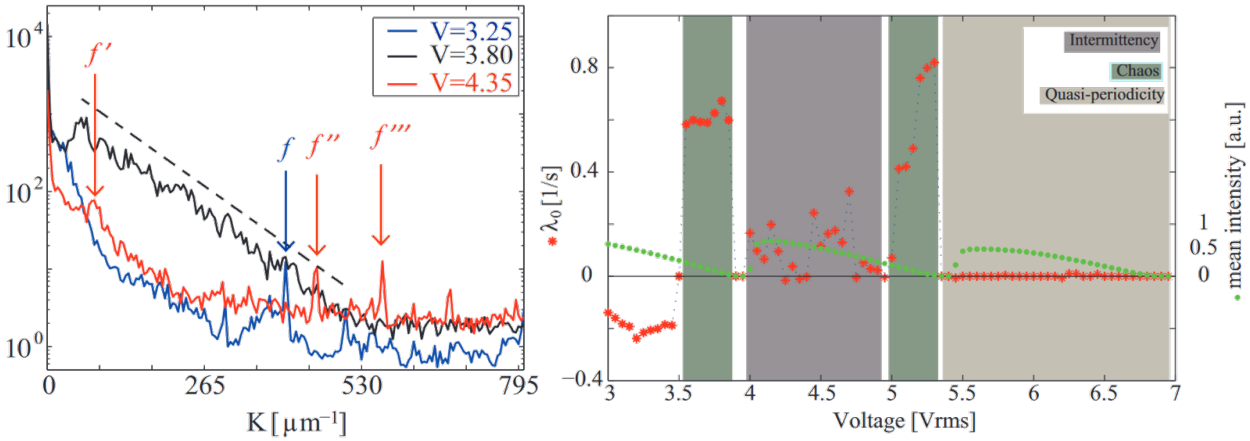

Figure 4.8: **Left**: Power density spectrum for patterns at different values of V_0. **Right**: Largest Lyapunov exponent for different values of V_0. Figure from [20].

each point of the cell.

$$\theta_0 = \frac{\pi}{2}\left(1 - \sqrt{\frac{\Gamma V_F}{\Gamma V_0 + \alpha I_w(\theta)}}\right). \tag{4.14}$$

Stationary and homogeneous solutions of equation 4.13 in terms of V_0 and I_0 are depicted in figure 4.9. The corrugated structure of this surface shows there exist regions having two stable and one unstable solution [21]. Close to the onset of bistability, a model describing an imperfect pitchfork bifurcation can be derived [21]. Let θ_0 be the equilibrium angle on the onset of bistability, an equation for the evolution of a perturbation $u(\vec{r}, t)$ of this angle is derived.

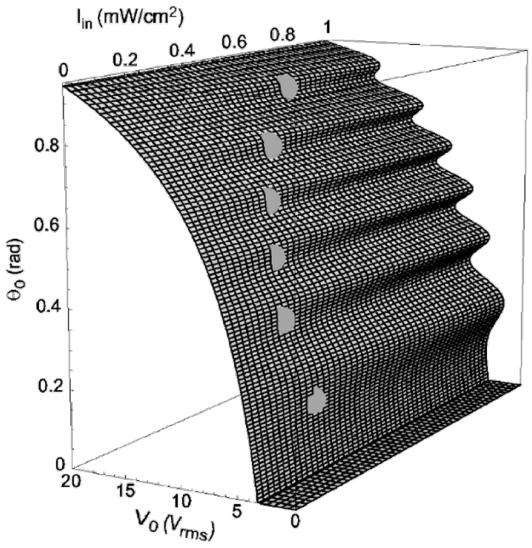

Figure 4.9: Surface defining the stationary solutions of equation 4.13. Figure from [21]

$$\theta = \theta_c + u, \tag{4.15}$$

$$\partial_t u = \eta + \varepsilon u - u^3 + h.o.t. \tag{4.16}$$

To add a spatial dependency to equation 4.16, we expand the diffraction operator in powers of L in equation 4.12

$$\mathrm{e}^{-\mathrm{i}\frac{L}{2k}\nabla_\perp^2} = 1 - \mathrm{i}\frac{L}{2k}\nabla_\perp^2 - \frac{L^2}{4k^2}\nabla_\perp^4 + O(L^3), \tag{4.17}$$

we keep up to second order in L because the diffusion in equation 4.13 can turn negative after the previous expansion. After some straightforward algebra one gets [4]

$$\partial_t u = \eta + \varepsilon u - u^3 + (l^2 - \nu(L))\nabla_\perp^2 u - h(L^2)\nabla_\perp^4 u + h.o.t., \tag{4.18}$$

$$\nu = \frac{\beta L \theta_c}{4k(\Gamma V_0 + \alpha I_0(1 + \cos\beta\cos^2\theta_c))} \sin 2\theta_c \sin\beta\cos^2\theta_c, \tag{4.19}$$

$$h = \frac{\theta_c L^2}{8k^2(\Gamma V_0 + \alpha I_0(1 + \cos\beta\cos^2\theta_c))}(1 + \cos\beta\cos^2\theta_c). \tag{4.20}$$

Equation 4.18 is the type Swift-Hohenberg model. As discussed in Chapter 3, this model can explain the formation of stripped and hexagonal patterns. However, this equation cannot describe the transition from quasiperiodicity into complex dynamics discussed in section 4.3.2. due to its variational nature.

4.5 Translational coupling

We propose that the origin of the complex spatiotemporal dynamics comes from the intrinsic misalignment into the experiment, which is also generic for every optics experiment. The experiment is modified to include movement in the transversal direction of the fiber bundle, depicted in figure 4.10. This has the consequence that the voltage in the LC at the point $\vec{r} = (x, y)$ now depends of the orientation of the LC at the point $\vec{r}+\vec{\delta}$. We called this a translational coupling and was introduced by F. del Campo in his Master's thesis [17, 30] studying the effects of misalignments in localized structures. Figure 4.11 shows spatiotemporal diagrams and power density spectra for patterns at different values of δ. We observe a transition from periodic waves into a state resembling spatiotemporal intermittency. The power density spectrum of figure 4.11 c) shows a power-law signaling a rather turbulent dynamic. The theoretical aspects of the translational coupling will be discussed in the next chapter.

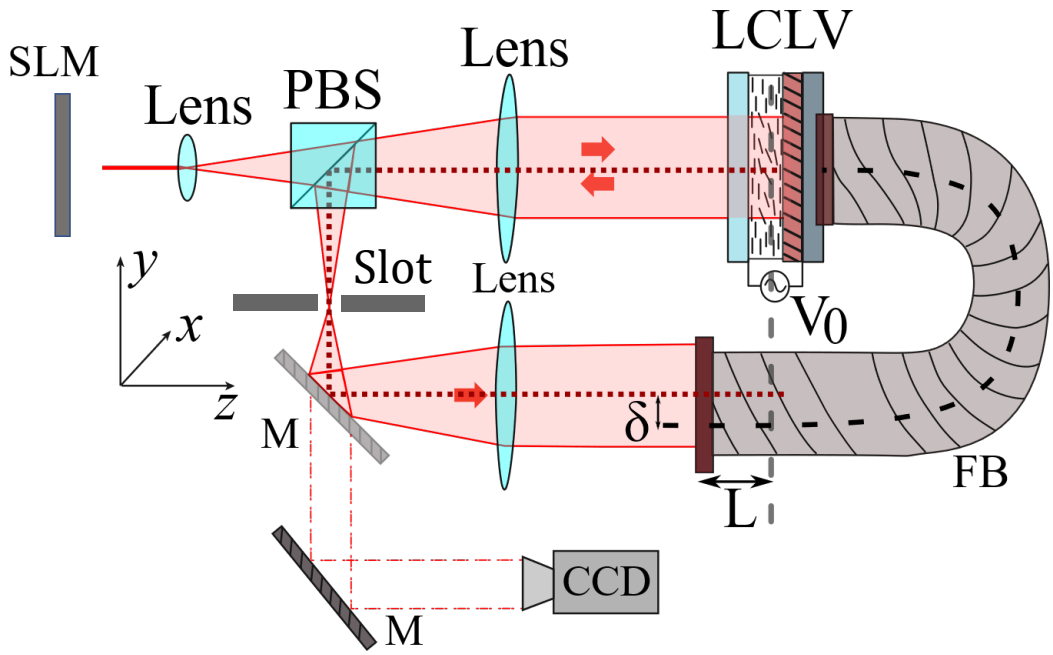

Figure 4.10: Modified LCLV where is possible to move the entry of the fiber bundle in the transversal direction

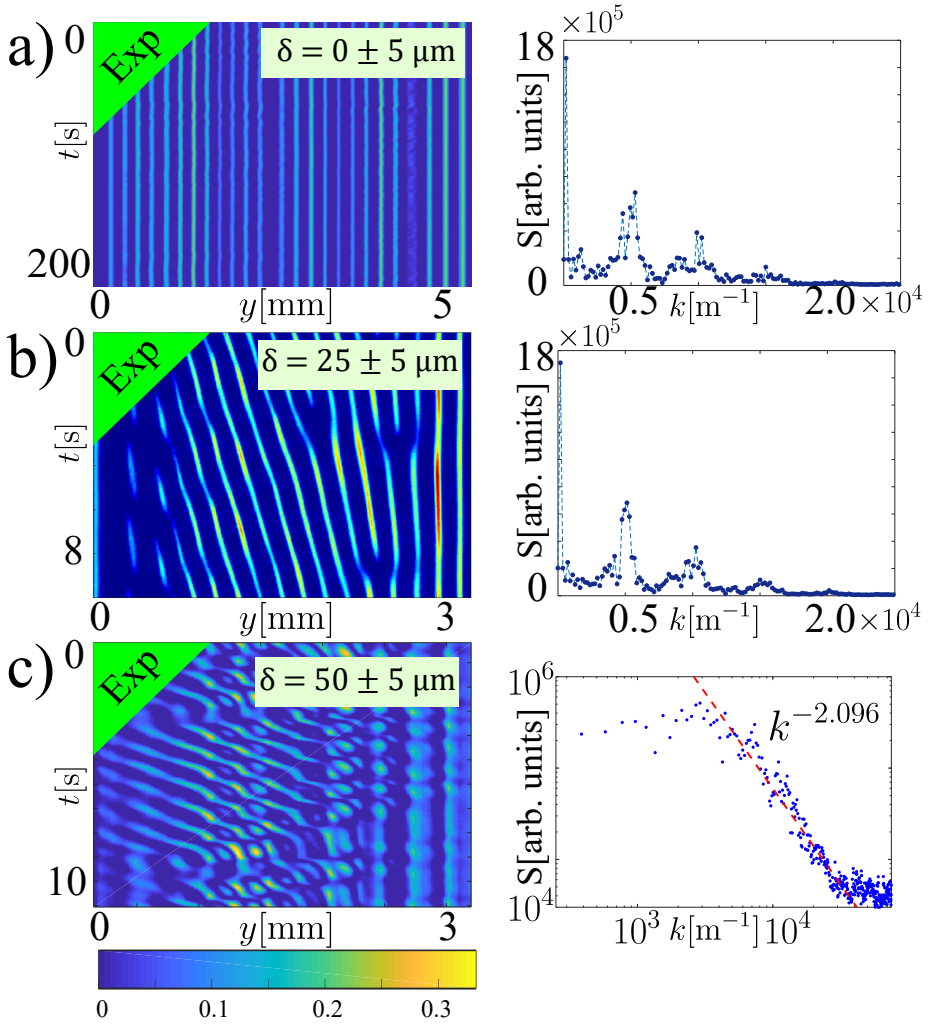

Figure 4.11: Spatiotemporal diagrams of patterns at different values of δ with their respective power density spectra.

Chapter 5

Route to the complexity

In the previous chapter, we showed that the generalized Swift-Hoheneberg equation can describe the molecular orientation in the Liquid crystal cell in some limit. This equation captures the emergence of stripped and hexagonal patterns in the experiment, however, due to its variational nature, it can not account for the complex spatiotemporal dynamics of the experiment. We showed that when the experiment is intentionally misaligned, it exhibits a transition from quasiperiodic behaviors to rather turbulent dynamics. To shed light on this complexity's origin, we consider a Swift-Hohenberg model with non-variational terms that account for the misalignment.

$$\partial_t u = \varepsilon\tilde{u} - \tilde{u} - \nu\nabla^2 u - \nabla^4 u, \tag{5.1}$$

where

$$\tilde{u} = u(\vec{r} + \vec{\delta}, t), \tag{5.2}$$

with $\vec{\delta}$ a constant vector. We refer to this equation as the Swift-Hohenberg equation with translational coupling (SHTC). It is possible to set the parameter ν equal to 1 by a re-scaling the time, the spatial coordinates the field u, so that the dynamics of equation (5.1) can be described only by the parameters ε and δ. We keep this parameter because it introduces a characteristic scale for the wavelength of the patterns, and thus, sets a limit for where our approximations remain valid. This equation was already studied to describe the effects of misalignment in localized structures by Francisco del Campo in his thesis [17, 30]. In his work, he reported the emergence of spatiotemporal intermittency, however, a full description of the origin of this complexity has not been made. The fact that the differential terms in equation 5.1 are not affected by the transnational coupling may seem like an arbitrary choice and not a completely realistic one. Recall that equation 5.1 is a prototype model for understanding the emergence of complexity in a general pattern-forming system and not a model of the liquid crystal light valve experiment.

In the first part of this chapter, we consider the one-dimensional SHTC. We explore its phenomenology and derive an amplitude equation that qualitatively accounts for its different dynamical regimes. In the second half, we briefly discuss the two-dimensional SHTC, and also talk about further generalizations of the one-dimensional SHTC. We finally relate this prototype model with the liquid crystal light valve experiment, and propose a modification to it.

5.1 The one-dimensional SHTC

5.1.1 Convective instability

Let us consider the one-dimensional SHTC

$$\partial_t u = \varepsilon\tilde{u} - \tilde{u} - \nu\partial_{yy}u - \partial_{yyyy}u, \tag{5.3}$$

where

$$\tilde{u} = u(y+\delta, t). \tag{5.4}$$

Equation (5.3) has a trivial homogeneous solution $u(y,t) = 0$, we start by studying the stability of this solution. We compute the dispersion relation for a perturbation δu to the homogeneous steady state

$$\delta u = \sum_q u_q \mathrm{e}^{\mathrm{i}qy+\lambda_q t}, \tag{5.5}$$

replacing this expression on the linear part of equation (5.3) we get the following relation

$$\lambda_{\vec{q}} = \varepsilon\mathrm{e}^{\mathrm{i}q\delta} + \nu q^2 - q^4. \tag{5.6}$$

We impose the conditions (2.9a) and (2.9b) for the system to have a Turing instability

$$0 = \varepsilon\cos(q\delta) + \nu q^2 - q^4, \tag{5.7a}$$
$$0 = \varepsilon\delta\sin(q\delta) + 2\nu q - 4q^3. \tag{5.7b}$$

These equations are difficult to solve algebraically. Since for the regular Swift-Hoheneberg equation $q_c \sim \sqrt{\nu}$, we expect that this also holds for the Swift-Hohenberg equation with translational coupling. It is reasonable then to expand $\cos(q\delta)$ and $\sin(q\delta)$ around $q = 0$

$$0 = \varepsilon + (\nu - \frac{\varepsilon\delta^2}{2})q^2 - (1 - \frac{\varepsilon\delta^4}{24})q^4 + O(q^6), \tag{5.8a}$$
$$0 = 2(\nu - \frac{\varepsilon\delta^2}{2})q - 4(\nu - \frac{\varepsilon\delta^4}{24})q^3 + O(q^5). \tag{5.8b}$$

We solve 5.8b and find an expression for q_c^2

$$q_c^2 = \frac{(\nu - \frac{\varepsilon\delta^2}{2})}{2(1 - \frac{\varepsilon\delta^4}{24})}. \tag{5.9}$$

Replacing (5.9) in (5.8a), we find a relation between ε and δ defining the curve of instability for the homogeneous steady state $u(y,t) = 0$

$$\delta_c = \sqrt{\frac{6\nu\varepsilon + 6|\varepsilon|\sqrt{\nu^2 - \frac{1}{3}(\nu^2 + 4\varepsilon)}}{\varepsilon^2}}. \tag{5.10}$$

This approximation remains fairly good when $\varepsilon \sim \nu^2$ or smaller. By making the transformation $\varepsilon = \nu^2\varepsilon'$, with ε' of order $O(1)$, we found that $\delta_c \sim \nu^{-1/2}$. The approximate instability

curve given by (5.10) is depicted in figure 5.1 along with the numerical solutions of equations 5.7 for $\nu = 1$. According to (5.9), the critical wavelength λ_c fulfills

$$\lambda_c = \frac{2\pi}{q_c} \approx \frac{10}{\sqrt{\nu}}, \tag{5.11}$$

$$\Rightarrow \frac{\delta_c}{\lambda_c} \sim \frac{1}{10}. \tag{5.12}$$

We conclude taht the instability happens when transnational coupling length is a fraction of the wavelength of the pattern. In the next section we show this enough for finding complex spatiotemproal dynamics.

The imaginary part of (5.6)

$$\mathrm{Im}\{\lambda_q\} = \varepsilon \sin q\delta. \tag{5.13}$$

Since this corresponds to an odd function of q, a traveling wave emerges when the instability threshold for the homogeneous steady state is reached. Thus, we say the instability is convective.

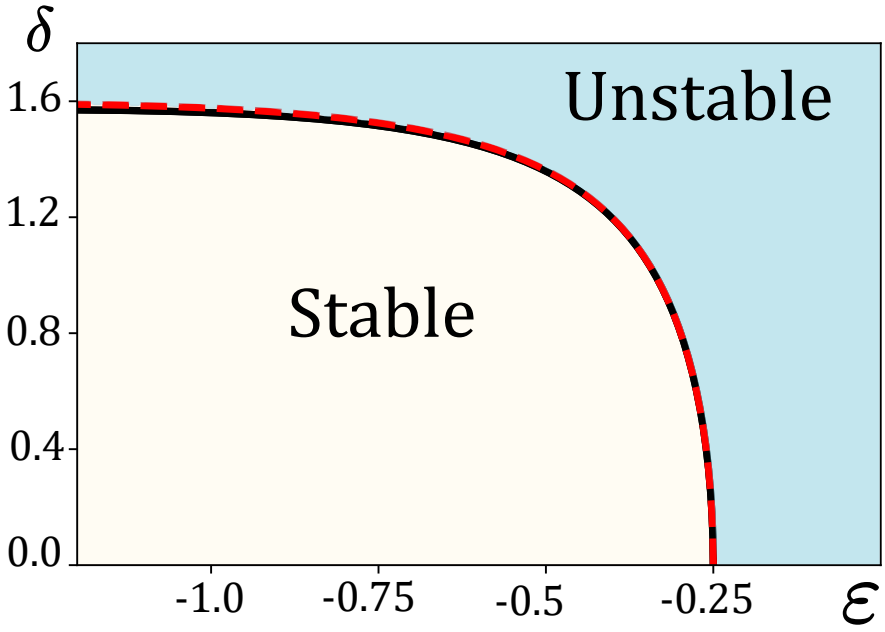

Figure 5.1: Stability limit for the homogeneous steady state $u(y,t) = 0$ to perturbations of finite wavelength for $\nu = 1$. The solid black curve correspond to the numerical solution $\delta(\varepsilon)$ of equations 5.7a and 5.7b. The dashed red curve correspond to the approximation given 5.10.

5.1.2 Phenomenology of states

We start by exploring the phenomenology of 5.1 for different values of ε and δ in the region where the homogeneous steady state is convectively unstable. We restrict to the case having $\nu = 1$ and impose periodic boundary conditions to the simulations. We also compute the envelope through the Hilbert transform, which is given by

$$\mathcal{H}(y,t) = 2\left| \int_0^\infty \mathrm{e}^{\mathrm{i}qy} \int_{-\infty}^\infty u(y',t)\mathrm{e}^{-\mathrm{i}qy'}\mathrm{d}y'\mathrm{d}q \right|. \tag{5.14}$$

Spatiotemporal diagrams of $u(y,t)$ for different regions of the $\varepsilon - \delta$ parameter space are

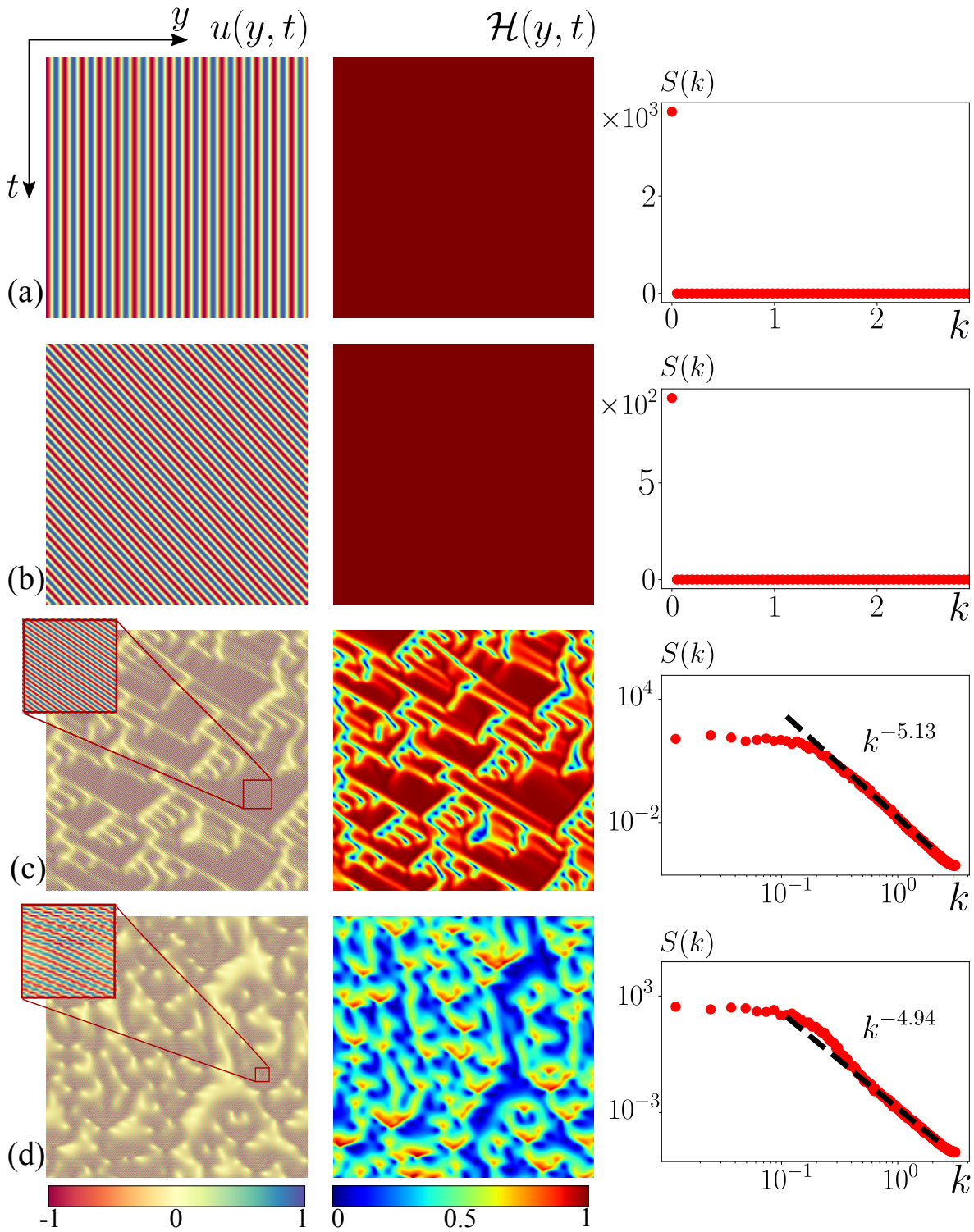

Figure 5.2: Spatiotemporal evolution of patterns in the Swift- Hohenberg model with translational coupling 5.1. The left, center, and right panels are spatiotemporal diagrams of $u(y,t)$, envelope $\mathcal{H}(y,t)$ of the patterns, and the temporal average power spectra S of the envelope, for (a) $\varepsilon = -0.08, \delta = 0.0$, (b)$\varepsilon = -0.3, \delta = 1.0$ (c) $\varepsilon = -0.3, \delta = 1.35$, and (d)$\varepsilon = -0.8, \delta = 1.51$. The insets illustrate a magnification of the temporal space diagram.

depicted in figure 5.2. We observe that complex spatiotemporal dynamics arises for high values of δ. Two different complex regimes can be distinguished: spatiotemporal intermittency and defect turbulence. The first regime is characterized by regions of a finite size separated by holes where the patterns' amplitude remains homogeneous. The second regime corresponds to a more isotropic state, where the dynamics are dominated by the appearance and disappearance of holes in a background pattern, leaving no extended laminar regions. We considered the the fraction $\chi = \delta/\lambda_p$, where λ_p is the wavelength of the background pattern. We found that $\chi = 0.18$ for the state represented in figure 5.2-c, and $\chi = 0.22$ for the state depicted in 5.2-d, which is consistent with what we concluded in the previous section.

5.1.3 Normal form

To elucidate the origin of the complex spatiotemporal dynamics, we derive an amplitude equation close to the homogeneous state's convective instability limit. Let q_c, ε_c and δ_c be solutions of (5.7). We introduce a perturbation to the parameters

$$\varepsilon = \varepsilon_c + \Delta\varepsilon, \tag{5.15}$$

$$\delta = \delta_c + \Delta\delta. \tag{5.16}$$

Now we propose the following Ansatz to equation (5.3)

$$u(y,t) = A(y_1,t)\mathrm{e}^{\mathrm{i}q_c y} + \bar{A}(y_1,t)\mathrm{e}^{\mathrm{i}q_c y} + W(A,\bar{A}), \tag{5.17}$$

$$y_1 = \xi y, \tag{5.18}$$

with ξ a dummy scaling parameter. Replacing the Ansatz, the left hand side of the equation reads

$$\partial_t A\mathrm{e}^{\mathrm{i}q_c y} + \partial_t \bar{A}\mathrm{e}^{-\mathrm{i}q_c y} + \frac{\partial W}{\partial A}\frac{\partial A}{\partial t} + \frac{\partial W}{\partial \bar{A}}\frac{\partial \bar{A}}{\partial t}. \tag{5.19}$$

The eigenvalues of the critical modes have non-zero imaginary parts given by (5.13), then to the lowest order in A we expect $\partial_t A \approx \mathrm{i}\Omega A$. By using this approximation, the left-hand side reads

$$\partial_t A\mathrm{e}^{\mathrm{i}q_c y} + \partial_t \bar{A}\mathrm{e}^{-\mathrm{i}q_c y} + \mathcal{G}W(A,\bar{A}). \tag{5.20}$$

$$\mathcal{G} = \mathrm{i}\Omega\left(A\frac{\partial}{\partial A} - \bar{A}\frac{\partial}{\partial \bar{A}}\right). \tag{5.21}$$

Since Ω is not a small parameter, then we can not neglect the time derivative of W in the equation. After replacing the Ansatz on the right hand side of (5.3), rearranging terms, and using (5.8a) and (5.7b) we get

$$\begin{aligned}\mathcal{L}W(A,\bar{A}) = [&\mathrm{i}\varepsilon_c \sin q_c\delta_c A + (\Delta\varepsilon\cos q_c\delta_c - \varepsilon_c q_c \Delta\delta_c \sin q_c\delta_c)A + \xi\varepsilon_c\delta_c\cos q_c\delta_c\partial_{y_1}A \\ &+ \xi^2(6q_c^2 - \nu + \frac{\varepsilon_c\delta_c^2}{2}\mathrm{e}^{\mathrm{i}q_c\delta_c})\partial_{y_1y_1}A - 3\mathrm{e}^{\mathrm{i}q_c\delta_c}A|A|^2 - \partial_t A]\mathrm{e}^{\mathrm{i}q_c y} \\ &- \mathrm{e}^{3\mathrm{i}q_c\delta_c}A^3\mathrm{e}^{3\mathrm{i}q_c y} + c.c. + O(\xi^3),\end{aligned} \tag{5.22}$$

where

$$\mathcal{L} = \mathcal{G} - \mathcal{L}_0, \tag{5.23}$$

$$\mathcal{L}_0 = \varepsilon\mathrm{e}^{\delta\partial_y} - \nu\partial_{yy} - \partial_{yyyy}. \tag{5.24}$$

The operator $\mathcal{L}_0$ operates only on functions of the fast variable y, while $\mathcal{G}$ only does it on the amplitudes of the critical modes. To apply the solvavility condition to (5.22) we need to introduce a proper inner product [78, 8]

$$f(y,A,\bar{A})\cdot g(y,A,\bar{A}) = \frac{2}{q_c}\int_{y_0}^{y_0+\frac{2\pi}{q_c}}\left[\int_{\mathbb{C}} \mathrm{e}^{-|A|^2} f(y,A,\bar{A})\bar{g}(y,A,\bar{A})\mathrm{d}u\mathrm{d}v\right]\mathrm{d}y, \tag{5.25}$$

where $A = u + \mathrm{i}v$ and the second integral is taken into the whole complex plane. Under this inner product, the adjoint of the operator $\sigma_A = A$ is $\sigma_A^\dagger = \frac{\partial}{\partial A}$. These operators can be regarded as creation and annihilation operators in a Segal-Bargmann space [78, 8]. Using this inner product we can compute the adjoints of $\mathcal{G}$ and $\mathcal{L}_0$, which are given by

$$\mathcal{G}^\dagger = -\mathrm{i}\Omega\left(A\frac{\partial}{\partial A} - \bar{A}\frac{\partial}{\partial \bar{A}}\right). \tag{5.26}$$

$$\mathcal{L}_0^\dagger = \varepsilon \mathrm{e}^{-\delta\partial_y} - \nu\partial_{yy} - \partial_{yyyy}. \tag{5.27}$$

Let us consider the actions of $\mathcal{H}^\dagger$ and $\mathcal{L}_0^\dagger$ on a function of the form $A|A|^m\mathrm{e}^{\mathrm{i}q_c y}$ with $m \in \mathbb{Z}$

$$\mathcal{G}^\dagger A|A|^m\mathrm{e}^{\mathrm{i}q_c y} = -\mathrm{i}\Omega[(m+1)A|A|^m - mA|A|^m]\mathrm{e}^{\mathrm{i}q_c y} = -\mathrm{i}\Omega A|A|^m\mathrm{e}^{\mathrm{i}q_c y}, \tag{5.28}$$

$$\mathcal{L}_0^\dagger A|A|^m\mathrm{e}^{\mathrm{i}q_c y} = -\mathrm{i}\Omega A|A|^m\mathrm{e}^{\mathrm{i}q_c y}, \tag{5.29}$$

then we have

$$\mathcal{L}^\dagger A|A|^m\mathrm{e}^{\mathrm{i}q_c y} = (\mathcal{G}^\dagger - \mathcal{L}_0^\dagger)A|A|^m\mathrm{e}^{\mathrm{i}q_c y} = 0. \tag{5.30}$$

Analogously, if we consider the actions of $\mathcal{H}^\dagger$ and $\mathcal{L}_0^\dagger$ on $\bar{A}|A|^m\mathrm{e}^{-\mathrm{i}q_c y}$ we have

$$\mathcal{L}^\dagger \bar{A}|A|^m\mathrm{e}^{-\mathrm{i}q_c y} = 0. \tag{5.31}$$

Since we have found the Kernel of $\mathcal{L}^\dagger$, we can apply the solvability condition to equation (5.22) and derive an equation for the evolution of A. After returning to the original coordinates, we get

$$\partial_t A = (\mu + \mathrm{i}\Omega)A - 3\mathrm{e}^{\mathrm{i}q_c\delta_c}|A|^2 A + \tilde{D}\partial_{yy}A + v\partial_y A, \tag{5.32}$$

where

$$\mu = \Delta\varepsilon\cos q_c\delta_c - \varepsilon_c q_c\Delta\delta\sin q_c\delta_c, \tag{5.33a}$$

$$\tilde{D} = 6q_c^2 - \nu + \frac{\varepsilon_c\delta_c^2}{2}\mathrm{e}^{\mathrm{i}q_c\delta_c}, \tag{5.33b}$$

$$v = \varepsilon_c\delta_c\cos q_c\delta_c. \tag{5.33c}$$

Even though the term proportional to $\partial_{yy}A$ is of a higher order than the drift term $v\partial_y A$, we keep it on the equation because, under periodic boundary conditions, the drift term can be eliminated by expressing the equation from a moving reference frame having the group velocity v. A more realistic model should have von Neumann or Dirichlet boundary conditions instead of periodic ones. In these scenarios, the amplitude equation is still valid far away from the boundaries, but it is not possible to express the equation in a moving frame because the translational symmetry is broken. We can renormalize the amplitude and the spatial coordinate y

$$A \to \sqrt{\frac{1}{3\cos q_c\delta_c}}B\mathrm{e}^{\mathrm{i}\omega t}, \tag{5.34}$$

$$y \to \sqrt{\frac{1}{6q_c^2 - \nu + \frac{\varepsilon_c \delta_c^2}{2} \cos q_c \delta_c}} Y, \tag{5.35}$$

the amplitude equation reads

$$\partial_t B = \mu B - (1 + \mathrm{i}\beta)|B|^2 B + (1 + \mathrm{i}\alpha)\partial_{YY} B + v' \partial_Y B, \tag{5.36}$$

where

$$\alpha = \frac{\sin q_c \delta_c}{6q_c^2 - \nu + \frac{\varepsilon_c \delta_c^2}{2} \cos q_c \delta_c} \tag{5.37a}$$

$$\beta = \tan q_c \delta_c \tag{5.37b}$$

$$v' = \frac{v}{\sqrt{6q_c^2 - \nu + \frac{\varepsilon_c \delta_c^2}{2} \cos q_c \delta_c}} \tag{5.37c}$$

Having α and β as functions of ε and δ allow us to map the bifurcation diagram of the complex Ginzburg-Landau equation into the $\varepsilon - \delta$ parameter space **close** to the instability curve as depicted in figure 5.3-a. The brown striped region in Figure 5.3-a corresponds to the zone where the parameters α and β are within the curve L_2 and the Benjamin-Fir curve in Figure 5.3-b. In this region, it possible to find spatiotemporal intermittency and traveling waves depending on the initial conditions. Recall the mechanism that gives rise to spatiotemporal intermittency, perturbations to the traveling waves may create holes in the pattern. These holes are unstable in this region of the parameter, and they can either fade out, or a phase slip event happens in the core of the hole, which nucleates a new defect, the new. Further up, traveling waves having a homogeneous envelope are no longer stable, so the system constantly creates and destroys holes in the pattern, leaving no laminar patches between them. We showed that the transition curves predicted by the Ginzburg-Landau normal form match well with the transitions points we have found by direct numerical simulations, which are represented by the red dot in figure 5.3-a. The figure 5.3-b is the bifurcation diagram of the complex Ginzburg-Landau equation, already presented in chapter 3. The solid red curve within this diagram corresponds to the mapping of $\alpha(\varepsilon_c, \delta_c(\varepsilon_c))$ and $\beta(\varepsilon_c, \delta_c(\varepsilon_c))$. Consistently with what we expect, this curve converges to the origin when $\varepsilon_c \to -0.25$ and $\delta_c \to 0$. For high values of δ_c the function $\beta(\varepsilon_c, \delta_c(\varepsilon_c))$ quickly diverges while $\alpha(\varepsilon_c, \delta_c(\varepsilon_c))$ remains a slow-growing function. Since the Benjamin-Feir and the L_1 curves match asymptotically for $\beta \to -\infty$ in the bifurcation of the complex Ginzburg-Landau equation, we do not observe a phase turbulence region; instead, we the observe a direct transition from spatiotemporal intermittency to defect turbulence.

5.2 Two dimensional SHTC

5.2.1 Convective instability

Let us now consider a two-dimensional Swift-Hohengerg equation with transnational coupling

$$\partial_t u = \varepsilon \tilde{u} - \tilde{u}^3 - \nabla^2 u - \nabla^4 u, \tag{5.38}$$

where

$$\tilde{u} = u(x, y + \delta, t). \tag{5.39}$$

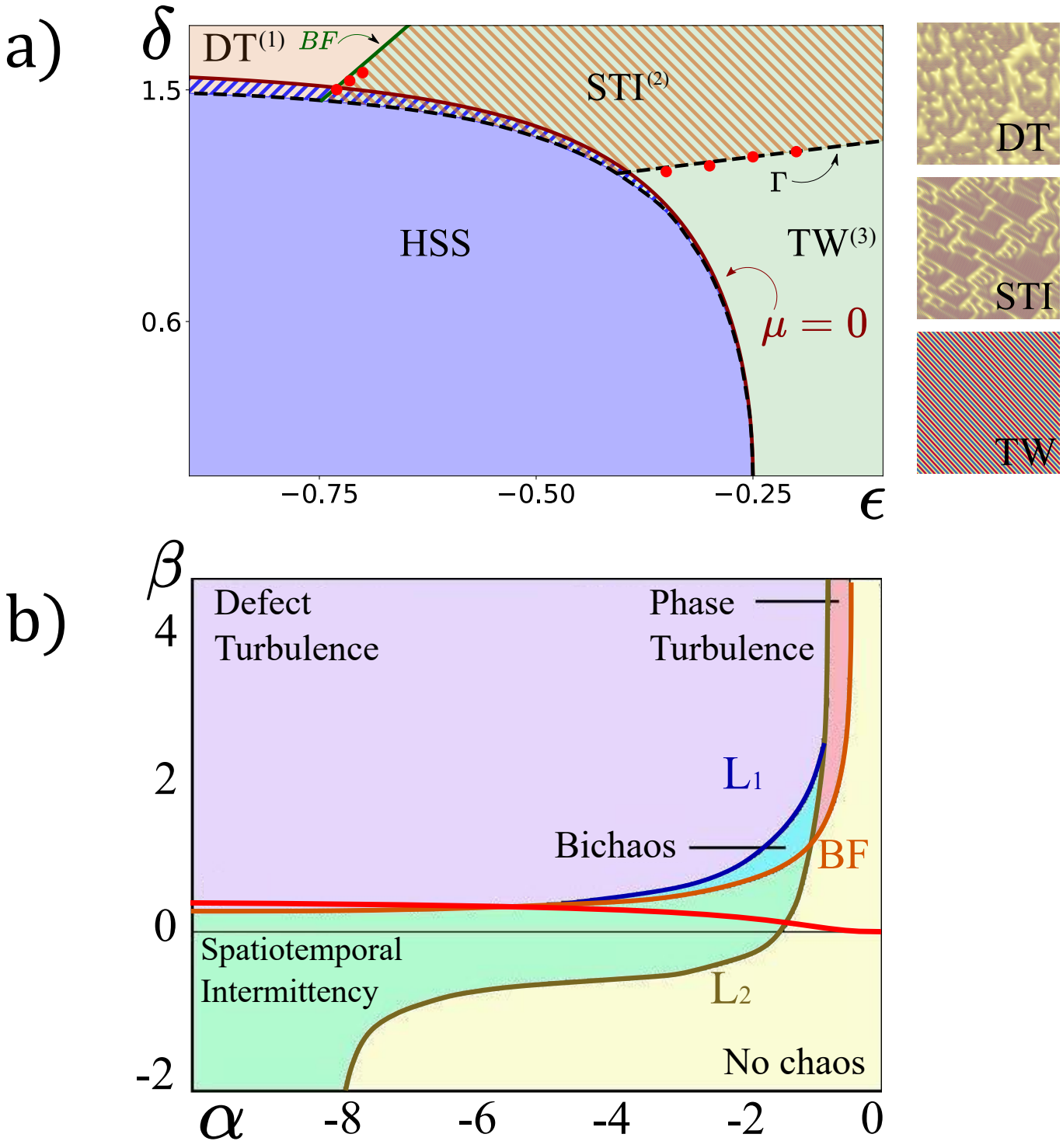

Figure 5.3: a) Bifurcation diagram of equation 5.1 for $\nu = 1$. HSS, TW STI, and DT stand for homogeneous steady state, traveliing wave, spatiotemporal intermittency, and defect turbulence respectively. The red dots correspond to the transition lines obtained by direct numerical simulations b) Bifurction diagram of the one dimensional complex Ginzburg-Landau equation. The red solid curve correspond to the mapping of $\alpha(\varepsilon_c, \delta_c(\varepsilon_c))$ and $\beta(\varepsilon_c, \delta_c(\varepsilon_c))$

Computing the dispersion relation we have

$$\lambda_{\vec{q}} = \mathrm{e}^{\mathrm{i}q_y\delta} + \nu q^2 - q^4. \tag{5.40}$$

The conditions for the Turing instabily read

$$0 = \varepsilon \cos q_y\delta + \nu q^2 - q^4, \tag{5.41}$$

$$0 = \varepsilon\delta \sin q_y\delta + 2\nu q - 4q^3. \tag{5.42}$$

Equation 5.41 reveals that the homogeneous steady state is more sensible to perturbation in y direction since when $\varepsilon < 0$, this is represented in figure 5.4. The convective instability is given by the same expression as the one-dimensional case (see figure 5.1). When reaching the threshold of instability, only two modes lose stability rather than a continuum of modes. Thus, close to instability we expect the emergence of a traveling wave in the y direction.

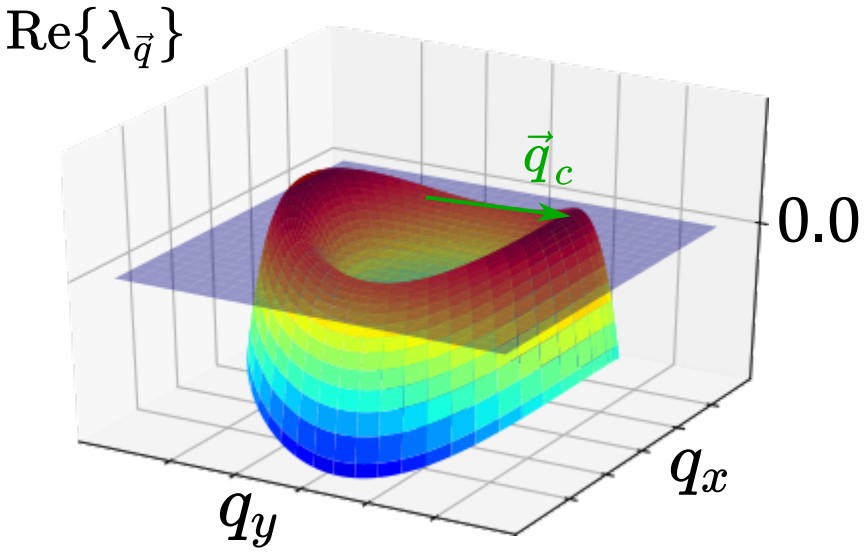

Figure 5.4: Turing instability for two dimensional Swift-Hohenberg with translational coupling

5.2.2 Phenomenonlogy of states

We have conducted simulations of equation 5.38 under periodic boundary conditions close to the instability curve considering $\nu = 1$. We used a random state as an initial condition. For values of δ ranging from 0 to around 1.3, we observe that the random initial condition first develops into a labyrinth pattern resembling figure 2.6. These labyrinths slowly evolve into a single traveling wave in the y direction. Depending on the initial conditions, bounded pairs of dislocations can be formed. When reaching the equilibrium state, these bounded states travel as rigid bodies along with the pattern at a constant speed. Starting from $\delta \sim 1.3$, we observe that system evolves into a background traveling wave in the y direction, but dislocations are constantly being created and destroyed, this is depicted in figure 5.5. We kept track of a traversal segment of the pattern; its spatiotemporal diagram resembles a distorted Sierpinski carpet, suggesting we face a rather intermittent state.

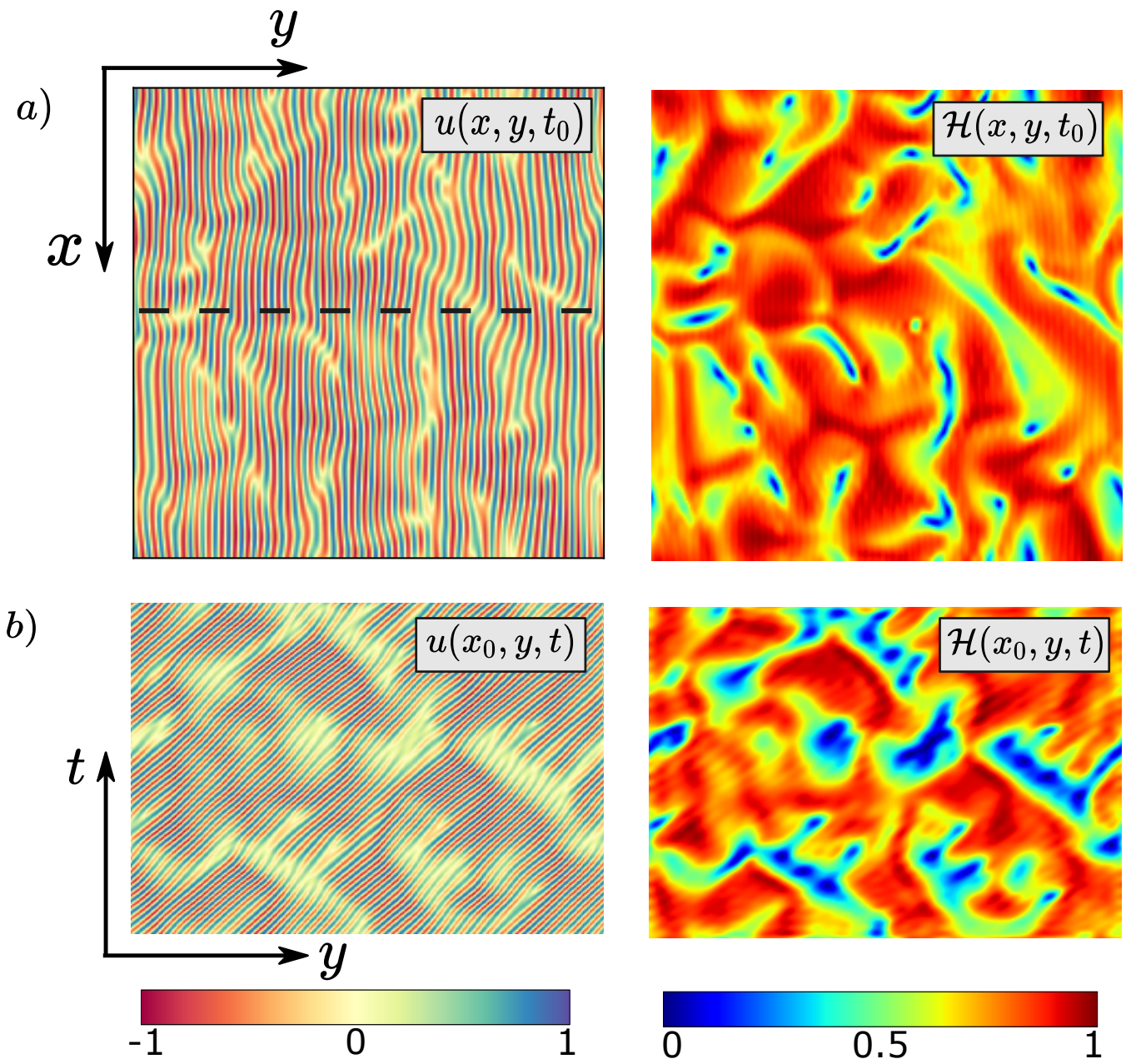

Figure 5.5: a)Snapshot of the two-dimensional SHTC in the region where is constant creation and destruction of defects and int envelope computed using the Hilbert transform. b) Spatiotemporal evolution with its envelope of the dashed black segment in the snapshot of the pattern.

5.2.3 Normal form

We propose the following Ansatz

$$u(x, y, t) = A(x_1, y_1, t)\mathrm{e}^{\mathrm{i}q_c y} + \bar{A}(x_1, y_1, t)\mathrm{e}^{-\mathrm{i}q_c y} + W(a, \bar{A}), \tag{5.43}$$

where

$$x_1 = \xi_1 x, \tag{5.44}$$

$$y_1 = \xi_2 y. \tag{5.45}$$

We get

$$\mathcal{L}W(A,\bar{A}) = [\mathrm{i}\varepsilon_c \sin q_c\delta_c A + (\Delta\varepsilon\cos q_c\delta_c - \varepsilon_c q_c \Delta\delta_c \sin q_c\delta_c)A + \xi_2\varepsilon_c\delta_c\cos q_c\delta_c\partial_{y_1}A + \xi_2^2(6q_c^2 - \nu + \frac{\varepsilon_c\delta_c^2}{2}\mathrm{e}^{\mathrm{i}q_c\delta_c})\partial_{y_1y_1}A - 3\mathrm{e}^{\mathrm{i}q_c\delta_c}A|A|^2 + \xi_1^2(2q_c^2-\nu)\partial_{x_1x_1}A - \partial_t A]\mathrm{e}^{\mathrm{i}q_c y} - \mathrm{e}^{3\mathrm{i}q_c\delta_c}A^3\mathrm{e}^{3\mathrm{i}q_c y} + c.c., \tag{5.46}$$

where

$$\mathcal{L} = \mathcal{G} - (\varepsilon\mathrm{e}^{\delta\partial_y} - \nu\nabla^2 - \nabla^4). \tag{5.47}$$

Differently from the regular Swift-Hohenberg equation, the term $(2q_c^2 - \nu)$ in (5.46) does not vanish,

$$(2q_c^2-\nu) \approx \frac{\nu\varepsilon_c\delta_c^2}{2}(\frac{\delta_c^2}{12} - 1). \tag{5.48}$$

If we are on a region where $\delta_c^2 < 12$, then $(2q_c^2 - \nu) > 0$ since $\varepsilon_c < 0$. We can neglect higher powers of ξ_1 in equation (5.46). Applying the solvavility condition an returning to the original coordinates we have

$$\partial_t A = (\mu + \mathrm{i}\Omega)A - 3\mathrm{e}^{\mathrm{i}q_c\delta}|A|^2A + D_1\partial_{xx}A + \tilde{D}_2\partial_{yy}A + v\partial_y A, \tag{5.49}$$

where

$$D_1 = (2q_c^2 - \nu), \tag{5.50}$$

and

$$\tilde{D}_2 = (6q_c^2 - \nu + \frac{\varepsilon_c\delta_c^2}{2}\cos(q_c\delta_c)\mathrm{e}^{\mathrm{i}q_c\delta_c}). \tag{5.51}$$

We introduce the following rescalings

$$A = \frac{1}{\sqrt{3\cos(q_c\delta_c)}}B, \tag{5.52a}$$

$$X = \frac{1}{\sqrt{D_1}}x, \tag{5.52b}$$

$$Y = \frac{1}{\sqrt{\mathrm{Re}\{\tilde{D}_2\}}}y \tag{5.52c}$$

we then get

$$\partial_t B = \mu B - (1+\mathrm{i}\beta)|A|^2A + \nabla'^2A + \mathrm{i}\alpha\partial_{YY}A + v'\partial_y A, \tag{5.53}$$

where

$$\nabla'^2 = \partial_{XX} + \partial_{YY}, \tag{5.54a}$$

$$\alpha = \frac{\sin q_c\delta_c}{6q_c^2 - \nu + \frac{\varepsilon_c\delta_c^2}{2}\cos q_c\delta_c}, \tag{5.54b}$$

$$\beta = \tan q_c\delta_c, \tag{5.54c}$$

$$v' = \frac{v}{\sqrt{6q_c^2 - \nu + \frac{\varepsilon_c\delta_c^2}{2}\cos q_c\delta_c}} \tag{5.54d}$$

This corresponds to a particular case of the anisotropic Ginzburg-Landau equation [6, 16]. Note that the parameters α and β have the same expressions as the one-dimensional SHTC. We computed these parameters in the regions where the solution SHTC converges into an almost homogeneous traveling wave, and where it has a permanent complex spatiotemporal dynamics. We then conducted simulations of the anisotropic Ginzburg-Landau equation using the computed parameter. For the first regime, we observe that the anisotropic Ginzburg-Landau converges into a solution having a homogeneous envelope $|A|$. On the other hand, in the complex regime, the anisotropic Ginzburg-Landau equation exhibit constant creation and destruction of spiral emitting holes. The bifurcation diagram of the anisotropic Ginzburg-Landau equation has not been fully characterized. Differences in the region of phase chaos respect to the isotropic Ginzburg-Landau equation have been reported [34]; nevertheless, a complete description of its other complex dynamical regimes has not been done. The anisotropic Ginzburg-Landau equation does not capture bounded states. These phenomenon has been reported in other anisotropic pattern-forming systems [89]. Amended amplitude equations with non-resonant terms that account for the background pattern have been derived in these systems. These terms successfully explain the bounding. We have not characterized the bifurcation diagram of the two-dimensional SHTC.

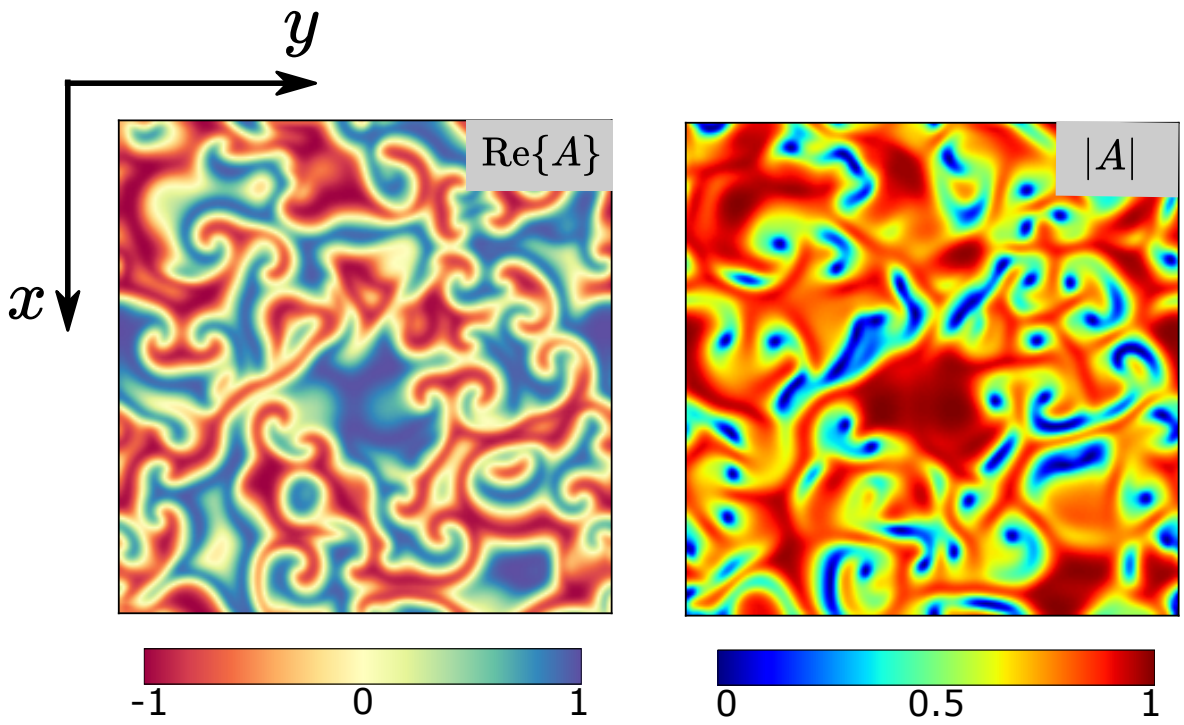

Figure 5.6: Snapshot of the anistropic Ginzburg-Landau in region of creation and destruction of spiral emitting holes for $\alpha = 0.15$ and $\beta = -2.0$.

5.3 Generalizations

A translational coupling can be regarded as a particular case of a more general kind of non-local interaction. Pattern-forming systems can have long-range interactions, which are modeled by means of integral Kernels. This kind of couplings has been introduced in reaction-diffusion models that describe vegetation patterns and population dynamics [56, 12]. We

show that transition from traveling waves to complex spatiotemporal dynamics can also be found in pattern-forming systems with asymmetric long-ranged interactions. Let us consider a Swift-Hoheneberg model with an interaction Kernel

$$\partial_t u = \varepsilon\tilde{u} - \tilde{u}^3 - \nu\partial_{yy} - \partial_{yyyy}u, \tag{5.55}$$

where

$$\tilde{u}(y,t) = \int_{-\infty}^{\infty} G(z,\vec{p})u(y+z)\mathrm{d}z. \tag{5.56}$$

The vector $\vec{p}$ correspond to the parameters that characterize each kernel, Note that is we choose $G(z,\delta) = \delta(z-\delta)$, we recover the Swift-Hoheneberg model with translational coupling.

For illustrative purposes, we conducted simulations using two different asymmetric integral kernels: A shifted uniform distribution, and a slightly asymmetric Gaussian function (see figure 5.7-a)

$$G_1(z)\begin{cases}\frac{1}{\sigma} & \text{if} \quad z\in[-\sigma/2+\delta,\sigma/2+\delta],\\ 0 & \text{else.}\end{cases} \tag{5.57}$$

$$G_2(z) = (1+bz)\mathrm{e}^{-(x/\sigma)^2}. \tag{5.58}$$

We observe that when the parameter that characterizes the asymmetry of the Kernels is tuned, δ for $G_1(z)$, and b for $G_2(z)$), we encounter the same kind of transitions we found in the one-dimensional SHTC. Spatiotemporal diagrams of the patterns observed and their envelopes are depicted in figure 5.7-b-c To generalize the previous results of this chapter, we compute the dispersion relation (5.55) for and arbitrary Kernel $G(z)$

$$\lambda_q = \varepsilon\int_{\infty}^{\infty} G(z,\vec{p})\mathrm{e}^{\mathrm{i}qz}\mathrm{d}z + \nu q_c^2 - q_c^4, \tag{5.59}$$

separating between real and imaginary parts we have

$$\mathrm{Re}\{\lambda_q\} = \varepsilon\int_{\infty}^{\infty} G(z,\vec{p})\cos(qz)\mathrm{d}z, + \nu q_c^2 - q^4, \tag{5.60}$$

$$\mathrm{Im}\{\lambda_q\} = \int_{\infty}^{\infty} G(z\vec{p})\sin(qz)\mathrm{d}z. \tag{5.61}$$

It is always possible to separate $G(z,\vec{p})$ into its symmetric and antisymmetric parts

$$G^S = \frac{G(z,\vec{p}) + G(-z,\vec{p})}{2}, \tag{5.62}$$

$$G^{AS} = \frac{G(z,\vec{p}) - G(-z,\vec{p})}{2}. \tag{5.63}$$

Using parity properties we have

$$\mathrm{Re}\{\lambda_q\} = \varepsilon\int_{\infty}^{\infty} G^S(z,\vec{p})\cos(qz)\mathrm{d}z + \nu q_c^2 - q^4, \tag{5.64a}$$

$$\mathrm{Im}\{\lambda_q\} = \int_{\infty}^{\infty} G^{AS}(z,\vec{p})\sin(qz)\mathrm{d}z. \tag{5.64b}$$

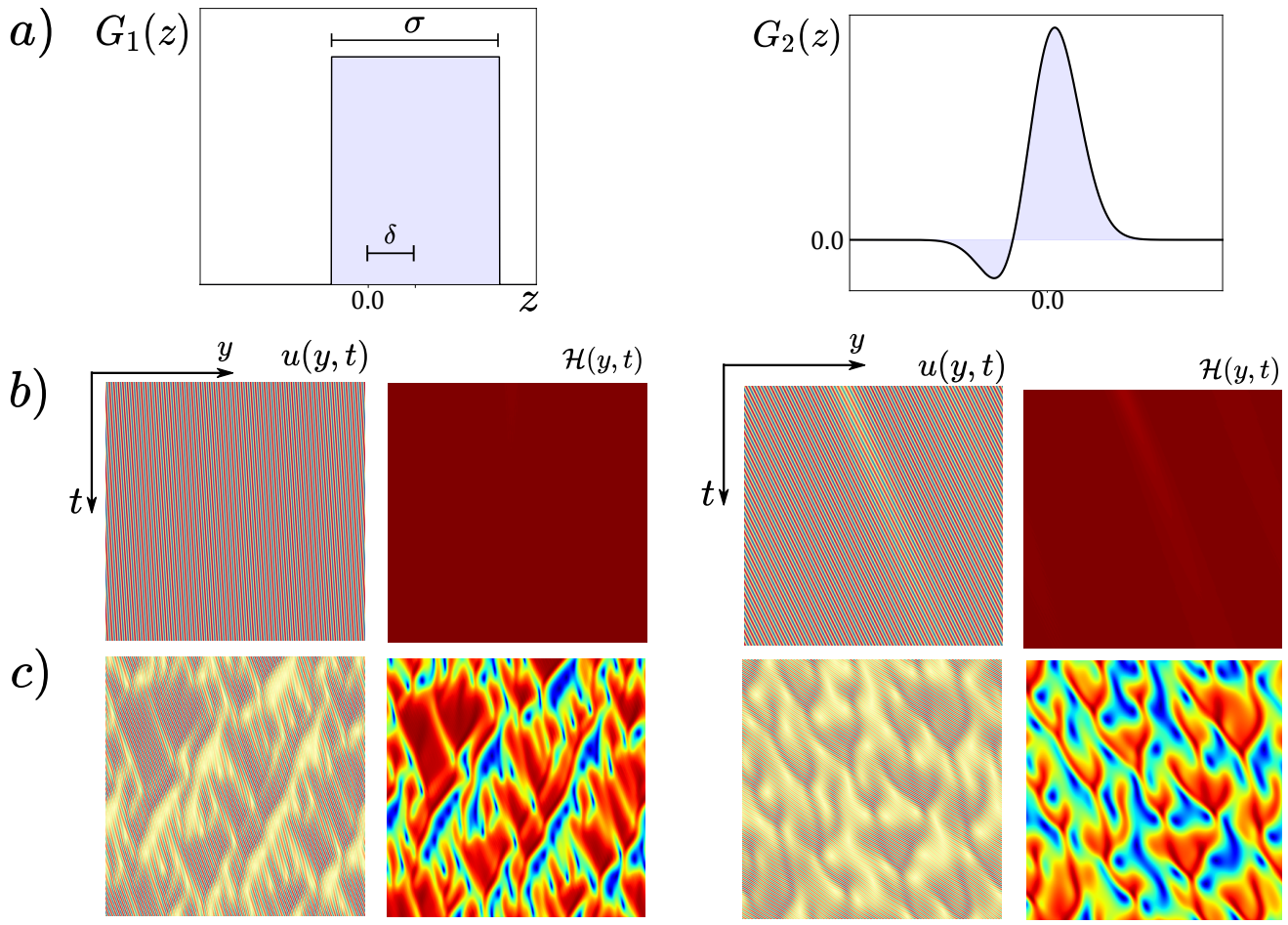

Figure 5.7: a) Plot of the different Kernels used in the numerical simulations. b) Traveling waves' regime for both Kernels; $\sigma =$ and $\delta =$ for $G_1(z)$; $\sigma =$ and $b =$ for $G_2(z)$. c) Spatiotemporal inttermittency regime for both kernels; $\sigma =$ and $\delta =$ for $G_1(z)$; $\sigma =$ and $b =$ for $G_2(z)$.

For simplicity we assume $G(z,\vec{p})$ is a rapid decaying function so that $\int_{-\infty}^{\infty} z^n G(z,\vec{p})\mathrm{d}z$ remains finite for $n \in \mathbb{N}_0$, this is refered as weak interaction [33]. We can expand (5.64a) around $q = 0$, and impose (2.9a) and (2.9b)

$$0 = \varepsilon + (\nu - \varepsilon\kappa_2)q^2 - (1 - \varepsilon\kappa_4)q^4 + O(q^6), \tag{5.65a}$$
$$0 = 2(\nu - \varepsilon\kappa_2)q_c - 4(1 - \varepsilon\kappa_4)q_c^3 + O(q^5), \tag{5.65b}$$

where

$$\kappa_n = \frac{1}{n!}\int_{-\infty}^{\infty} z^n G(z,\vec{p})\mathrm{d}z. \tag{5.66}$$

It is in principle possible to find solutions to equations (5.65a) and (5.65b) which depend on the shape of $G(z)$. In the other hand we have that after the expansion, the expression (5.64b) reads

$$\mathrm{Im}\{\lambda_q\} = \int_{\infty}^{\infty} G^{AS}(z,\vec{p})\sin(qz)\mathrm{d}z = \kappa_1 q + O(q^3), \tag{5.67}$$

which is always an odd function of q when $G^{AS} \neq 0$. This means that if the system has a

Turing instability, it will always be of a convective nature when the interaction Kernel has an antisymmetric part.

Assuming we choose the parameters ε and $\vec{p}$ so that we are close to the convective instability, we propose the following Ansatz

$$u(y,t) = A(y,t)\mathrm{e}^{\mathrm{i}q_c y} + \bar{A}(y,t)\mathrm{e}^{-\mathrm{i}q_c y} + W(A,\bar{A}). \tag{5.68}$$

The following approximation can be made

$$\int_{\infty}^{\infty} G(z,\vec{p})A(y+z)\mathrm{e}^{\mathrm{i}q_c(y+z)} \approx \gamma_0 A(y,t)\mathrm{e}^{\mathrm{i}q_c y} + \gamma_1 \partial_y A\mathrm{e}^{\mathrm{i}q_c y} + \gamma_2 \partial_{yy} A\mathrm{e}^{\mathrm{i}q_c y}. \tag{5.69}$$

where

$$\gamma_n = \frac{1}{n!}\int_{-\infty}^{\infty} z^n G(z,\vec{p})\mathrm{e}^{\mathrm{i}q_c z}\mathrm{d}z. \tag{5.70}$$

We also define the following linear operator

$$\mathcal{L} = \mathcal{G} - \left(\varepsilon\int_{\infty}^{\infty} G^S(z,\vec{p})\{\cdot\}(y+z)\mathrm{d}z - \nu\partial_{yy} - \partial_{yyyy}\right). \tag{5.71}$$

which is analogous to the operator defined at (5.23). Replacing the Ansatz on (5.55) and rearranging terms, we get

$$\begin{aligned}\mathcal{L}W(A,\bar{A}) = [&\mathrm{iRe}\{\gamma_0\}A + \mu A + \xi\mathrm{Re}\{\gamma_1\}\partial_{y_1}A + \xi^2(6q_c^2 - \nu + \gamma_2)\partial_{y_1y_1}A \\ &- 3|\gamma_0|^2\gamma_0 A|A|^2 - \partial_t A]\mathrm{e}^{\mathrm{i}q_c y} - \mathrm{e}^{3\mathrm{i}q_c\delta_c}A^3\mathrm{e}^{3\mathrm{i}q_c y} + c.c. + O(\mu^3).\end{aligned} \tag{5.72}$$

Applying the solvability condition, we again get a cubic complex Ginzburg-Landau equation

$$\partial_t A = \mu A + \mathrm{i}\Omega A - 3|\gamma_0|^2\gamma_0|A|A^2 + \tilde{D}\partial_{yy}A + v\partial_y A, \tag{5.73}$$

where

$$\Omega = \int_{-\infty}^{\infty} G^{AS}(z,\vec{p})\sin(qz)\mathrm{d}z, \tag{5.74a}$$

$$\mu = \Delta\varepsilon + \sum_{p_\mathrm{i}}\Delta p_\mathrm{i}\int_{-\infty}^{\infty}\frac{\partial G}{\partial p_\mathrm{i}}(z,\vec{p})\mathrm{e}^{\mathrm{i}q_c z}\mathrm{d}z, \tag{5.74b}$$

$$v = \int_{-\infty}^{\infty} zG^{AS}(z,\vec{p})\cos(qz)\mathrm{d}z, \tag{5.74c}$$

$$\tilde{D} = 6q_c^2 - \nu + \gamma_2. \tag{5.74d}$$

Asymmetry in the interaction kernel is necessary for the coefficients γ_0 and $\tilde{D}$ to be complex numbers since Fourier transforms of even and odd functions are purely real and purely imaginary numbers, respectively. Equation (5.73) is enough to capture the transition into spatiotemporal intermittency we observe in figure 5.7. Some considerations need to be taken to 5.72 before applying the solvability condition. If the real part of $\gamma_0 < 0$, the bifurcation turns subcritical and becomes necessary to add higher-order terms of A and $\bar{A}$ to saturate the instability. This is done by explicitly computing the correction $W(A,\bar{A})$ up to third order in A, and then add these terms to the Ansatz (5.68), this allows to get a term proportional to $A|A|^4$ in the normal form becoming a quintic Ginzburg-Landau equation. A similar situation happens if the real part of D turns negative. In this case, we need to keep higher-order spatial derivatives and obtain a different amplitude equation.

5.4 Relation to the LCLV

Recall equation (5.1) is just a prototype pattern forming model which accounts for a translational coupling or a misalignment in the context of optics. Nevertheless, this model captures the transition qualitatively into the complexity of stripped patterns. A comparison between the experimental results an numerical simulations are depicted in figure 5.8. Experimentally, it is possible to observe patterns of around 20 wavelengths. To perform a fair comparison, we choose a simulation domain so that the patterns have no more than 20 wavelengths. We also consider Dirichlet boundary conditions ($u(0,t) = u(L,t) = 0$). The wavelength of the experimental patters $\lambda_e \sim 250\mu m$. Numerical simulations and experimental observations show a qualitative agreement. We considered the fraction between the translational coupling length and the wavelength of the background pattern in the experiment $\chi_e = \delta/\lambda_e$. In the complex regime, depicted in figure 5.8-f, $\chi_e \approx 0.2$, which is consistent with our theoretical results.

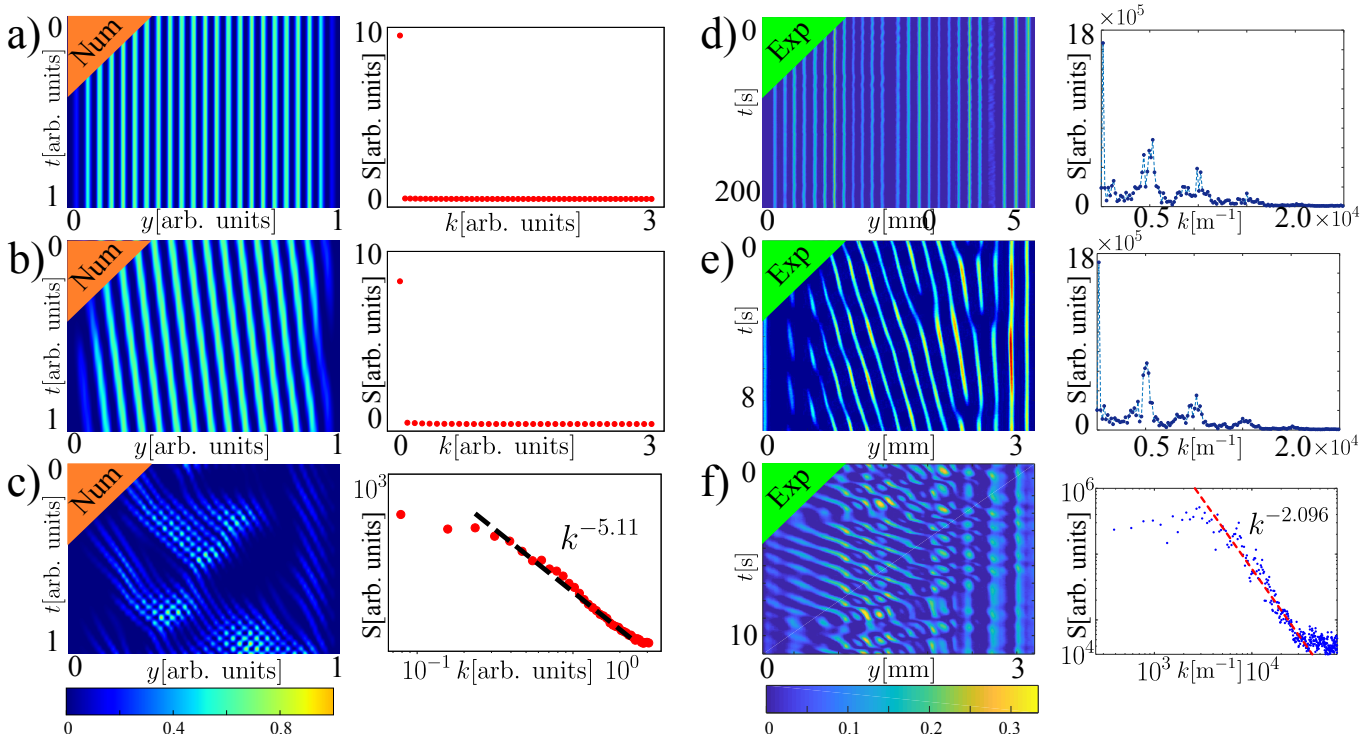

Figure 5.8: Spatiotemporal evolution and the temporal average power spectra $S(k)$ of the envelope of the pattern observed in the one dimensional SHTC for $\varepsilon = -0.1$ and the liquid crystal valve with translational optical feedback. Left panels numerical simulations with $\delta = 0.0$ (a), 0.2 (b), and 1.51(c).Left panels experimental observations with $\delta = 0 \pm 5$ μm (d), $\delta = 25 \pm 5$ μm (e), and $\delta = 50 \pm 5$ μm (f).

In chapter 4 showed that the generalized Swift-Hohenberg equation is derived by some limit of a reaction-diffusion model for the experiment. This reaction-diffusion system is a simplification of a model for the local molecular orientation derived from a variational principle. The linear term in this model depends on the local electric field applied to the liquid crystal molecules. This electric field is a function of the molecular orientation at a distance δ. To account for this, we propose a modified reaction-diffusion model with a

translational coupling

$$\tau\partial_t\theta = -(\tilde{\theta} - \tilde{\theta}_0) + l^2\nabla_\perp^2\theta, \tag{5.75}$$

where

$$\tilde{\theta} = \theta(x, y+\delta, t), \tag{5.76a}$$

$$\tilde{\theta}_0 = \frac{\pi}{2}\left(1 - \sqrt{\frac{\Gamma V_F}{\Gamma V_0 + \alpha\tilde{I}_w}})\right), \tag{5.76b}$$

$$\tilde{I}_w = \frac{I_0}{4}|\mathrm{e}^{-\mathrm{i}\frac{L}{2k}\nabla_\perp^2}(1 + \mathrm{e}^{-\mathrm{i}\beta\cos^2\theta(x,y+\delta)})|^2. \tag{5.76c}$$

Homogeneous solutions are not affected by the translational coupling, so these solutions are still represented by the surface in figure 4.13. Performing the same analysis we made in chapter 4, we stand on the onset of bistability of the homogeneous solution at θ_c, and derive an equation for a perturbation u

$$\theta = \theta_c + u, \tag{5.77}$$

$$\partial_t u = \eta + \varepsilon\tilde{u} - \tilde{u}^3 + l^2\nabla_\perp^2 u - \nu(L)\nabla_\perp^2\tilde{u} + h(L)\nabla_\perp^4\tilde{u}. \tag{5.78}$$

This corresponds to a more general version of the Swift-Hohenberg equation with transnational coupling. We need to take some consideration in this equation. Since the differential terms are now affected by the translational coupling, when computing the dispersion relation for perturbations of definite wavenumber q, we find terms of the form $q^2\mathrm{e}^{\mathrm{i}q\delta}$ and $q^4\mathrm{e}^{\mathrm{i}q\delta}$, whose real parts can become an arbitrarily large number for $q \to \infty$. We can overcome this by introducing a cut-off wavenumber q_0 before the change of sign of $\cos q\delta$. Experimentally this can be made by filtering short wavelength modes in the Fourier plane of the experiment.

5.4.1 Experimental proposition

A long-ranged interaction can be introduced to the experiment using a spatial light modulator in the Fourier plane. This device can change the phase and the intensity of the beam at each point; this is equivalent to multiplying the envelope of the beam's electric field by some complex function. Since at the spatial light modulator the envelope is given by the Fourier transform of the envelope of the beam just coming out from the liquid crystal cell, then the change of the Fourier transform of the envelope while passing through all the 4-f array is given by

$$\hat{E}_{out}(\vec{q}) = \hat{G}(\vec{q})\hat{E}_{out}(\vec{q}), \tag{5.79}$$

with $\hat{G(\vec{q})}$ a complex transmission factor at each point of the spatial light modulator. Recall that multiplication in the Fourier space is equivalent to do convolution in the spatial coordinates. Then the relation between the envelopes at the start and the end of the 4-f array reads

$$E_{out}(\vec{r}) = \int_{\mathbb{R}^2} G(\vec{r}')E_{\mathrm{in}}(\vec{r} - \vec{r}')\mathrm{d}x'\mathrm{d}y'. \tag{5.80}$$

This makes it possible to introduce an interaction Kernel to the system. We expect that in the pattern forming regime, the orientation of the molecules can be described by a Swift-Hoheneberg equation. A rigorous derivation of this kind of model has not been done in this thesis.

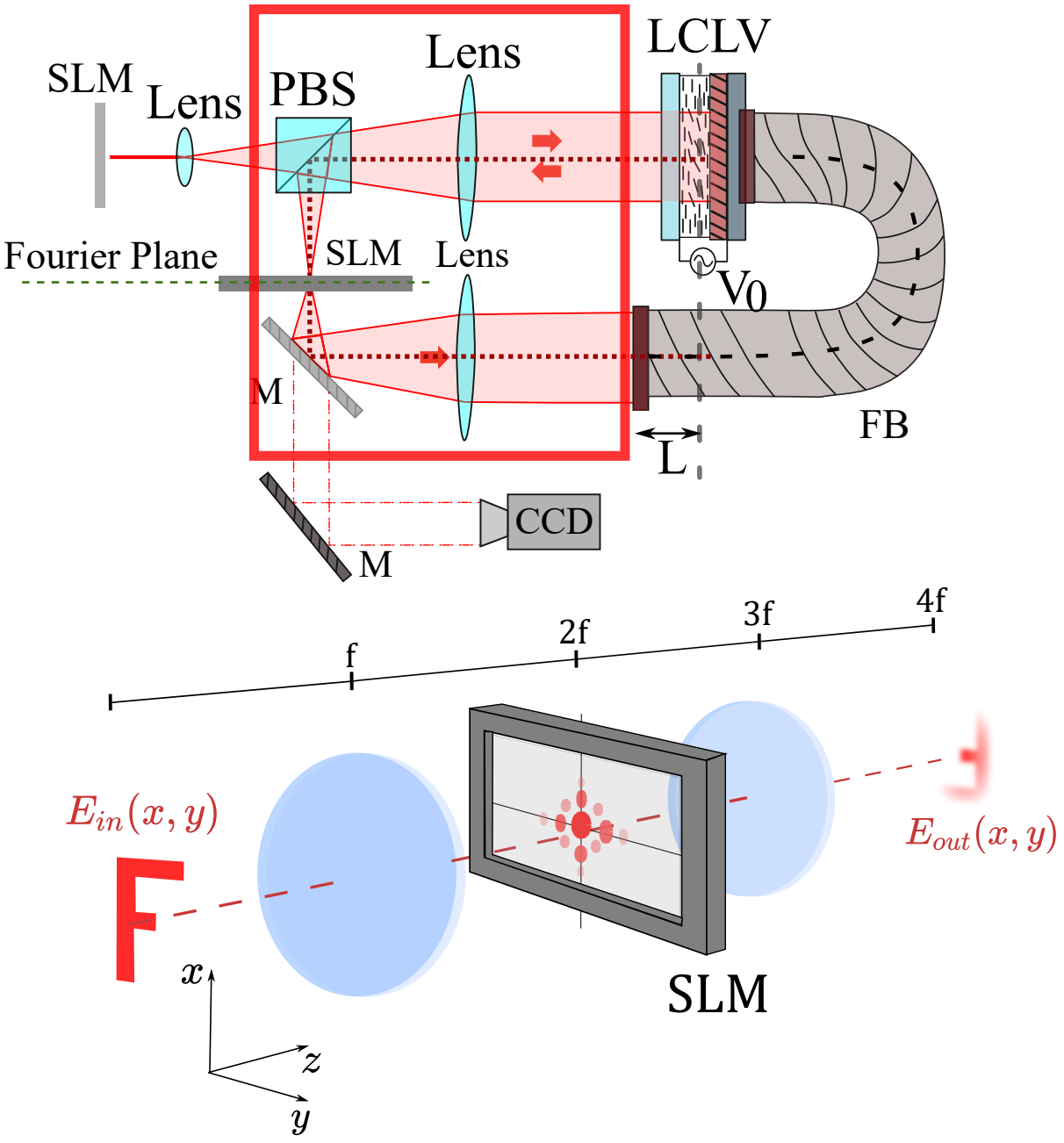

Figure 5.9: Liquid crystal light valve experiment with a spatial light modulator (SLM) in the Fourier plane.

Chapter 6

The Lugiato-Lefever equation with Raman interaction

Other optical pattern-forming systems are optical cavities filled with a Kerr medium. When a light beam passes through a Kerr medium, its refraction index is modified by a quantity proportional to the intensity of the beam. This phenomenon accounts for the non-linearity in the equation that governs the evolution of the electric field's envelope within an optical cavity known as the Lugiato-Lefever equation [54]. This model neglects the inelastic scattering of photons that happens when light interacts with matter. When these effects are considered into the model, they result in long-ranged temporal couplings, which are intrinsically asymmetric since they must respect causality. In this chapter, we briefly discuss the model that describes the evolution of the electric field's envelope of light beam injected in a fiber ring, which constitutes an optical cavity. We then introduce the effects of the Raman stimulated scattering into the model and explore its consequences.

6.1 The longitudinal Lugiato-Lefever equation

A fiber ring is depicted in figure 6.1. Let t_R be the round trip time of the fiber ring; short pulses are injected into the fiber with frequency $1/t_R$. The system has two different time scales: t is slow time representing the evolution after each successive roundtrip of a pulse in the fiber; τ is a fast time variable in the moving reference frame of the pulse traveling inside the fiber. A longitudinal Lugiato-Lefever equation can be derived for the evolution of the envelope the electric field as a first approximation [41]

$$\partial_t E = S - (\alpha + \mathrm{i}\theta)E - \mathrm{i}|E|^2 E + \mathrm{i}\partial_{\tau\tau} E, \tag{6.1}$$

where S in the amplitude of the injected pulses, α is the dissipation coefficient of the ring. The coefficient α can always be set to 1 by a rescaling the coordinates and the amplitude E. For the rest of this chapter, we will assume $\alpha = 1$. Homogeneous solutions to equation (6.1) are found by solving the following algebraic equation

$$|S|^2 = [1 + (\theta - |E|^2)^2]|E|^2. \tag{6.2}$$

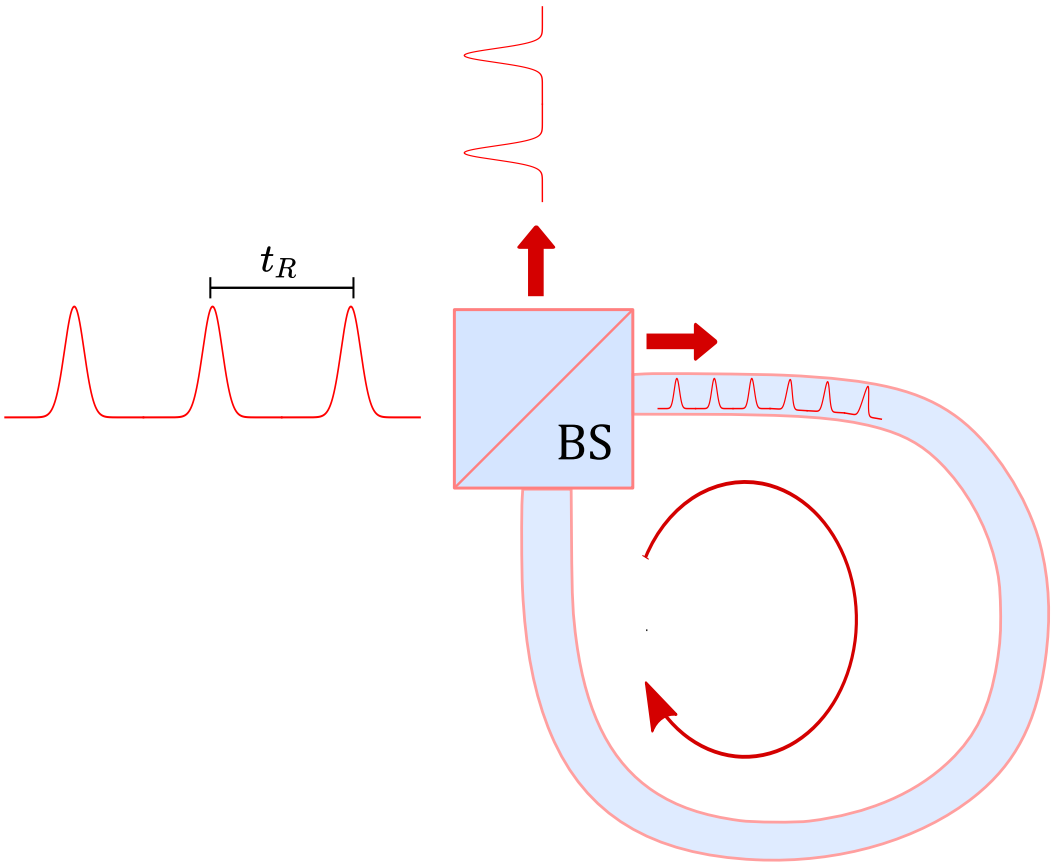

Figure 6.1: Fiber ring. A beam splitter (BS) of low transmittance is used to inject the pulses into the fiber.

The system has an imperfect and supercritical pitchfork bifurcation at $\theta_c = \sqrt{3}$ [54]. For our further analysis, we restrict the monostable regime ($\theta < \sqrt{3}$). We study the stability of the homogeneous solution to linear perturbations to the homogeneous solutions of the form

$$\begin{pmatrix} E \\ \bar{E} \end{pmatrix} = \begin{pmatrix} E_H \\ \bar{E}_H \end{pmatrix} + \begin{pmatrix} \delta E \\ \delta \bar{E} \end{pmatrix} \mathrm{e}^{\mathrm{i}q\tau + \lambda_q t}. \tag{6.3}$$

The system has a Turing instability at $q_c = \pm\sqrt{2-\theta}$, for $|S_c| = \sqrt{1+(\theta-1)^2}$ [54]. Close to the instability, a real Ginzburg-Landau equation can be derived to evolution the amplitude of the emerging pattern [61]. However, far away from the instability, the system exhibits a transition to a complex spatiotemporal intermittency, for even higher injection of energy, the system exhibits a transition into turbulence [23]. We note that the real Ginzburg-Landau equation captures none of these transitions due to its variational nature.

Equation (6.1) is a good approximation when the width of the pulses is much longer that 1 ps. However, for widths shorter than 1 ps, the effects of inelastic scattering of photons within the fiber can not be neglected. In the next section, we discuss this phenomenon and introduce a modified version of (6.1)

6.2 The Raman scattering

When a photon of given frequency ω interacts with a molecule in the fiber, it can excite a vibrational state of the molecule. This state can decay into a lower energy state, emitting a new photon. If the final state of the molecule is the same as the initial one, the emitted photon has the same frequency as the absorbed one; this phenomenon is known as Rayleigh scattering [70]. However, suppose the final state of the molecules is not the same as its initial state. In that case, the emitted photon will have a lower frequency given by $\omega - \Delta\omega$; this phenomenon is known as spontaneous Raman scattering [68, 51]. This process can be enhanced when two beams of different frequencies ω_p, and $\omega_s = \omega_p - \Delta\omega$, interact with the fiber. Let I_p and I_s be the intensities of each of these beams. The rate at which photons of frequency ω_p into photons of frequency ω_s is proportional to a coefficient g_R, which depends on the frequency difference $\Delta\omega$, and to the product of the intensities of the beams. This process is known as stimulated Raman scattering [91, 90, 43]. The following set of equations describe the evolution of the intensity of the beams while traversing a fiber

$$\partial_z I_p = -\frac{\omega_p}{\omega_s} g_R(\Delta\omega) I_p I_s - \alpha' I_p, \tag{6.4a}$$

$$\partial_z I_s = g_R(\Delta\omega) I_p I_s - \alpha' I_s, \tag{6.4b}$$

where z is a spatial coordinate in the propagation axis, and α' is a dissipation coefficient. The function $g_R(\Delta\omega)$ is referred to as the Raman gain. This function can be experimentally measured and reaches its maximum at $\Delta\omega \approx 10THz$ in Silica fibers (see Figure 6.3-a). The width of the spectrum of ultrashort pulses ($<$ 1ps) can be of the order of tens of Terahertz so that the effect of the stimulated Raman interaction can not be neglected. The Raman gain

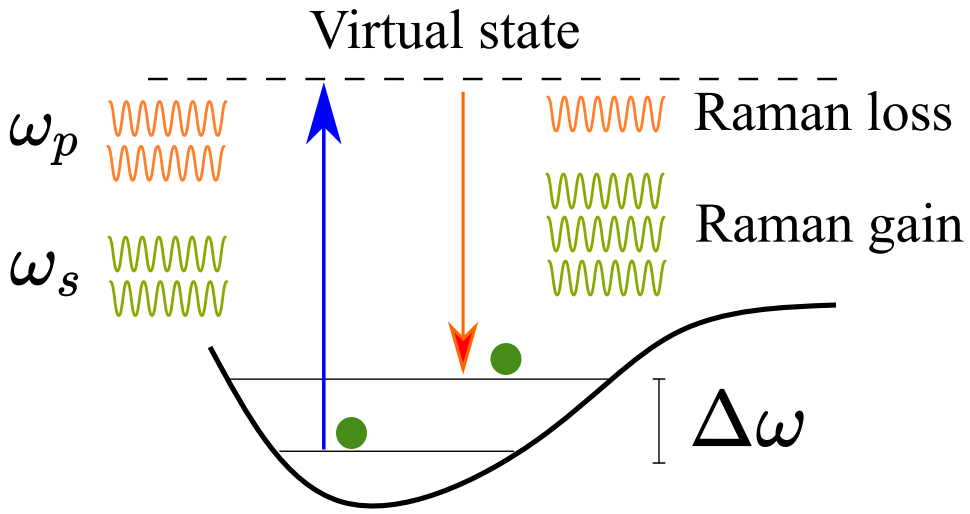

Figure 6.2: Pictorial represetantion of the Raman stimulated scttering.

is proportional to imaginary part of the third-order electric suceptibility of the fiber [1].

$$g_R(\Delta\omega) \propto \mathrm{Im}\{\chi^{[3]}(\Delta\omega)\} = \mathrm{Im}\{\hat{h}_R(\Delta\omega)\}, \tag{6.5}$$

where $\hat{h}_R(\Delta\omega)$ if the Fourier transform of the Raman response function $h_R(t)$ (see figure 6.3-b). The whole third-order response of the fiber will have an instantaneous part, associated with the Kerr effect, and a delayed response associated with Raman scattering. The equation

that governs the evolution of the envelope of the electric field is equation (6.1) with another non-linearity that accounts for the Raman response [22], this equation reads

$$\partial_t E = S - (\alpha + \mathrm{i}\theta)E + \mathrm{i}(1 - f_R)|E|^2 E + \mathrm{i}\partial_{\tau\tau} E + \mathrm{i} f_R E \int_{-\infty}^{\tau} h'_R(\tau - \tau')|E|^2(\tau')\mathrm{d}\tau'. \quad (6.6)$$

where

$$h'_R(\tau) = \tau_0 h_R(\tau_0 \tau), \quad (6.7)$$

The integral in the right-hand side is taken up to τ, since it has to respect causality. The parameter τ_0 sets a characteristic time scale for the fast time variable τ; it depends on the length of the cavity and its dissipation coefficient. The parameter f_R reflects the relevance of the Raman interaction in the system, and it depends on the properties of the fiber. The response function $h_R(\tau)$ is determined by experimentally measuring $g_R(\Delta\omega)$ and then using the Kramers-Kronig relations [14]. Nevertheless, a good approximation for the response function in Silica fiber is given by [2]

$$h_R = \frac{\tau_1^2 + \tau_2^2}{\tau_1 \tau_2^2} \sin \tau/\tau_1 \mathrm{e}^{-\tau/\tau_2}, \quad (6.8)$$

where τ_1 and τ_2 depend on the properties of the fiber-.

6.3 Convective instability

The integral term in equation (6.6) breaks the symmetry $\tau, -\tau$; thus, the Turing instability of the original system turns into a convective one. To illustrate this, let us linearize equation (6.6) around its homogeneous solution and consider linear perturbations to it

$$\begin{pmatrix} E \\ \bar{E} \end{pmatrix} = \begin{pmatrix} E_H \\ \bar{E}_H \end{pmatrix} + \begin{pmatrix} \delta E \\ \delta \bar{E} \end{pmatrix} \mathrm{e}^{\mathrm{i}q\tau + \lambda_q t}. \quad (6.9)$$

Replacing this expression in equation (6.6) and keeping just linear terms in δE we get the following problem of eigenavalues

$$\begin{aligned} \lambda_q \begin{pmatrix} \delta E \\ \delta \bar{E} \end{pmatrix} = & \begin{bmatrix} -1 + \mathrm{i}(2|E_H|^2 - \theta - q^2) & \mathrm{i}E_H^2 \\ -\mathrm{i}\bar{E}_H^2 & -1 - \mathrm{i}(2|E_H|^2 - \theta - q^2) \end{bmatrix} \begin{pmatrix} \delta E \\ \delta \bar{E} \end{pmatrix} \\ & + f_R \gamma \begin{bmatrix} \mathrm{i} & \mathrm{i}E_H^2 \\ -\mathrm{i}\bar{E_H}^2 & -\mathrm{i} \end{bmatrix} \begin{pmatrix} \delta E \\ \delta \bar{E} \end{pmatrix}, \end{aligned} \quad (6.10)$$

where we have defined

$$\gamma(q) = \int_0^\infty h'_R(\tau')\mathrm{e}^{-\mathrm{i}q\tau'}\mathrm{d}\tau' - 1 = \frac{q^2\tau_1^2/\tau_0^2 - 2\mathrm{i}q\tau_1^2\tau_2/\tau_0}{\tau_1^2 + \tau_2^2(1 - q^2\tau_1^2/\tau_0^2) + 2\mathrm{i}q\tau_1^2\tau_2/\tau_0} = \gamma_r + \gamma_\mathrm{i}. \quad (6.11)$$

If $f_R \ll 1$, then the second term in (6.10) can be taken as perturbative. We already know at which parameter the spatial instability happens for the system without the Raman interaction. With the Raman term, the spatial instability should happen at

$$|E_H^c| \approx 1 + f_R E_R, \quad (6.12)$$

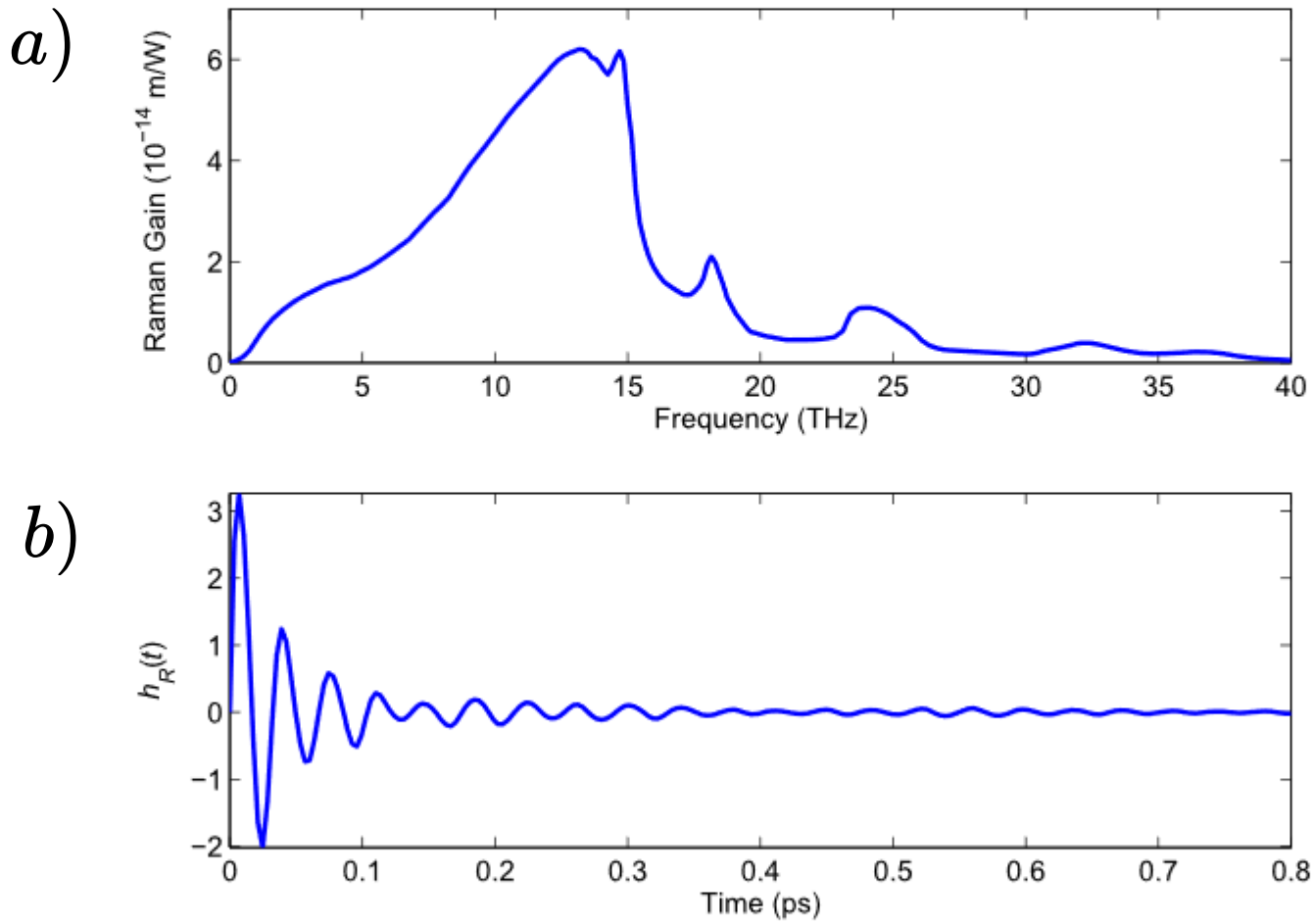

Figure 6.3: a) Raman gain in Silica fibers b)Raman response function in Silica fibers.

using this approximation, equation (6.10) reads

$$\lambda_q \begin{pmatrix} \delta E \\ \delta \bar{E} \end{pmatrix} = \begin{bmatrix} -1 + \mathrm{i}(2 - \theta - q^2) & \mathrm{i}e^{2\mathrm{i}\phi} \\ -\mathrm{i}e^{-2\mathrm{i}\phi} & -1 - \mathrm{i}(2 - \theta - q^2) \end{bmatrix} \begin{pmatrix} \delta E \\ \delta \bar{E} \end{pmatrix} + f_R \gamma \begin{bmatrix} \mathrm{i} & \mathrm{i}e^{2\mathrm{i}\phi} \\ -\mathrm{i}e^{-2\mathrm{i}\phi} & -\mathrm{i} \end{bmatrix} \begin{pmatrix} \delta E \\ \delta \bar{E} \end{pmatrix} + f_R E_R \begin{bmatrix} 2\mathrm{i} & \mathrm{i}e^{2\mathrm{i}\phi} \\ -\mathrm{i}e^{-2\mathrm{i}\phi} & -2\mathrm{i} \end{bmatrix} \begin{pmatrix} \delta E \\ \delta \bar{E} \end{pmatrix}, \tag{6.13}$$

where $E_H = \mathrm{e}^{\mathrm{i}\phi}$, with ϕ some phase that is not relevant for solving the eigenvalue problem. Since we know the solution of the unperturbed case, we use standard perturbation theory to find the corrections to critical eigenvalues. To first order in f_R we have

$$E_R = -\gamma_r(q_c), \tag{6.14}$$

$$\lambda_{q_c} = \mathrm{i} f_R \gamma_{\mathrm{i}}(q_c), \tag{6.15}$$

With $q_c = \pm\sqrt{2-\theta}$, corrections to q_c are of order f_R^2. According to (6.11) $\gamma_{\mathrm{i}}(q)$ is an odd function, so the instability becomes convective.

We conducted numerical simulations of equation (6.6); we found that close to the onset of instability for different values of f_R, the system converges into a traveling wave solution. Due to symmetry breaking, the amplitude equation that describes the evolution of the envelope of these waves is a complex cubic Ginzburg-Landau equation whose imaginary terms are proportional to f_R; however, since simulations show the Raman interaction induces no transition into complex dynamics, we did not characterize this amplitude equation. The Raman interaction has a relevant effect on solutions far away from the convective instability; this is discussed in the following section.

6.4 Reducing the complexity

We conducted numerical simulations of equation (6.6), using $\tau_0 = 1, \tau_1 = 0.12, \tau_2 = 0.32, S = 2.15$ and $\theta = 1$, in this region the unperturbed Lugiato-Lefever equation converges into a complex intermittent state. We tuned the value of f_R starting from this complex state and found that for $f_R \sim 0.06$, the system transitions into a different type of spatiotemporal intermittency. This new dynamical regime resembles to the spatiotemporal intermittency exhibited the complex cubic Ginzburg-Landau equation. Further up, for values $f_R \sim 0.12$ and higher, the drift induced by the Raman interaction too strong and drags away the characteristic structures of the spatiotemporal intermittency. Figure 6.4 depicts the different regimes observed while increasing f_R.

The transition between the different regimes can be characterized using the fast time correlation length τ_{corr}. We computed this by the method of Cross [27] (see figure 6.5). When approaching the region of Sierpinsky spatiotemporal intermittency, we observe an increase in the correlation length and observe a peak at the transition point. Moreover, we computed the Lyapunov spectra and the Yorke-Kaplan dimension for different values of f_R(see figure 6.6). We found that the Raman interaction effectively lowers the complexity of the system since there is a diminution in the Yorke-Kaplan dimension. We have not characterized the bifurcation diagram of equation (6.6), but we have found enough tools to characterize this transition. Experimentally, it is only possible to tune the coefficient τ_0, the parameters f_R, τ_1, τ_2 depend on the Fiber material. As future perspectives, we expect to conduct simulations of equation (6.6) fixing all parameters except for τ_0 and try to find the same transition. If this is possible, we also expect this phenomenon to be found in the fiber ring experiment.

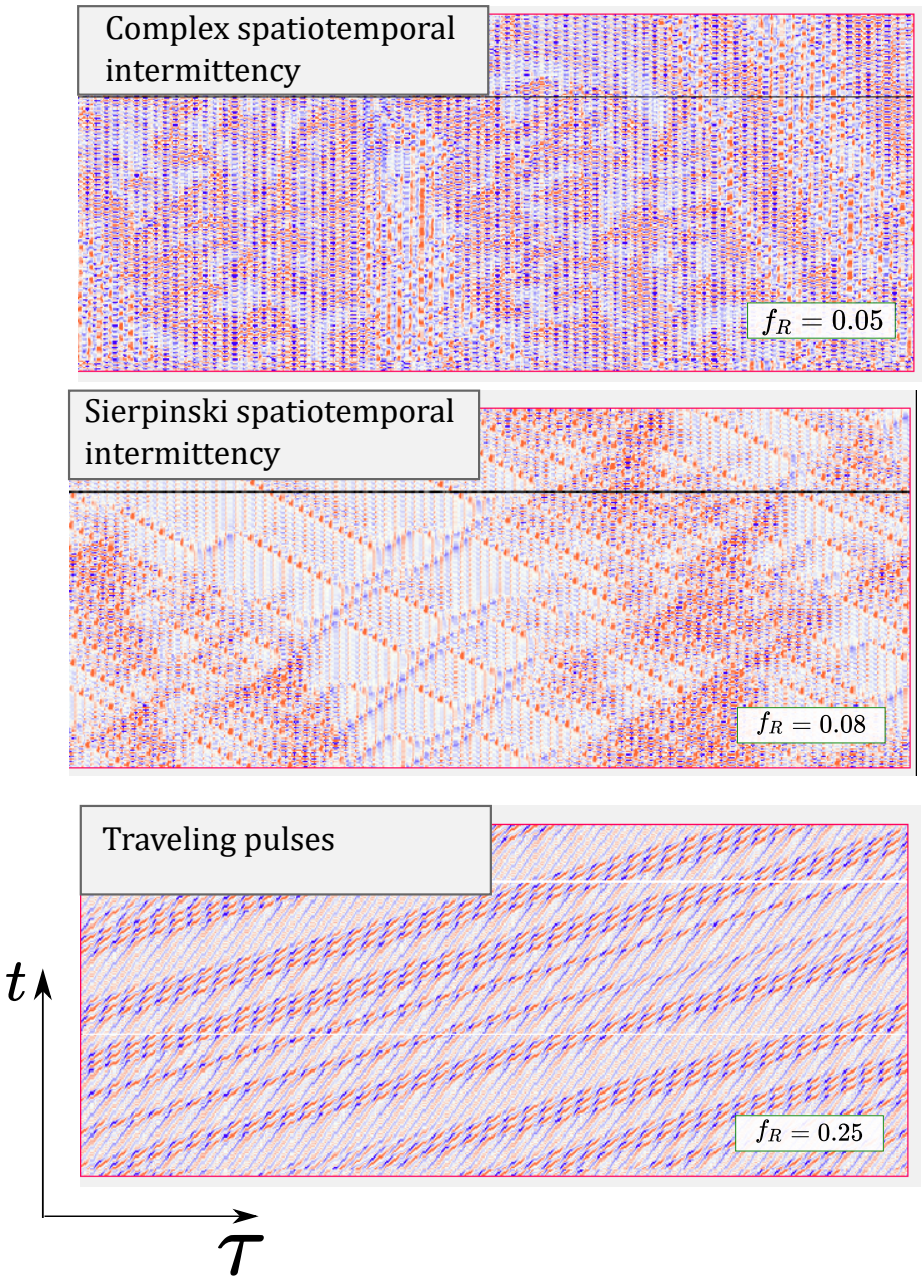

Figure 6.4: Different dynamical regimes found at different values of f_R

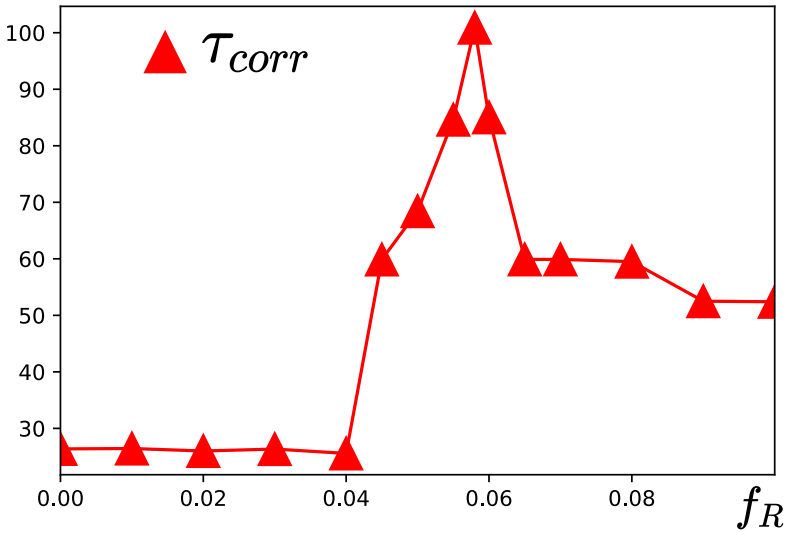

Figure 6.5: Spatial correlation length for the asympotic states for different values of f_R

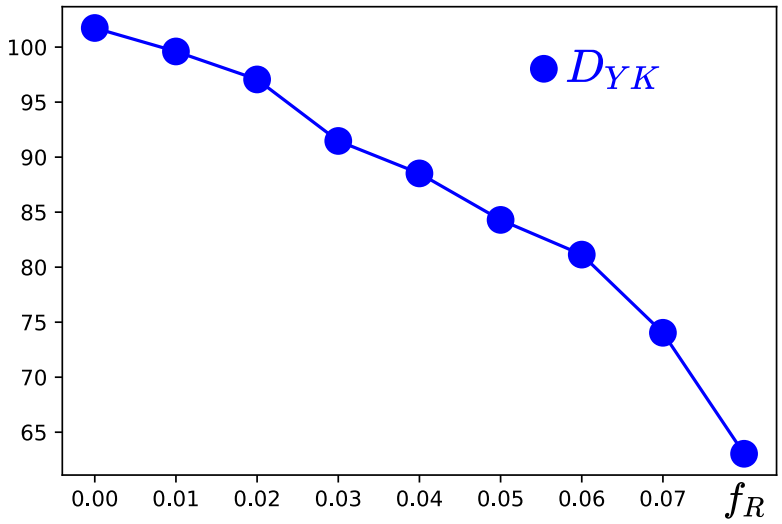

Figure 6.6: The Yorke-Kaplan dimension of the Lugiato-Lefever equation with Raman interaction for different values of f_R

Conclusion

In this dissertation, we presented experimental observations from the liquid crystal light valve experiment that shows a transition which is triggered form stationary patterns to propagation, spatiotemporal intermittency, and defect turbulence of stripped waves. To shed light on the origin of this complexity, we proposed a prototype pattern forming system that considers the effect of misalignment, characterized by a parameter δ, namely, the one-dimensional Swift-Hoheneberg model with translational coupling. We showed that this equation has a convective instability that gives rise to traveling stripped waves from the homogeneous state. When increasing the value of δ, the envelope of these waves exhibits transition into spatiotemporal intermittency defect turbulence, which is in qualitative agreement with the experimental observations. We derived an amplitude equation close to the convective instability of our model, namely, the cubic complex Ginzburg-Landau equation, which successfully accounts for the complex regimes of the prototype model. This allowed us to reveal the bifurcation diagram of the model close to its convective instability and understand the mechanisms that give rise to its complexity. We explored the two-dimensional extension of the prototype model, where we found a complex regime. When considering the temporal evolution of a line segment parallel to the translational coupling direction, we found a spatiotemporal diagram resembling the one-dimensional Siperpinski spatiotemporal intermittency. We generalized our results for more general long-ranged and asymmetric interaction mediated through interactions kernels; we showed that the same phenomenology, and that the cubic complex Ginzburg-Landau equation can also be derived in these models. This allows us the apply our results to pattern-forming systems in contexts other than nonlinear optics, such as population dynamics and ecology. We proposed a modification to the liquid crystal light valve experiment, introducing a spatial light modulator in the Fourier plane, which allows us to experimentally explore the effects of different interaction Kernels in a pattern-forming system. Finally, we explored a specific pattern-forming system with a long-ranged asymmetric interaction. We studied a specific pattern-forming system with an asymmetric interaction far from its convective instability, the longitudinal Lugiato-Lefever equation with Raman interaction, which describes the evolution of the envelope of the electric field of short light pulses injected in a fiber ring. We showed that the inclusion of the Raman interaction induces a transition between different types of spatiotemporal intermittency. We characterized this change in the complexity by means of Lyapunov Spectra and spatial correlation functions. Experimental observations can be done in a fiber ring to compare with the theoretical predictions

Bibliography

[1] Gonzague Agez, Pierre Glorieux, M Taki, and E Louvergneaux. Two-dimensional noise-sustained structures in optics: Theory and experiments. *Physical Review A*, 74(4):043814, 2006.

[2] Govind P Agrawal. Nonlinear fiber optics. In *Nonlinear Science at the Dawn of the 21st Century*, pages 195–211. Springer, 2000.

[3] SA Akhmanov, MA Vorontsov, V Yu Ivanov, AV Larichev, and NI Zheleznykh. Controlling transverse-wave interactions in nonlinear optics: generation and interaction of spatiotemporal structures. *JOSA B*, 9(1):78–90, 1992.

[4] F Alvarez-Garrido, MG Clerc, and Gregorio Gonzalez-Cortes. Transition to spatiotemporal intermittency and defect turbulence in systems under translational coupling. *Physical Review Letters*, 124(16):164101, 2020.

[5] Aleksandr Aleksandrovich Andronov, Aleksandr Adol'fovich Vitt, and Semen Emmanuilovich Khaikin. *Theory of Oscillators: Adiwes International Series in Physics*, volume 4. Elsevier, 2013.

[6] Igor S Aranson and Lorenz Kramer. The world of the complex ginzburg-landau equation. *Reviews of Modern Physics*, 74(1):99, 2002.

[7] Philip Ball and Neil R Borley. *The self-made tapestry: pattern formation in nature*, volume 198. Oxford University Press Oxford, 1999.

[8] Valentine Bargmann. On a hilbert space of analytic functions and an associated integral transform part i. *Communications on pure and applied mathematics*, 14(3):187–214, 1961.

[9] Naoaki Bekki and Kazuhiro Nozaki. Formations of spatial patterns and holes in the generalized ginzburg-landau equation. *Physics Letters A*, 110(3):133–135, 1985.

[10] Henri Bénard. Les tourbillons cellulaires dans une nappe liquide. *Rev. Gen. Sci. Pures Appl.*, 11:1261–1271, 1900.

[11] T Brooke Benjamin and JE Feir. The disintegration of wave trains on deep water. *J. Fluid mech*, 27(3):417–430, 1967.

[12] G Bertram Jr et al. *Population dynamics: alternative models*. Elsevier, 2013.

[13] Max Born and Emil Wolf. *Principles of optics: electromagnetic theory of propagation, interference and diffraction of light*. Elsevier, 2013.

[14] RW Boyd and BR Masters. Nonlinear optics 3rd edn (new york: Academic). 2008.

[15] Richard J Briggs. Electron-stream interaction with plasmas. 1964.

[16] R Brown, AL Fabrikant, and MI Rabinovich. Evolution of patterns in the anisotropic complex ginzburg-landau equation: Modulational instability. *Physical Review E*, 47(6):4141, 1993.

[17] Francisco Daniel del Campo Rojas. Efectos del acoplamiento traslacional y el ruido en sistemas extendidos. 2013.

[18] S. Chandrasekhar. Liquid crystals, 1992.

[19] Hugues Chate. Spatiotemporal intermittency regimes of the one-dimensional complex ginzburg-landau equation. *Nonlinearity*, 7(1):185, 1994.

[20] Marcel G Clerc, Gregorio González-Cortés, Vincent Odent, and Mario Wilson. Optical textures: characterizing spatiotemporal chaos. *Optics express*, 24(14):15478–15485, 2016.

[21] Marcel G Clerc, Artem Petrossian, and Stefania Residori. Bouncing localized structures in a liquid-crystal light-valve experiment. *Physical Review E*, 71(1):015205, 2005.

[22] MG Clerc, S Coulibaly, and M Tlidi. Time-delayed nonlocal response inducing traveling temporal localized structures. *Physical Review Research*, 2(1):013024, 2020.

[23] Saliya Coulibaly, Majid Taki, Abdelkrim Bendahmane, Guy Millot, Bertrand Kibler, and Marcel Gabriel Clerc. Turbulence-induced rogue waves in kerr resonators. *Physical Review X*, 9(1):011054, 2019.

[24] P Coullet, L Gil, and F Rocca. Optical vortices. *Optics Communications*, 73(5):403–408, 1989.

[25] John Crank. *The mathematics of diffusion*. Oxford university press, 1979.

[26] Mark C Cross and Pierre C Hohenberg. Pattern formation outside of equilibrium. *Reviews of modern physics*, 65(3):851, 1993.

[27] MC Cross and DI Meiron. Domain coarsening in systems far from equilibrium. *Physical review letters*, 75(11):2152, 1995.

[28] Michael Cross and Henry Greenside. *Pattern formation and dynamics in nonequilibrium systems*. Cambridge University Press, 2009.

[29] James P Crutchfield. Space-time dynamics in video feedback. *Physica D: Nonlinear*

Phenomena, 10(1-2):229–245, 1984.

[30] F Del Campo, F Haudin, RG Rojas, U Bortolozzo, MG Clerc, and S Residori. Effects of translational coupling on dissipative localized states. *Physical Review E*, 86(3):036201, 2012.

[31] David A Egolf and Henry S Greenside. Characterization of the transition from defect to phase turbulence. *Physical review letters*, 74(10):1751, 1995.

[32] Christian Elphick, Enrique Tirapegui, ME Brachet, Pierre Coullet, and Gérard Iooss. A simple global characterization for normal forms of singular vector fields. *Physica D: Nonlinear Phenomena*, 29(1-2):95–127, 1987.

[33] D Escaff. Non-local defect interaction in one-dimension: weak versus strong non-locality. *The European Physical Journal D*, 62(1):33–38, 2011.

[34] Roland Faller and Lorenz Kramer. Phase chaos in the anisotropic complex ginzburg-landau equation. *Physical Review E*, 57(6):R6249, 1998.

[35] Michael Faraday. On a peculiar class of acoustical figures; and on certain forms assumed by groups of particles upon vibrating elastic surfaces. In *Abstracts of the Papers Printed in the Philosophical Transactions of the Royal Society of London*, number 3, pages 49–51. The Royal Society London, 1837.

[36] Ronald Aylmer Fisher. The wave of advance of advantageous genes. *Annals of eugenics*, 7(4):355–369, 1937.

[37] Ivar Fredholm. Sur une classe d'équations fonctionnelles. *Acta mathematica*, 27(1):365–390, 1903.

[38] V Fréedericksz and A Repiewa. Theoretisches und experimentelles zur frage nach der natur der anisotropen flüssigkeiten. *Zeitschrift für Physik*, 42(7):532–546, 1927.

[39] Uriel Frisch and Andreĭ Kolmogorov. *Turbulence: the legacy of AN Kolmogorov*.

[40] LP GORKOV and GM Eliashberg. Generalization of the equations in the ginzburg-landau theory of non-stationary problems in the case of alloys containing paramagnetic impurities. *ZH EKSPER TEOR FIZ*, 54(2), 1968.

[41] Marc Haelterman, Stefano Trillo, and Stefan Wabnitz. Dissipative modulation instability in a nonlinear dispersive ring cavity. *Optics communications*, 91(5-6):401–407, 1992.

[42] Mariana Haragus and Gérard Iooss. *Local bifurcations, center manifolds, and normal forms in infinite-dimensional dynamical systems*. Springer Science & Business Media, 2010.

[43] Robert W Hellwarth. Theory of stimulated raman scattering. *Physical Review*, 130(5):1850, 1963.

[44] Elizabeth E Holmes, Mark A Lewis, JE Banks, and RR Veit. Partial differential equations in ecology: spatial interactions and population dynamics. *Ecology*, 75(1):17–29, 1994.

[45] Béatrice Janiaud, Alain Pumir, David Bensimon, Vincent Croquette, Helga Richter, and Lorenz Kramer. The eckhaus instability for traveling waves. *Physica D: Nonlinear Phenomena*, 55(3-4):269–286, 1992.

[46] James L Kaplan and James A Yorke. Chaotic behavior of multidimensional difference equations. In *Functional differential equations and approximation of fixed points*, pages 204–227. Springer, 1979.

[47] AN Kolmogorov, IG Petrovskii, and NS Piskunov. Study of a diffusion equation that is related to the growth of a quality of matter, and its application to a biological problem. *Byul. Mosk. Gos. Univ. Ser. A Mat. Mekh*, 1(1):26, 1937.

[48] Lorenz Kramer and Werner Pesch. Convection instabilities in nematic liquid crystals. *Annual review of fluid mechanics*, 27(1):515–539, 1995.

[49] Yoshiki Kuramoto. Diffusion-induced chaos in reaction systems. *Progress of Theoretical Physics Supplement*, 64:346–367, 1978.

[50] LD Landau and VL Ginzburg. On the theory of superconductivity,[in:] collected papers of ld landau, d. ter haar [ed.], 546–568, 1965.

[51] Gr Landsberg and L Mandelstam. Über die lichtzerstreuung in kristallen. *Zeitschrift für Physik*, 50(11-12):769–780, 1928.

[52] Joceline Lega. Traveling hole solutions of the complex ginzburg–landau equation: a review. *Physica D: Nonlinear Phenomena*, 152:269–287, 2001.

[53] Marcel Lesieur. *Turbulence in fluids*, volume 40. Springer Science & Business Media, 2012.

[54] Luigi A Lugiato and René Lefever. Spatial dissipative structures in passive optical systems. *Physical review letters*, 58(21):2209, 1987.

[55] Paul Manneville and Hugues Chaté. Phase turbulence in the two-dimensional complex ginzburg-landau equation. *Physica D: Nonlinear Phenomena*, 96(1-4):30–46, 1996.

[56] Ehud Meron. *Nonlinear physics of ecosystems*. CRC Press, 2015.

[57] Wolf-Christian Müller, Shiva Kumar Malapaka, and Angela Busse. Inverse cascade of magnetic helicity in magnetohydrodynamic turbulence. *Physical Review E*, 85(1):015302, 2012.

[58] Alan C Newell and John A Whitehead. Finite bandwidth, finite amplitude convection. *Journal of Fluid Mechanics*, 38(2):279–303, 1969.

[59] Grégoire Nicolis. *Introduction to nonlinear science*. Cambridge University Press, 1995.

[60] Gregoire Nicolis and Ilya Prigogine. Self-organization in nonequilibrium systems. *Dissipative Structures to Order through Fluctuations*, 1977.

[61] Nicolas Périnet, Nicolas Verschueren, and Saliya Coulibaly. Eckhaus instability in the lugiato-lefever model. *The European Physical Journal D*, 71(9):243, 2017.

[62] Arkady Pikovsky and Antonio Politi. *Lyapunov exponents: a tool to explore complex dynamics*. Cambridge University Press, 2016.

[63] Len M Pismen. *Patterns and interfaces in dissipative dynamics*. Springer Science & Business Media, 2006.

[64] Len M Pismen, Len M Pismen, et al. *Vortices in nonlinear fields: From liquid crystals to superfluids, from non-equilibrium patterns to cosmic strings*, volume 100. Oxford University Press, 1999.

[65] Henri Poincaré. Sur l'équilibre d'une masse fluide animée d'un mouvement de rotation. *Acta mathematica*, 7(1):259–380, 1885.

[66] EB Priestley, Peter J Wojtowicz, and Ping Sheng. Introduction to liquid crystals.

[67] Mikhail I Rabinovich, Alexander B Ezersky, and Patrick D Weidman. *The dynamics of patterns*. World Scientific, 2000.

[68] Chandrasekhara Venkata Raman. A new radiation. 1928.

[69] PL Ramazza, S Ducci, and FT Arecchi. Optical diffraction-free patterns induced by a discrete translational transport. *Physical review letters*, 81(19):4128, 1998.

[70] John William Strutt Baron Rayleigh. *On the scattering of light by small particles*. 1871.

[71] Lord Rayleigh. Lix. on convection currents in a horizontal layer of fluid, when the higher temperature is on the under side. *The London, Edinburgh, and Dublin Philosophical Magazine and Journal of Science*, 32(192):529–546, 1916.

[72] Stefania Residori. Patterns, fronts and structures in a liquid-crystal-light-valve with optical feedback. *Physics Reports*, 416(5-6):201–272, 2005.

[73] Daniel Revuz and Marc Yor. *Continuous martingales and Brownian motion*. Number 293 in Grundlehren der mathematischen Wissenschaften. Springer, Berlin [u.a.], 3. ed edition, 1999.

[74] David Ruelle. Large volume limit of the distribution of characteristic exponents in turbulence. *Communications in Mathematical Physics*, 87(2):287–302, 1982.

[75] Bahaa EA Saleh and Malvin Carl Teich. *Fundamentals of photonics*. john Wiley & sons, 2019.

[76] Albert Schmid. A time dependent ginzburg-landau equation and its application to the problem of resistivity in the mixed state. *Physik der kondensierten Materie*, 5(4):302–317, 1966.

[77] Wolfgang Schöpf and Walter Zimmermann. Results on wave patterns in binary fluid convection. *Physical Review A*, 41(2):1145, 1990.

[78] Irving Ezra Segal and George W Mackey. *Mathematical problems of relativistic physics*, volume 2. American Mathematical Soc., 1963.

[79] Boris I Shraimanlk2puco, Alain Pumir, Wim van Saarloos, Pierre C Hohenberg, Hugues Chaté, and Margaret Holen. Spatiotemporal chaos in the one-dimensional complex ginzburg-landau equation. *Physica D: Nonlinear Phenomena*, 57(3-4):241–248, 1992.

[80] Waclaw Sierpinski. Sur une courbe cantorienne qui contient une image biunivoque et continue de toute courbe donnée. *CR Acad. Sci. Paris*, 162:629–632, 1916.

[81] Ch Skokos. The lyapunov characteristic exponents and their computation. In *Dynamics of Small Solar System Bodies and Exoplanets*, pages 63–135. Springer, 2010.

[82] K Stewartson and JT Stuart. A non-linear instability theory for a wave system in plane poiseuille flow. *Journal of Fluid Mechanics*, 48(3):529–545, 1971.

[83] Steven H Strogatz. *Nonlinear dynamics and chaos with student solutions manual: With applications to physics, biology, chemistry, and engineering*. CRC press, 2018.

[84] Jack B Swift and Pierre C Hohenberg. Hydrodynamic fluctuations at the convective instability. *Physical Review A*, 15(1):319, 1977.

[85] Geoffrey Ingram Taylor. Viii. stability of a viscous liquid contained between two rotating cylinders. *Philosophical Transactions of the Royal Society of London. Series A, Containing Papers of a Mathematical or Physical Character*, 223(605-615):289–343, 1923.

[86] Alan Mathison Turing. The chemical basis of morphogenesis. *Bulletin of mathematical biology*, 52(1-2):153–197, 1990.

[87] Martin van Hecke. Building blocks of spatiotemporal intermittency. *Physical review letters*, 80(9):1896, 1998.

[88] Wim van Saarloos and PC Hohenberg. Fronts, pulses, sources and sinks in generalized complex ginzburg-landau equations. *Physica D: Nonlinear Phenomena*, 56(4):303–367, 1992.

[89] Estefanía Vidal Henríquez. Phase singularity dynamics in out of equilibrium anisotropic systems. 2015.

[90] Chen-Show Wang. Theory of stimulated raman scattering. *Physical Review*, 182(2):482, 1969.

[91] EJ Woodbury and WK Ng. Ruby laser operation in near ir. *Proceedings of the Institute of Radio Engineers*, 50(11):2367, 1962.

[92] Vladimir E Zakharov, Victor S L'vov, and Gregory Falkovich. *Kolmogorov spectra of turbulence I: Wave turbulence*. Springer Science & Business Media, 2012.

Appendix A

Transition to Spatiotemporal Intermittenct and Defect Turbulence in Systems under Translational Coupling

In this section we include a copy of the paper titled "Transition to Spatiotemporal Intermittenct and Defect Turbulence in Systems under Translational Coupling" published in Physical Review Letters.

Transition to Spatiotemporal Intermittency and Defect Turbulence in Systems under Translational Coupling

F. Alvarez-Garrido, M. G. Clerc, and G. Gonzalez-Cortes
Departamento de Física and Millennium Institute for Research in Optics, Facultad de Ciencias Físicas y Matemáticas, Universidad de Chile, Casilla 487-3, Santiago, Chile

(Received 4 November 2019; accepted 30 March 2020; published 21 April 2020)

Out of equilibrium systems under the influence of enough energy injection exhibit complex spatiotemporal behaviors. Based on a liquid crystal light valve experiment with translational optical feedback, we observe propagation, spatiotemporal intermittency, and defect turbulence of striped waves. A prototype model of pattern formation with translational coupling shows the same phenomenology. Close to the spatial instability, a local amplitude equation is derived. This amplitude equation allows us to reveal the origin and bifurcation diagram of the observed complex spatiotemporal dynamics. Experimental observations have a qualitative agreement with theoretical findings.

DOI: 10.1103/PhysRevLett.124.164101

Nonequilibrium processes often lead to the formation of dissipative structures in nature [1–4]. These processes are characterized by constantly injecting and dissipating energy. When the injection of energy is small compared to dissipation, equilibria are usually characterized by being uniform and stationary. Increasing the energy injection can develop a pattern from a homogeneous state through spontaneous breaking of symmetries [1–4]. At the onset of this instability, a general strategy to describe the dynamics is achieved through amplitude equations [3–5]. This description permits us to explain the emergence of stripes, hexagons, rhombic, quasicrystals, superlattice textures, and the alternation between them among other phenomena [3–7]. In nonlinear optics, the coupling of light to a polarizable medium is the primary mechanism of pattern formation (see review [8] and references therein). One of the difficulties to face is the proper alignment of the light since a small deviation can generate deformations and dynamics of patterns. This misalignment can trigger a transition from hexagon to stripe or square pattern [9,10]. From a theoretical point of view, optical misalignment can be modeled by *translational couplings*. Namely, the dynamics that are steering the system under study depend on physical variables in its local position and on what happens in a position at a given distance [10–12]. This type of dynamics can induce that localized patterns to propagate and even emit vortices with a structure such as von Kármán street [12]. Asymmetric differential integral terms can be described by translational couplings. This type of coupling has been used to describe the dynamical behaviors of several systems such as neurons [13], vegetation self-organization in nonuniform topography [14], fluid surface dynamics, and optical fibers [15]. Selection and transition of stationary two-dimensional patterns in optical experiments with translational coupling have been established [9,10]. However, the understanding of complex spatiotemporal patterns remains unexplored.

This Letter aims to investigate how the translational coupling in pattern-forming systems brings out the emergence and transition of complex spatiotemporal behaviors. Based on a liquid crystal light valve experiment with translational optical feedback, we observe the emergence of striped patterns. Increasing the length of the translational coupling, the system exhibits transitions to traveling, spatiotemporal intermittency, and defect turbulence of striped waves. A universal pattern model, the Turing-Swift-Hohenberg equation [16,17] with translational coupling, is analyzed. Increasing the length of the translational coupling, this model exhibits a transition between traveling, spatiotemporal intermittency, and defect turbulence of waves. Close to spatial instability, the complex Ginzburg-Landau equation is derived. This local model allows us to reveal the origin and bifurcation diagram of the observed dynamical behaviors. The sequence of experimental bifurcations and observations have a qualitative agreement with theoretical findings.

A flexible and straightforward experiment that displays pattern formation is the liquid crystal light valve (LCLV) with optical feedback (see review [18] and references therein). Figure 1 shows a schematic representation of a LCLV with an optical feedback. The LCLV is composed of a nematic liquid crystal (LC) film between a glass and a photoconductive plate. A dielectric mirror is deposed over the photoconductive plate. The LC film is planarly aligned, with a thickness $d = 15\ \mu$m. The liquid crystal used is a nematic LC-654 (NIOPIK) with positive dielectric anisotropy $\Delta\varepsilon = 10.7$, and large optical birefringence $\Delta n = 0.2$. To obtain the maximum polarization change on the light, we set an angle $\pi/4$ between the electric field orientation of the incident light and the anchoring of the

 © 2020 American Physical Society

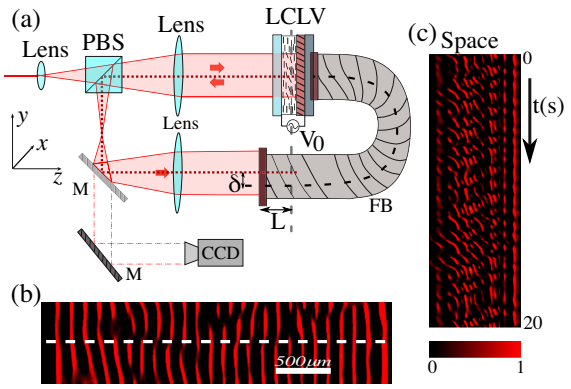

FIG. 1. (a) Schematic representation of the setup. LCLV is a liquid crystal light valve, PBS polarized beam splitter, M accounts for mirrors, V_0 the voltage applied to the liquid crystal layer, CCD charge-coupled device camera, L free propagation length, FB optical fiber bundle, and δ translational length. (b) Snapshot of the striped pattern obtained with $L = -4.0$ cm and $\delta = 50$ μm. (c) Spatiotemporal evolution of the profile of the striped pattern in the dashed line illustrated in (b).

cell. Transparent electrodes permit the application of an external electrical potential $V = V_0 \cos(\omega t)$ across the LC layer ($\omega = 1.0$ kHz). The LCLV is illuminated by an expanded He-Ne laser beam, $\lambda = 633$ nm, with 1.5 cm transverse radius and power $I_{\text{in}} = 7.0$ mW/cm^2. Once the light is injected into the LCLV, the beam is reflected by the dielectric mirror. Light is sent to the polarizing beam splitter cube (PBS), which will carry the light into the feedback loop given the polarization change the light has undergone in the LCLV. A nonpolarized beam splitter M and an optical fiber bundle (FB) have been used to close the loop. To record the liquid crystal cell plane, we collect the light with a coupled charge device (CCD) camera.

A $4-f$ array is placed in the optical feedback loop to obtain a self-imaging and the Fourier plane. By means of the optical fiber bundle, it is possible to adjust the free propagation length characterized by the L parameter [18]. In order to introduce a translational coupling on the LCLV, the FB also is displaced in a distance δ in the y direction (cf. Fig. 1) [9]. When considering a negative free propagation length and a translational coupling ($\delta \neq 0$), the hexagonal patterns become striped patterns. Figure 1(b) shows a typical striped pattern as the consequence of translational coupling. Unexpectedly, these patterns are not static. To characterize its dynamics, we monitor the spatiotemporal evolution of an arbitrary horizontal line of these patterns. Figure 1(c) illustrates the spatiotemporal dynamics exhibited by the LCLV with translational coupling. This dynamic behavior presents complex spatiotemporal evolution similar to that exhibited by the optical valve with an anisotropic filter in the Fourier plane [19]. Observe that if one considers another line, the dynamical behavior exhibited by the system is similar.

To shed light on the observed dynamics in the LCLV with optical feedback and translational coupling, let us consider a simplified mathematical model of pattern formation with translational coupling, which reads (the Swift-Hohenberg model with translational coupling [11])

$$\partial_t u(y,t) = \epsilon\tilde{u} - \tilde{u}^3 - \nu\partial_{yy}u - \partial_{yyyy}u, \tag{1}$$

where $u(y,t)$ is a scalar order parameter, y and t account for the spatial coordinate and time, respectively, $\tilde{u} \equiv u(y+\delta,t)$ stands for the translational coupling, ϵ is a bifurcation parameter, and ν accounts for the local spatial coupling (coupling to nearest neighbors). When ν is negative (positive) the term proportional to it accounts for a diffusive (antidiffusive) process. ∂_{yy} and ∂_{yyyy} are the Laplacian and bi-Laplacian operator, respectively. For the sake of simplicity, we consider periodic boundary conditions. A qualitatively similar model to Eq. (1) has been used to describe the LCLV with translational coupling [9]. When $\delta = 0$, model Eq. (1) becomes the Swift-Hohenberg model [20]. This paradigmatic equation was deduced originally to describe the pattern formation on Rayleigh-Bénard convection [20]. The Swift-Hohenberg equation is the most simple isotropic and reflection symmetry real model that shows pattern formation [4].

For $\epsilon < -\nu^2/4$ and $\delta = 0$, the only equilibrium presented by the model Eq. (1) is $u(y,t) = 0$. When $\epsilon \geq -\nu^2/4$ and $\delta = 0$, the model presents a family of motionless patterns of wave number of the order $\sqrt{\nu}$, which emerge through a supercritical transition. Figure 2(a) shows the spatiotemporal evolution and envelope of $u(y,t)$ of the typically observed pattern. The envelope of $u(y,t)$ is computed by the transformation $\mathcal{H}(y,t) = |\int_{-\infty}^{\infty}[\int_0^{\infty} u(y',t)e^{ik(y'-y)}dy']dk/\pi|$ [21]. In addition, the right panels display the temporal average of the power spectrum of the envelope $S(k) = \int_0^T |\int_{-\infty}^{\infty} \mathcal{H}(y,t)e^{-iky}dy|^2 dt/\sqrt{2\pi T}$. From this figure, we infer that the pattern has a well-defined dominant wavelength. By increasing the translational parameter, stationary patterns become propagative waves in a direction determined by the δ sign [see Fig. 2(b)]. Note that these waves are slightly asymmetric and have a uniform envelope. This propagative phenomenon can be understood as a result that small translational coupling induces linear and nonlinear drag effects [22]. Namely, it is possible to approximate the nonlocal term by $\tilde{u} \approx u(y,t) + \delta\partial_y u$ when $\delta \ll 1$.

Notwithstanding, when δ is large enough, uniform traveling waves suffer an instability that gives rise to the emergence of defects in the traveling wave. Defects are characterized by being zero of the envelope wave, i.e., the wave exhibits a phase singularity. Observe that defects separate regions with almost uniform wave amplitudes. Defect dynamics present complex spatiotemporal evolution characterized by generating triangular shaped regions of uniform wave amplitude with different sizes. Figure 2(c)

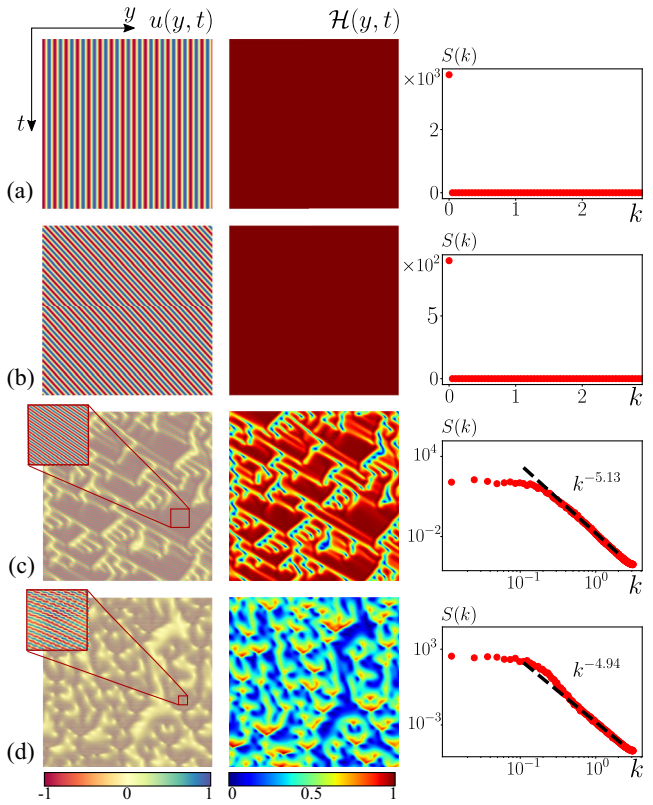

FIG. 2. Spatiotemporal evolution of patterns in the Swift-Hohenberg model with translational coupling Eq. (1). The left, center, and right panels are spatiotemporal diagrams of $u(y,t)$, envelope of $u(y,t)$ [$\mathcal{H}(u)$], and the temporal average power spectra $S(k)$ of the envelope. (a) $\epsilon = -0.08$, $\delta = 0.0$, (b) $\epsilon = -0.3$, $\delta = 1.0$, (c) $\epsilon = -0.3$, $\delta = 1.35$, and (d) $\epsilon = -0.8$, $\delta = 1.51$. The insets illustrate a magnification of the temporal space diagram.

shows the typical observed dynamics. The envelope $\mathcal{H}(y,t)$ allows us to clearly visualize the complex dynamics. Hence, in the spatiotemporal diagram, the system is characterized by presenting an alternation between regular and irregular region. This type of dynamical behavior is usually called spatiotemporal intermittency [23]. The temporal average of the power spectrum of the envelope allows us to find relationships between the dynamics of different spatial modes. Right panel of Fig. 2(c) illustrates this power spectrum $S(k)$. This spectrum is characterized by having a power law for large wave numbers, $S(k) \sim k^{-5}$. From this figure, we infer that the dynamics exhibited by the defects of the traveling waves has a turbulentlike nature [24]. Further increasing the translational coupling parameter δ, the spatiotemporal intermittency is replaced by the permanent or almost uniform emergence of defects [see Fig. 2(d)]. Namely, the appearance of defects is not intermittent. From the behavior of the envelope and its respective power spectrum, we conclude that this type of spatiotemporal dynamics corresponds to defect turbulence [23]. The power spectrum is characterized by maintaining a

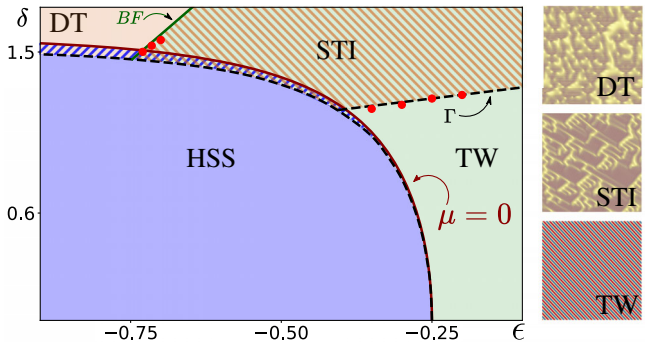

FIG. 3. Phase diagram of the Swift-Hohenberg model with translational coupling Eq. (1) with $\nu = 1.0$. HSS, TW, STI, and DT account for the homogeneous steady state $u = 0$, traveling wave with uniform envelope, spatiotemporal intermittency, and, defect turbulence, respectively. The solid (red) curve, $\mu = 0$, accounts for the convective instability. The solid curve BF describes the Benjamin-Fair instability. The dashed line Γ accounts for the transition between spatiotemporal intermittency to traveling waves. Red dots are the transition lines obtained by direct numerical simulations. The insets show the respective dynamic behaviors observed.

power law for large wave number $S(k) \sim k^{-5}$. From the point of view of defect production, it is not possible to identify the transition between spatiotemporal intermittency and defects turbulence. An efficient way to determine this transition is characterizing the statistics of regular and irregular regions of spatiotemporal evolution [25,26]. From defect turbulence equilibrium, when one decreases δ the emergence of spatiotemporal intermittency is observed, which remains in a large area of the parameter space coexisting with the uniform traveling wave. Hence, spatiotemporal intermittency presents a hysteresis loop with the traveling wave of uniform amplitude. Figure 3 shows the numerical phase diagram of the Swift-Hohenberg model with translational coupling Eq. (1).

To shed light on the origin of the previous dynamical behaviors, we will perform a weakly nonlinear analysis. Close to the transition between the homogeneous state and the traveling waves, *convective instability* induced by the nonlocal term [27,28], we can introduce the envelope ansatz

$$u(x,t) = aAe^{i(k_c y - \omega_c t)} + a\bar{A}e^{-i(k_c y - \omega_c t)} + W(A,\bar{A}), \quad (2)$$

in Eq. (1), where A is the complex amplitude of the critical wave, k_c is the critical wave number that satisfies the relation $k_c^4 = \epsilon\cos(k_c\delta) + \nu k_c^2$, $\omega_c = \epsilon\sin(k_c\delta)$ is the wave frequency, $\mu = \Delta\epsilon\cos(k_c\delta) - \epsilon k_c\Delta\delta\sin(k_c\delta)$ is the bifurcation parameter that characterizes the convective instability, $a = 1/\sqrt{3\cos(k_c\delta)}$ is a normalization constant, and $W(A,\bar{A})$ accounts for nonlinear corrections in amplitude A. Linearizing in W and imposing a solvability condition, the amplitude satisfies the convective and complex Ginzburg-Landau equation [29]

$$\partial_t A = \mu A - (1 + i\beta)|A|^2 A + (1 + i\alpha)\partial_z^2 A + v\partial_z A, \quad (3)$$

where the dimensionless spatial coordinate $z \equiv x/z_0$ with $z_0 = \sqrt{6k_c^2 - \nu + \varepsilon\delta^2 \cos(k_c\delta)/2}$, diffraction $\alpha \equiv \varepsilon\delta^2 \sin(k_c\delta)/2z_0^2$, nonlinear frequency response $\beta \equiv \tan(k_c\delta)$, and advective speed $v = \varepsilon\delta \cos(k_c\delta)/z_0$.

In the limit of local dynamic, $\delta = 0$, one recovers the Ginzburg-Landau equation with real coefficients ($\alpha = \beta = v = \omega = 0$), which describes the emergence of patterns [3]. In the case of periodic boundary conditions by considering the comobile coordinate system, the advective term in Eq. (3) can be eliminated. However, for other boundary conditions, this advective term is relevant to explain the transition from convective and absolute instability [27] and pinning-depinning of patterns [30]. The bifurcation parameter $\mu = 0$ accounts for the convective instability of the homogeneous state (see Fig. 3). This instability gives rise to a family of traveling waves of the form $A_p(y,t) = \sqrt{\mu - p^2}e^{i[py+(v-\beta(\mu-p^2)-\alpha p^2)t]}$. Stability analysis of this traveling wave for $p = 0$, allows obtaining the Benjamin-Fair (BF) critical curve, $1 + \alpha\beta = 0$ [29]. Figure 3 shows the BF curve in the parameter space $\{\epsilon, \delta\}$. It is expected to find phase turbulence for small β and significant α [23]. However, this is not possible to observe for the parameters generated from the $\{\epsilon, \delta\}$ space. The only phenomenon observed from the Ginzburg-Landau equation is the transition from waves to defect turbulence, which is expected for small α and large β [23]. It is also well known that this instability is of a subcritical nature; that is, coexistence is observed between the defects turbulence and traveling waves. By decreasing the parameter of instability, the defects' turbulence is replaced by spatiotemporal intermittency, which coexists with the traveling waves. Note that this dynamical behavior is consistent with the phenomena observed in the spatiotemporal intermittency region in Fig. 3. The transition between spatiotemporal intermittency to traveling waves was characterized numerically [23]. Using this numerical characterization, we have interpolate this transition curve, indexed by Γ, in the phase space represented in Fig. 3. In brief, the Ginzburg-Landau equation allows us to reveal the origin of all the intricate dynamics exhibited by the prototype pattern formation model with the translational coupling Eq. (1).

To compare the entire previous scenario with experimental observations onto the liquid crystal light valve with optical translational feedback, we must first consider more realistic boundary conditions than periodic ones and adequate domain of simulation. We have conducted numerical simulations of model Eq. (1), where a few numbers of wavelength is allowed. Note that experimentally, we observe about 20 wavelengths. Furthermore, we have considered Dirichlet boundary conditions $u(y = 0, t) = u(y = L, t) = 0$.

Experimentally and numerically, the parameters are in the region where pattern formation is observed. When a small translational length is included, we observe a static pattern due to pinning, induced by the boundary conditions [30] (see top panels in Fig. 4). When δ is increased, the pattern become propagative, but as a consequence of the boundary conditions, systematically appear and disappear dislocations in the spatiotemporal diagrams [cf. Figs. 4(b) and 4(e)]. Further increasing the translational coupling length, patterns exhibit intermittent behaviors, characterized by having a power spectrum with power laws. Figure 4 summarizes the spatiotemporal evolution of the pattern observed in the model Eq. (1) and the liquid crystal valve

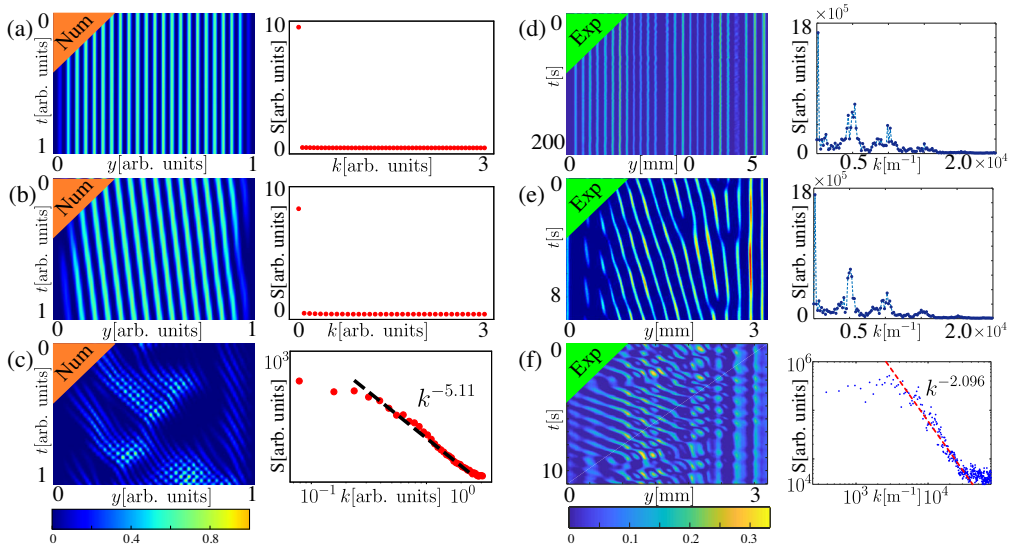

FIG. 4. Spatiotemporal evolution and the temporal average power spectra $S(k)$ of the envelope of the pattern observed in the model Eq. (1) by $\epsilon = -0.1$ and the liquid crystal valve with translational optical feedback. Left panels: numerical simulations with $\delta = 0.0$ (a), 0.2 (b), and 1.51(c). Right panels: experimental observations with $\delta = 0 \pm 5$ μm (d), $\delta = 25 \pm 5$ μm (e), and $\delta = 50 \pm 5$ μm (f).

with optical translated feedback. Hence, experimental observations and sequence of transitions have a qualitative agreement with theoretical findings. However, the critical exponents of the spatiotemporal intermittency are not the same. Theoretical characterization from a first principles model is in progress.

In conclusion, we have shown that systems under translational coupling exhibit transition to spatiotemporal intermittency and turbulence of defects. The translational coupling can be described as an asymmetric differential integral term. This type of coupling has been used to describe various systems in population dynamics, nonlinear optics, fluids, and ecology. Hence, the results presented are relevant in various physical contexts.

The authors thank F. del Campo for his discussions and primary numerical observations. We wish to acknowledge the economic support of Millennium Institute for Research in Optics and Fondecyt 1180903. G. G.-C. acknowledges the support of CONICYT-PFCHA Doctorado Nacional 2017211716.

[1] P. Glansdorff and I. Prigogine, *Thermodynamic Theory of Structures. Stability and Fluctuations* (Wiley, New York, 1971).
[2] G. Nicolis and I. Prigogine, *Self-Organization in Non-equilibrium Systems* (John Wiley & Sons, New York, 1977).
[3] L. M. Pismen, *Patterns and Interfaces in Dissipative Dynamics* (Springer, Berlin, 2006).
[4] M. Cross and H. Greenside, *Pattern Formation and Dynamics in Non-Equilibrium Systems* (Cambridge University, New York, 2009).
[5] A. C. Newell, T. Passot, and J. Lega, Annu. Rev. Fluid Mech. **25**, 399 (1993).
[6] R. B. Hoyle, *Pattern Formation: An Introduction to Methods* (Cambridge University Press, Cambridge, England, 2006).
[7] A. O. Leon, M. G. Clerc, and S. Coulibaly, Phys. Rev. E **89**, 022908 (2014).
[8] F. T. Arecchi, S. Boccaletti, and P. Ramazza, Phys. Rep. **318**, 1 (1999).
[9] P. L. Ramazza, S. Ducci, and F. T. Arecchi, Phys. Rev. Lett. **81**, 4128 (1998).
[10] G. Agez, P. Glorieux, M. Taki, and E. Louvergneaux, Phys. Rev. A **74**, 043814 (2006).
[11] F. del Campo, F. Haudin, R. G. Rojas, U. Bortolozzo, M. G. Clerc, and S. Residori, Phys. Rev. E **86**, 036201 (2012).
[12] F. Haudin, R. G. Rojas, U. Bortolozzo, M. G. Clerc, and S. Residori, Phys. Rev. Lett. **106**, 063901 (2011).
[13] J. D. Murray, *Mathematical Biology* (Springer, New York, 1990).
[14] E. Meron, *Nonlinear Physics of Ecosystems* (CRC Press, Boca Raton, 2015).
[15] M. G. Clerc, S. Coulibaly, and M. Tlidi, Phys. Rev. Research **2**, 013024 (2020).
[16] J. Swift and P. C. Hohenberg, Phys. Rev. A **15**, 319 (1977).
[17] J. H. P. Dawes, Historia mathematica **43**, 49 (2016).
[18] S. Residori, Phys. Rep. **416**, 201 (2005).
[19] M. G. Clerc, G. Gonzalez-Cortes, V. Odent, and M. Wilson, Opt. Express **24**, 15478 (2016).
[20] J. Swift and P. C. Hohenberg, Phys. Rev. A **15**, 319 (1977).
[21] J. Claerbout, *Fundamentals of Geophysical Data Processing* (McGraw-Hill, New York, 1976).
[22] M. G. Clerc, S. Coulibaly, F. del Campo, M. A. Garcia-Nustes, E. Louvergneaux, and M. Wilson, Phys. Rev. E **92**, 050902(R) (2015).
[23] H. Chate, Nonlinearity **7**, 185 (1994).
[24] U. Frisch, *Turbulence: The Legacy of AN Kolmogorov* (Cambridge University Press, Cambridge, England, 1995).
[25] S. Ciliberto and P. Bigazzi, Phys. Rev. Lett. **60**, 286 (1988).
[26] S. Coulibaly, M. Taki, A. Bendahmane, G. Millot, B. Kibler, and M. G. Clerc, Phys. Rev. X **9**, 011054 (2019).
[27] R. J. Briggs, *Electron-Stream Interaction with Plasmas* (MIT Press, Cambridge, MA, 1964).
[28] F. Papoff and R. Zambrini, Phys. Rev. Lett. **94**, 243903 (2005); Phys. Rev. E **73**, 016611 (2006); Eur. Phys. J. D **58**, 235 (2010).
[29] I. S. Aranson and L. Kramer, Rev. Mod. Phys. **74**, 99 (2002).
[30] M. G. Clerc, C. Fernandez-Oto, M. A. Garcia-Nustes, and E. Louvergneaux, Phys. Rev. Lett. **109**, 104101 (2012).